BENCHMARKING TADF ACTIVITY OF SULFONE BASED COMPOUNDS

by

Aslıhan Hepgüler

B.S., Chemistry, Yıldız Technical University, 2018

Submitted to the Institute for Graduate Studies in
Science and Engineering in partial fulfillment of
the requirements for the degree of
Master of Science

Graduate Program in Chemistry

Boğaziçi University

2022

ACKNOWLEDGEMENTS

First of all, I want to thank my advisor Assoc. Prof. Şaron Çatak for her support, interest and sharing her knowledge.

I wish to extend my gratitude to my thesis committee members: Prof. Ayşe Neren Ökte and Prof. Alimet Sema Özen.

I want to thank TUBITAK for TUBITAK 2210-A National Scholarship Programme for MSc Students and their support. This study has been supported by TUBITAK Project No. 118Z914. I acknowledge TUBITAK ULAKBIM High Performance Computing Center for computational resources.

I thank current and former members of CCBG: Başak Fındık, Beyza Horoz, Busenur Aslanoğlu, Ege Uyar, Gamze Tanrıver, Mert Bozoflu, Pelin Ulukan and Zeynep Aktaş for their friendship and support. I studied with Pelin during this project and I am very grateful to work with her. I want to thank Pelin for her assistance and support.

Finally, I thank my family. They always believe me in all situations and stand next to me in my all decisions. I always feel strong and lucky with their presence. I dedicate my thesis to my family.

ABSTRACT

BENCHMARKING TADF ACTIVITY OF SULFONE BASED COMPOUNDS

Thermally activated delayed fluorescence (TADF) mechanism can be explained as transfer of excitons from the first triplet excited state (T_1) to the first singlet excited state (S_1) by reverse intersystem crossing (RISC). In this study, the activity of sulfone-based TADF compounds was examined with descriptors by using density functional theory (DFT). Besides structural properties, photophysical properties of studied compounds were investigated. Dihedral angles obtained from optimized geometries are shown to change with respect to donor units. The nature of excited states was examined because of its impact on TADF efficiency. As seen in results, we can say that M062X functional is the only functional that gives locally excited (LE) character at triplet excitations. The energy difference between S_1 and T_1 excited states (ΔE_{ST}) is one of the analyzed descriptors and generated with three different functionals. The calculated ΔE_{ST} values are consistent with experimental values. To evaluate efficiency of functionals, the relationship of experimental k_{RISC} with calculated $1/\Delta E_{ST}$ and spin-orbit coupling (SOC) that is required for reverse intersystem crossing (RISC) process is examined. As a result, B3LYP accidentally generates the best ΔE_{ST} values while M062X is the only functional that gives correct relationship between k_{RISC}-SOC. According to comparison based on the effect of ΔE_{ST} and SOC values on the (R)ISC possibility (χ), M062X is the most reliable functional. The obtained visualization of the highest occupied molecular orbital (HOMO) and the lowest unoccupied molecular orbital (LUMO) and Φ_s indices are consistent with other descriptors. Finally, absorption and emission spectra are generated and compared with experimental spectra. The obtained results will have contributions to the selection of the most reliable functional and design strategies for TADF compounds.

ÖZET

SÜLFON İÇEREN MOLEKÜLLERİN TADF AKTİVİTESİNİN KARŞILAŞTIRILMASI

Termal aktif gecikmeli floresans (TADF), eksitonların geri sistemiçi geçiş (RISC) ile ilk uyarılmış triplet halden (T_1) ilk uyarılmış singlet hale (S_1) transferi olarak açıklanabilir. Bu çalışmada yoğunluk fonksiyonel teorisi (DFT) kullanılarak sülfon içeren TADF moleküllerin aktivitesi çeşitli parametreler ile incelenmiştir. Moleküllerin yapısal özelliklerinin yanısıra fotofiziksel özellikleride araştırılmıştır. Optimize olmuş geometrilerden elde edilen dönme açılarının donör gruplarına bağlı olarak değiştiği görülmüştür. TADF verimine olan etkisinden dolayı uyarılmış hallerin karakterleri incelenmiştir. Elde edilen sonuçlara göre M062X fonksiyonelinin triplet uyarılmalarda lokal uyarılmış karakter (LE) veren tek fonksiyonel olduğunu söyleyebiliriz. Analiz edilen parametrelerden biri olan S_1 ve T_1 arasındaki enerji farkı (ΔE_{ST}), üç farklı fonksiyonel ile elde edilmiştir. Hesaplanan ΔE_{ST} değerleri deneysel değerler ile uyumludur. Deneysel k_{RISC} değerleri ile hesaplanan $1/\Delta E_{ST}$ ve RISC için gerekli olan spin yörünge etkileşimi (SOC) değerleri arasındaki bağlantı kullanılan fonksiyonellerin etkisini görmek için incelenmiştir. Sonuç olarak B3LYP fonksiyoneli ΔE_{ST} değerlerini kazara en iyi şekilde elde ederken M062X k_{RISC}-SOC arasındaki bağlantıyı doğru veren tek fonksiyoneldir. M062X, ΔE_{ST} ve SOC değerlerinin (R)ISC olasılığı (χ) üzerindeki etkisine dayanan karşılaştırmaya göre en güvenilir fonksiyoneldir. En yüksek enerjili dolu orbital (HOMO) ve en düşük enerjili boş orbitalden (LUMO) elde edilen görseller ve Φ_s indeksleri diğer parametreler ile uyumludur. Absorpsiyon ve emisyon spektrumları elde edilerek deneysel spektrumlar ile karşılaştırılmıştır. Elde edilen sonuçlar en güvenilir fonksiyonel seçimine ve TADF moleküllerin dizayn stratejilerine katkı sağlayacaktır.

TABLE OF CONTENTS

LIST OF FIGURES

LIST OF TABLES

LIST OF SYMBOLS

$E_{ext[n(r)]}$	Interaction between Electron and the External Potential
E_{xc}	Exchange-Correlation Functional
$\hat{H}$	Hamiltonian Operator
k_B	Boltzmann's Constant
k_{RISC}	Reverse Intersystem Crossing Rate Constant
$n(r)$	Electron Density
r_s	Radius of Sphere
S_n	Singlet Excited States
T_n	Triplet Excited States
$T_{[n(r)]}$	Kinetic Energy
$V_{xc[n(r)]}$	Non-classical Exchange-correlation Energy
$\nu_{xc}(r)$	Exchange Correlation Potential
Z	Atomic Number
χ	(R)ISC Possibility
ΔE_{ST}	Singlet-Triplet Energy Gap
Γ	Detachment Density Matrix
Λ	Attachment Density Matrix
μ	Magnetic Moment
ω_p	TDA Excitation Energy
Φ_s	Quantitative Topological Descriptor
Π	Bridge
Ψ	Wavefunction
θ	Dihedral Angle
φ_j	Number of Atomic Orbitals
X_p	Amplitude Vector

LIST OF ACRONYMS/ABBREVIATIONS

A	Acceptor
B3LYP	Becke-3-parameter Lee-Yang-Parr Functional
BLYP	Becke-Lee-Yang-Parr Functional
BSE	Bethe-Salpeter Equation
CT	Charge Transfer
Cz	Carbazole
C-PCM	Conductor-like Polarizable Continuum Model
D	Donor
DBSO	Dibenzothiophene Sulfone
DFT	Density Functional Theory
DMAC	Dimethylacridine
DPA	Diphenylamine
DPS	Diphenylsulfone
D-PCM	Dielectric Polarizable Continuum Model
EIL	Electron Injection Layer
EML	Emission Layer
EQE	External Quantum Efficiency
ETL	Electron Transporting Layer
GGA	General Gradient Approximation
GTO	Gaussian Type Orbitals
HIL	Hole Injection Layer
HOMO	Highest Occupied Molecular Orbital
HTL	Hole Transporting Layer
ICT	Intramolecular Charge Transfer
IEF-PCM	Integral Equation Formalism Polarizable Continuum Model
IQE	Internal Quantum Efficiency
ISC	Intersystem Crossing
LCAO	Linear Combination of Atomic Orbitals

LDA	Local Density Approximation
LE	Local Excited
LUMO	Lowest Unoccupied Molecular Orbital
M062X	Hybrid Meta Exchange-Correlation Functional
NTO	Natural Transition Orbital
OLEDs	Organic Light-Emitting Diodes
PBE0	Perdew–Burke-Ernzerhof Hybrid Functional
PCM	Polarizable Continuum Model
PhOLEDs	Phosphorescent OLEDs
PTZ	Phenothiazine
PXZ	Phenoxazine
RISC	Reverse Intersytem Crossing
SOC	Spin-Orbit Coupling
STO	Slater Type Orbitals
TADF	Thermally Activated Delayed Fluorescence
TDA	Tamm-Dancoff Approximation
TD-DFT	Time-Dependent Density Functional Theory

1. INTRODUCTION

Electroluminescence of organic compounds was one of the research fields that takes great attention for ideal lighting sources. The process of electroluminescence can be described as generating light by application of an electric field. Organic Light-Emitting Diodes (OLEDs) which has a working principle based on electroluminescence is reported by Tang et al. in 1987 [1]. Besides lighting, OLEDs have come to the forefront of display applications because of their properties such as providing improved image quality, high brightness, low fabrication costs, low power consumption and high durability [2, 3]. The five functional layers which are hole injection layer (HIL), hole transporting layer (HTL), emission layer (EML), electron transporting layer (ETL) and electron injection layer (EIL) located between two electrodes constitute the structure of OLEDs as seen in Figure 1.1 [4]. When electrical voltage is applied to electrodes, the holes which are injected from anode and electrons which are injected from cathode meet and recombine at emissive layer. After recombination, emitters release their excess energy as photons [5].

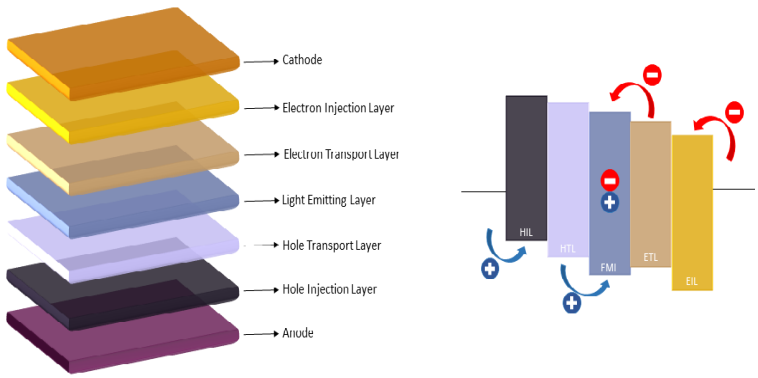

Figure 1.1. Device structure and working principle of OLEDs.

Efficiency of an OLED device can be described by external quantum efficiency (EQE) and internal quantum efficiency (IQE) values. EQE is described as the ratio of the photons escaped from the OLED device over the number of electrons injected while IQE is the ratio of the photons emitted over the number of electrons injected [6]. To increase the efficiency, OLEDs are based on different processes and divided into three

generations. Fluorescent materials are used as emitters at first generation OLEDs. Due to spin-statistics, 25% of the excitons formed by the recombination of electrons and holes go to singlet excited state while 75% of the excitons are located at triplet excited state [7, 8]. The first generation OLEDs suffer from an intrinsically low 25% IQE and 5% EQE because the singlet state is the only emissive state and 75% of the excitons cannot be harvested [7, 8]. Then, two new mechanisms have been proposed to overcome this limitation by triplet harvesting. Phosphorescent OLEDs (PhOLEDs) which are known as second generation OLEDs use phosphorescent materials as emitters that harvest both singlet and triplet excitons by intersystem crossing (ISC) which led to 100% IQE and 20-30% EQE as shown in Figure 1.2 [9]. ISC is the transfer of excitons from singlet excited states to the triplet excited states. Heavy atoms (Pt, Ir) that are used in phosphorescent materials cause high spin-orbit coupling (SOC) that accelerates the ISC. However, these atoms are not environmentally friendly, and besides, the rarity of these atoms increases the production cost [10–16].

Thermally activated delayed fluorescence (TADF) mechanism which is utilized in third generation OLEDs offers us a low cost channel to overcome the limitations of the first two generations. Thermally activated delayed fluorescence (E-type delayed fluorescence) is an intramolecular mechanism and up conversion process is the reason for delayed fluorescence [17].

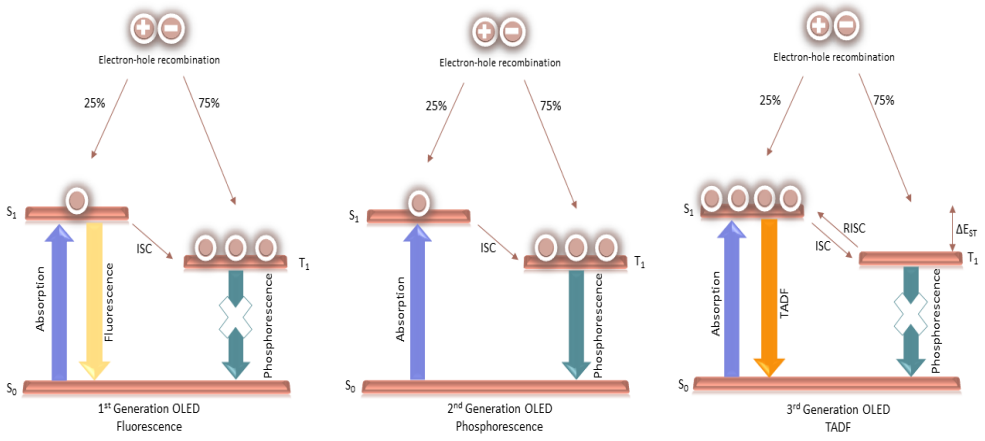

Figure 1.2. Schematic representation of three generations of OLEDs.

The first organic TADF emitter was reported by Adachi [18]. TADF mechanism is not completely understood [19, 20]. Triplet excitons are harvested by reverse intersystem crossing (RISC) in TADF mechanism, thus, 100% IQE with 30% EQE is achieved. RISC can be described as the up-conversion process of electrons from the lowest triplet excited state (T_1) to the lowest singlet excited state (S_1) and it is known that SOC and thermal energy are required for RISC. Studies show that room temperature is enough for RISC [21]. A small ΔE_{ST} that describes the energy difference between S_1 and T_1 states is required for efficient TADF mechanism. ΔE_{ST} is important, but not sufficient, to observe efficient TADF process [22–25]. A relatively large rate constant of reverse intersystem crossing (k_{RISC}) and small overlap between highest occupied molecular orbital (HOMO) and lowest unoccupied molecular orbital (LUMO) are other primary factors for generating efficient TADF mechanism. k_{RISC} can be expressed by the following equation:

$$k_{RISC}\,\alpha\,exp(-\frac{\Delta E_{ST}}{k_B T}). \tag{1.1}$$

Relationship between ΔE_{ST} and k_{RISC} can be seen from Equation (1.1). ΔE_{ST} can be defined by the following equations:

$$\Delta E_{ST} = 2J \tag{1.2}$$

$$E_S = E + K + J \tag{1.3}$$

$$E_T = E + K - J \tag{1.4}$$

$$J = \int \varphi_1 \varphi_2^* \frac{1}{r_{12}} \varphi_2 \varphi_1^* dr \tag{1.5}$$

where E represents the orbital energy, K represents the electron repulsion energy. Electron arrangement at singlet and triplet states is the same for the same molecule and this results in the same E and K values in singlet and triplet states. J represents the degree of stabilization and destabilization [9]. The overlap integral of frontier molecular orbitals (HOMO and LUMO) determines the value of J. Small overlap between HOMO and LUMO resulted in small J value and this situation provides small ΔE_{ST} which is one of the requirements of efficient TADF process [9]. This can be achieved by

a molecule that has an excited state with a strong charge transfer character resulted from the presence of electron donor and electron acceptor units.

There are two ways to excite a TADF molecule. The molecule can be excited to local excited state ^{1}LE (locally excited) which can radiatively decay to the ground state (S_0) or transfer an electron to ^{1}CT (charge transfer) state [23, 26]. On the other hand, the molecule can be excited directly to the ^{1}CT state [23, 27]. Both ^{1}CT and ^{1}LE states can decay radiatively but ^{1}LE contribution at emission spectra vanishes while ^{1}CT emission continues because of the repopulation of ^{1}CT state by RISC [23]. For that reason, only one singlet state (S_1) is considered. The TADF mechanism shows four state model which is the second order coupling of ^{1}CT, ^{3}LE, ^{3}CT [23, 28–31]. ^{1}CT state can either decay radiatively forming prompt fluorescence which has a fast radiative transition from an excited singlet state to a ground singlet state with approximately in nanoseconds or it can undergo ISC and populate ^{3}LE state as shown in Figure 1.3. ^{3}CT and ^{3}LE states are mixed by non-adiabatic coupling and thermal energy. However, studies show that the equilibrium between ^{3}CT and ^{3}LE is weakly temperature dependent and small ΔE_{ST} and vibronic coupling are enough for populating ^{3}CT even at 0 K. To sum up, there is only one mixed triplet state as the lowest excited triplet state (T_1) [23, 29, 32].

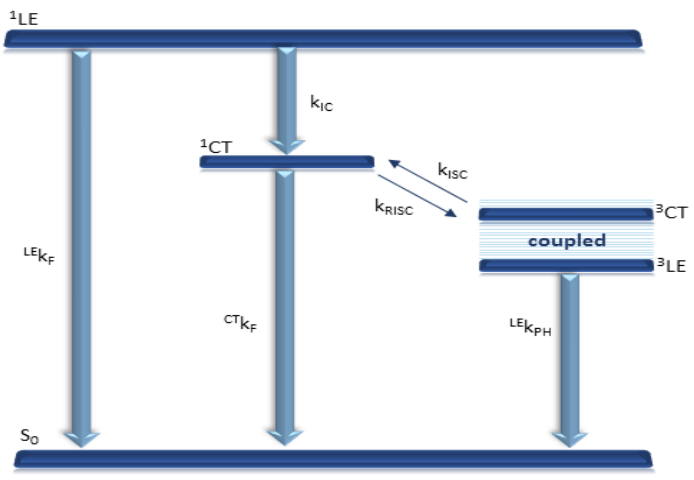

Figure 1.3. Representation of TADF mechanism.

Up to date, many studies have been conducted to get the answer of how to design an efficient TADF molecule which is constructed by acceptor and donor units and some design techniques are reported. There are some structure types of TADF molecules such as donor (D) – acceptor (A), D–π–A, D–A–D and D–π–A–π–D. Donors that are used in the construction of TADF molecules are diphenylamine [2,33–35], carbazole [36–44], acridine [45, 46], phenothiazine [47], phenoxazine [48–51], 5,10-dihydrophenazine [52] and thianthrene [53] derivatives. The commonly used acceptor moieties are sulfone [33, 47, 54–59], boron [60] and benzophenone [45] derivatives. The structures of donor and acceptor moieties are shown in Figure 1.4. Selection of these donor and acceptor moieties plays a critical role in the performance of devices. In addition, the selection of building units provides a way for tuning emission color.

In this study, molecules under investigation are sulfone group containing organic compounds in which the sulfur atom is bonded to two carbon atoms and two oxygens in a tetrahedral arrangement. Sulfone has become attractive part of the TADF emitters due to its outstanding electron accepting and transporting ability [61]. Sulfone containing molecules exhibit S_1 and T_1 states which have large CT excitation characteristics that help to reduce the ΔE_{ST} and enhance the RISC [58]. However, sulfone based TADF emitters can show instability which limits their applications in OLEDs because of the low bond dissociation energy of C-S bonds. For that reason, both high efficiency and long-term stability should be considered for designing sulfone based emitters [62]. In comparison with traditional sulfone counterparts, the effective conservation of relatively weak C-S bonds by rigid cyclic systems can enhance their chemical and electrochemical stability [63].

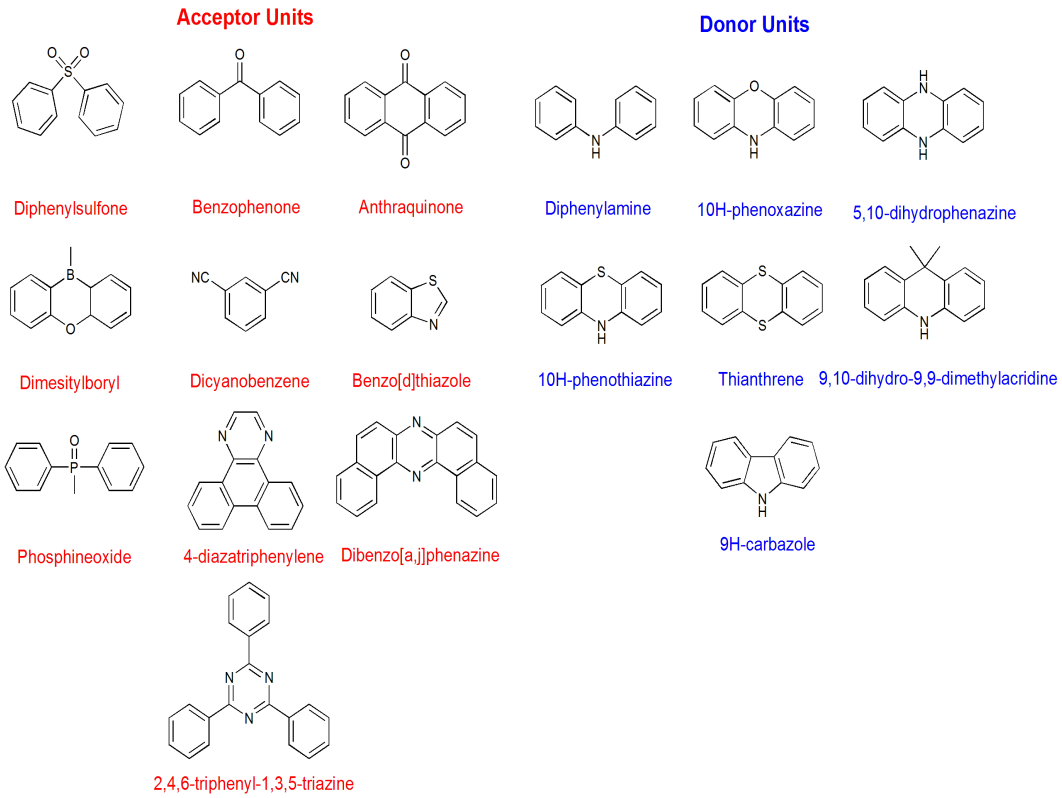

Figure 1.4. Chemical structures of acceptor and donor units.

The studied compounds have different type of sulfone-based acceptor units. One of the building block as acceptor unit which is the diphenylsulfone (DPS) has come to the forefront especially in TADF based OLEDs thanks to the strong electron affinity, good thermal stability, and unique steric effect of sulfone and two phenyl ring [64]. DPS has outstanding electron withdrawing property due to a twist angle in the middle and it is the third most widely used acceptor for the design of blue TADF emitter because of its low LUMO energy level and obvious twist configuration [65–68]. The sulfone derivatives are generated to increase the electron accepting strength. The stronger electron withdrawing property of sulfone groups is resulted in the lower LUMO energy level [63]. The narrow emission spectrum can be generated by increasing rigidity of acceptor unit [69]. The DMTDAC emitter contains rigid acceptor unit called as DMTD and exhibits narrow emission band because the interlocking of the two phenyl units which are linked to the sulfone unit prevents molecular motion of the acceptor unit [62,70,71]. TADF molecule DMAC-TTR contains additional sulfone unit as acceptor. The addition of another sulfone unit as acceptor improves the charge separation and this resulted in a stronger intramolecular charge transfer (ICT) characteristic [72].

The two phenyl rings could be fused to construct a five-membered ring system which is called dibenzothiophene sulfone (DBSO) and DBSO is used to prepare green TADF emitter such as DTC-DBT [24, 62, 73, 74]. High efficiency blue TADF emitter Ac-OSO which contains angular linked phenoxathiin dioxide as acceptor unit is reported with 20.5% EQE [63]. A C=O bridge was introduced in another study with cyclic biarylsulfones to form thioxanthones, constructing emitters which are called as TXO-TPA and TXO-PhCz with 18.5% and 21.5% EQE [73, 75].

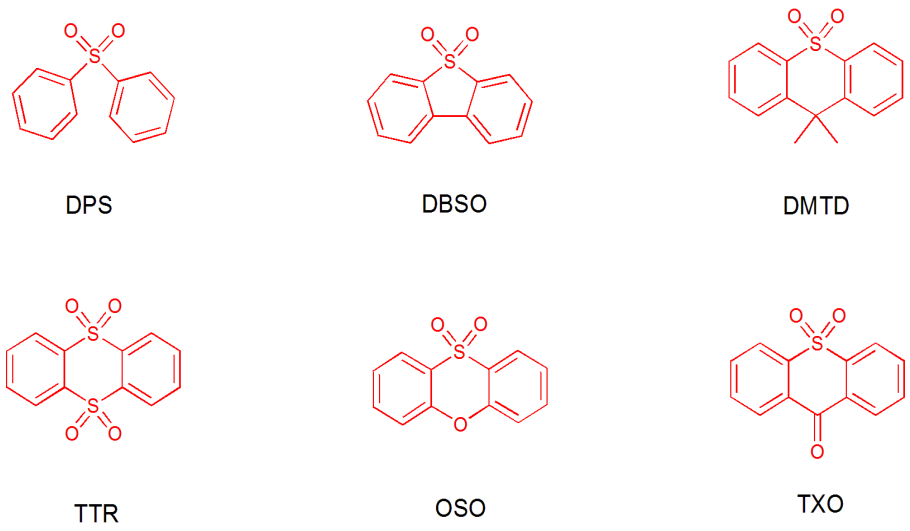

Figure 1.5. Chemical structures of acceptor moieties studied in this work.

Molecules under investigation are divided into six groups. Group 1 contains compounds named 1 [47], 2 [47], 3 [47], 4 [47] and 5. Compounds have carbazole (Cz), dimethylacridine (DMAC), phenoxazine (PXZ), phenothiazine (PTZ) and diphenylamine (DPA) as donor units and DPS as an acceptor unit. Donor units are located to the acceptor unit at the meta position. All of the compounds have D-A-D type structure. Compound 5 does not have experimental data.

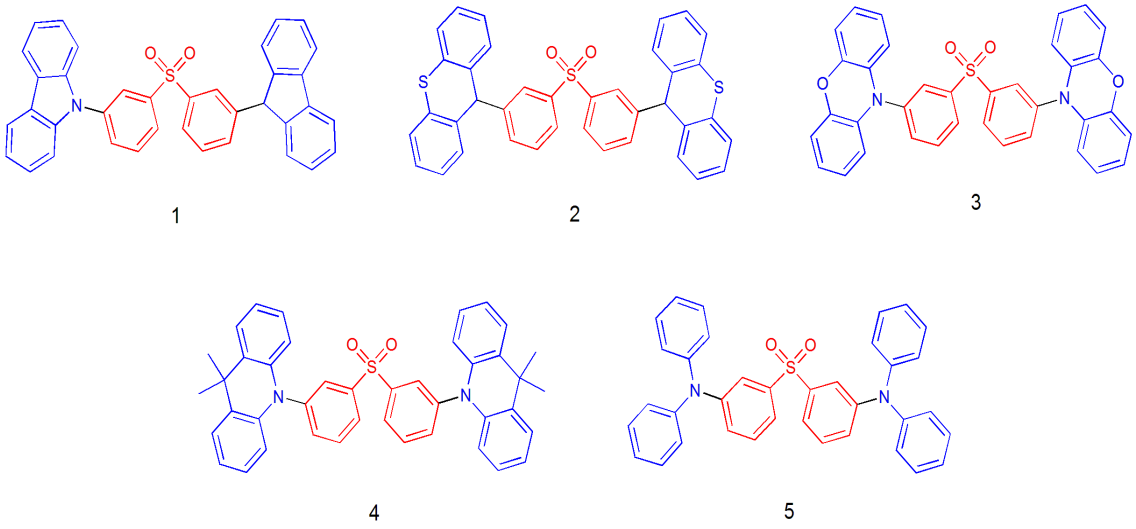

Figure 1.6. TADF emitters which have been included in Group 1 [47].

SF2C [56, 57, 59], PTSOPT [55, 56, 58, 59, 76], PXZ-DPS [54, 58, 75, 77], DMAC-DPS [54, 75, 77] and DPA-DPS [33, 75, 78] construct Group 2. These compounds have the same structure type and donor-acceptor unit as Group 1 compounds. However, donor units are located to the acceptor unit at the para position.

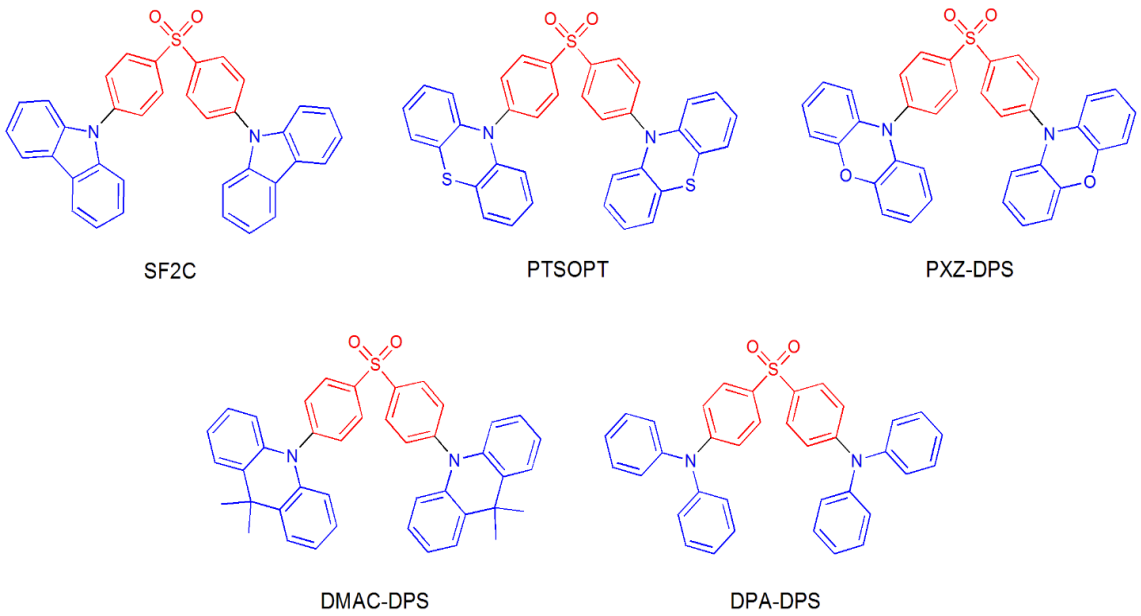

Figure 1.7. TADF emitters which have been included in Group 2 [33,54,55,59].

Group 3 consists of rigid acceptor and donor units with D-A-D and D-A types. PXZ and DMAC are used as donor units while DBSO and DMTD are used as acceptor units. 1a [20, 79], 4ASOA [80, 81], DPO-TXO2 [82] and DDMA-TXO2 [71, 82, 83] have D-A-D type structures. PXZ-DBTO2 [22] has D-A type structure.

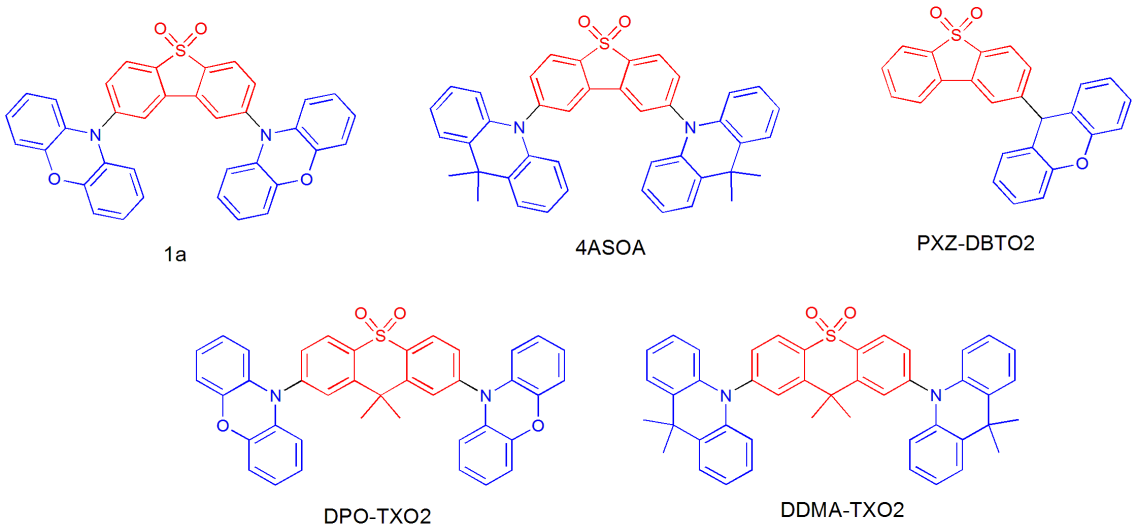

Figure 1.8. TADF emitters which have been included in Group 3 [20,22,81-83].

Group 4 contains compounds Cz-TTR [36], DMAC-TTR [84, 85], PXZ-TTR [85] and PTZ-TTR [84] with D-A type structure. These compounds have TTR as an acceptor unit and Cz, DMAC, PXZ and PTZ are used as donor units. PXZ-TTR has just theoretical data in the literature.

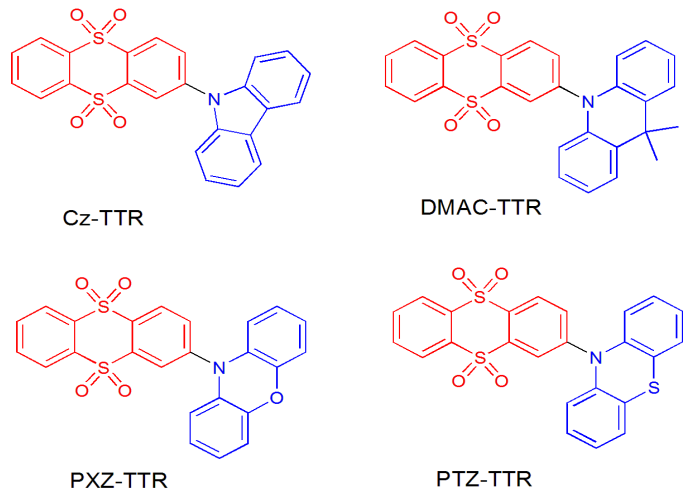

Figure 1.9. TADF emitters which have been included in Group 4 [36,84,85].

Group 5 contains CzPhDSO2 [86], ACRDSO2 [84, 87], PXZDSO2 [87] and PTZ-Ph-TTR [84]. These compounds have D-B-A structure type which is the bridge form of Group 4 compounds. TTR is used as an acceptor unit while Cz, DMAC, PXZ and PTZ are used as donor units.

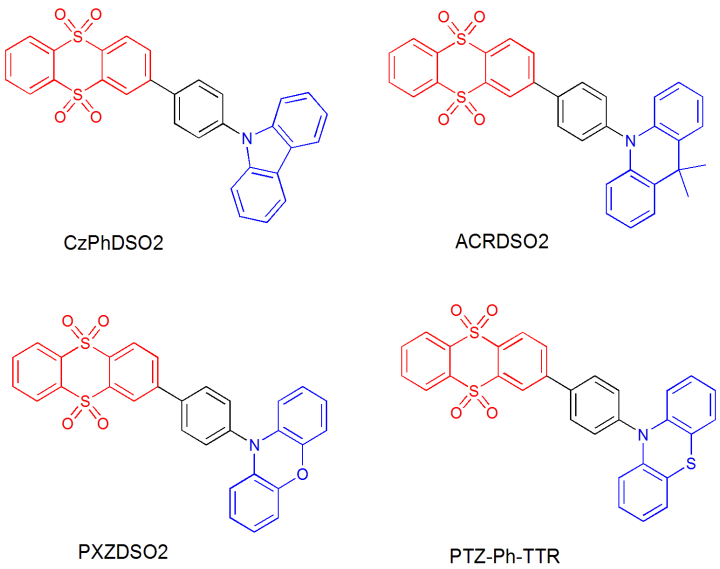

Figure 1.10. TADF emitters which have been included in Group 5 [84,86,87].

Group 6 is the smallest group that contains 3 TADF emitters. Ac-OSO [63, 88], CzSOXO [89, 90] and TXO-PhCz [75, 91] have D-A type structures. Ac-OSO consists of DMAC donor unit and OSO as an acceptor unit. CzSOXO and TXO-PhCz have TXO as an acceptor unit and Cz as donor unit. However, TXO-PhCz has Cz unit that is located to the acceptor unit at different position and has additional phenyl unit.

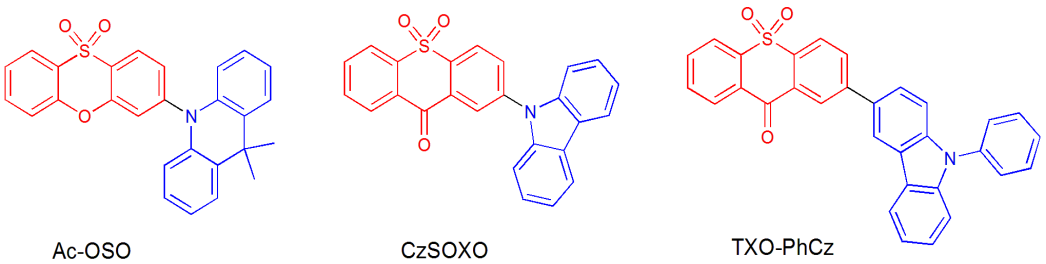

Figure 1.11. TADF emitters which have been included in Group 6 [63,75,90].

Computational studies provide information to make more clear way for designing efficient TADF molecules. In this study, DFT calculations are used to get a clear design strategy for sulfone-based TADF emitters. To provide rationale, different sulfone-based TADF emitters are modeled and comprehensive conformer search is done. The absorption and emission spectra are generated and compared with experimental spectra. The descriptors such as dihedral angle, ΔE_{ST}, SOC constants and Φ_s indices are investigated with different donor and sulfone based acceptor units. In addition, the χ term which represents the effect of ΔE_{ST} and SOC constant on (R)ISC process is examined. The χ term can be expressed as

$$\chi \, \alpha \, \frac{H_{SO}}{\Delta E_{ST}}. \tag{1.6}$$

As seen in Equation (1.6), small ΔE_{ST} and high H_{SO} are required for effective TADF mechanism mathematically. χ term is used to get effective functional for calculations.

1.1. Aim of the study

Computational studies provide information to make more clear way for designing efficient TADF molecules. Sulfone becomes attractive part as an acceptor unit in TADF emitters due to its outstanding electron accepting ability. Molecules under investigation contain different sulfone groups as acceptor units and donor units that are found at studied compounds are Cz, DMAC, PXZ, PTZ and DPA. In addition, investigated TADF emitters have different structural types such as D-A-D, D-A, D-π-A and different substitution position. To provide rationale, the relationship between structure of compounds and TADF activity is examined. Descriptor analysis is done to describe the TADF activity. In theoretical calculations, the reliability of methods used for calculations needs to be benchmarked toward efficient design of TADF emitter. Dihedral angle, nature of states, ΔE_{ST}, SOC and Φ_S indices are the analyzed descriptors and three different functionals are B3LYP, PBE0 and M062X are used at descriptor analysis. According to obtained results, M062X is the most reliable functional among all of the used functionals. The results of descriptor analysis are in good correlation between each other. Besides descriptors, absorption spectra and emission spectra are

reproduced and compared with experimental spectra. However, the generated emission spectra are not correlated with experimental spectra. In conclusion, the important strategies for efficient structural design of TADF emitters are obtained and the best functional to observe TADF activity is provided by comparing experimental and theoretical results. This study can be used as a reference study for both experimental and theoretical studies about sulfone-based TADF emitters.

2. METHODOLOGY

2.1. Density Functional Theory

The Schrödinger's equation is important for quantum mechanics [92]. It is called the most comprehensive description of any system and wavefunction is obtained by solution of the Schrödinger's equation. Equations can be expressed as

$$i\hbar\frac{\partial}{\partial t}\Psi(r,t) = \widehat{H}\Psi(r,t) = -\frac{\hbar^2}{2m}\nabla^2\Psi(r,t) + V(r)\Psi(r,t) \tag{2.1}$$

$$E\psi(r) = -\frac{\hbar^2}{2m}\nabla^2\psi(r) + V(r)\psi(r). \tag{2.2}$$

Equation (2.1) is the time-dependent Schrödinger's equation while Equation (2.2) is the time-independent Schrödinger's equation. $\Psi(r,t)$ is the wavefunction, r is the position in three-dimensional space, $\widehat{H}$ is the Hamiltonian operator, m is the mass and V(r) is the potential at point r. The Schrödinger's equation can be solved for small systems such as hydrogen atom but how about the larger systems? The equation is many-body problem and the solution of equation for large systems is complicated. Different approximations are built to solve this complication.

Density Functional Theory (DFT) introduces electron density to solve many-body problem. DFT was first reported by Hohenberg-Kohn and Kohn-Sham in 1960s [93,94]. The Hohenberg-Kohn theorem consists of the uniqueness and variational theorems. According to the first theorem, the unique functional of ground state electron density $n_0(r)$ gives the ground state energy from Schrödinger's equation. Uniqueness theorem proves the existence of functional but does not obtain that functional. Variational theory proves an important property of that functional. Variational theory states that the full solution of Schrödinger's equation (ground state energy) can be obtained by minimizing the energy in terms of electron density n(r). The energy can be expressed by summation of kinetic energy, electrostatic energy and the energy of non-interacting

electron moving under external potential as

$$E_{[n(r)]} = T_{[n(r)]} + U_{[n(r)]} + \int V(\vec{r})n(\vec{r})d^3r. \tag{2.3}$$

By using universal functional of the electron density n(r) the first two terms can be written as

$$T = \int \frac{3}{10}[3\pi^2 n(r)]^{\frac{2}{3}} n(r)dr \tag{2.4}$$

$$U = \frac{1}{2}\int \frac{n(r')}{\mid r - r' \mid} dr'dr. \tag{2.5}$$

The Hohenberg-Kohn theory found a way for calculating energy in terms of electron density. However, the method is not accurate because the presentation of kinetic energy T is not adequate.

According to Kohn-Sham theory, finding the true ground state electron density resulted in finding the lowest energy of the system and the ground state of the system. In addition, ground state density can be found by theorem. Kohn-Sham states the ground state energy as a functional of the charge density:

$$E_{[n(r)]} = T_{[n(r)]} + E_{ext[n(r)]} + \frac{1}{2}\int \frac{n(r)n(r')}{\mid r - r' \mid} + \nu_{xc[n(r)]}. \tag{2.6}$$

Terms represent the kinetic energy, interaction between electron and the external potential, electron-electron electrostatic interaction and the non-classical exchange-correlation energy. Then, Kohn and Sham reintroduced the single particle wavefunctions as

$$n(r) = \sum_{i=1}^{n} \psi_i^*(r)\psi_i(r). \tag{2.7}$$

Representation of kinetic energy in terms of wavefunctions:

$$T[n(r)] = -\frac{\hbar^2}{2m}\sum_{i=1}^{n}\langle\psi_i \mid \nabla^2 \mid \psi_i\rangle. \tag{2.8}$$

Schrödinger's equation of non-interacting particles moving in an effective potential ν_{eff}(r):

$$-\frac{\hbar^2}{2m}\nabla^2\psi_i(r) + \nu_{eff}(r)\psi_i(r) = \varepsilon_i\psi_i(r). \tag{2.9}$$

ν_{eff}(r) can be written as

$$\nu_{eff}(r) = \nu_{ext}(r) + \nu_{xc}(r) + \frac{1}{2}\int\frac{n(r')}{\mid r - r' \mid}dr'. \tag{2.10}$$

The exchange-correlation potential is expressed as

$$\nu_{xc}(r) = \frac{\delta E_{xc[n(r)]}}{\delta n(r)}. \tag{2.11}$$

Finally, equation of energy can be expressed as

$$E_{[n]} = \sum_{i=1}^{n}\varepsilon_i - \frac{1}{2}\int\frac{n(r')}{\mid r - r' \mid} + E_{xc[n(r)]} - \int\frac{\delta E_{xc[n(r)]}}{\delta n(r)}n(r)dr. \tag{2.12}$$

The term ε_i is an exact term. The exchange-correlation functional, E_{XC}, creates problem for solution of equation because the term is not known. The problem of exchange-correlation functional will be discussed at following section.

2.2. Functionals

As mentioned above, the exchange-correlation term is not known and approximation functionals are proposed for exchange-correlation term. The development of these functionals is based on simplicity and accuracy. Exchange-correlation functionals can be divided into three categories that are the local density approximation (LDA),

general gradient approximations (GGA) and hybrid functionals.

LDA is the reasonable first and simplest approximation for exchange-correlation functionals [95]. The idea behind LDA is based on uniform electron gas of the same local density as

$$E_{ex(n)} = \int e_{xc}(n(r))n(r)dr. \tag{2.13}$$

e_{xc}(n) refers to the exchange-correlation energy of a uniform electron gas that has density n. The opening versions of e_x(n) and e_c(n) are shown as

$$e_x(n) = -\frac{0.458}{r_s} \tag{2.14}$$

$$e_c(n) = -\frac{0.44}{r_s + 7.8}. \tag{2.15}$$

r_s means radius of sphere containing one electron. Distribution of electron density in a system is not homogenous in real and this creates some drawbacks for LDA such as overestimating exchange-correlation energy and insufficient calculations that have dominant electron-electron interaction effect.

The addition of gradient expansion term to the LDA functional resulted in the GGA functional as

$$E_{ex}(n) = \int e_{xc}(n(r), \mid \partial n(r) \mid)n(r)dr. \tag{2.16}$$

BLYP, PBE and PW91 are examples of GGA functionals [96]. A.D. Becke has contributions to some of the first GGA exchange functionals that have abbreviations as “B” while C. Lee, W. Yang and R. G. Parr have contributions to the correlation functional that has abbreviations as “LYP”.

Hybrid method is the mixture of Hartree-Fock theory that ignores electron correlation energy and exchange-correlation from other sources. The rationale of hybrid

functional was first proposed by Axel Becke in 1993. B3LYP is the famous hybrid functional and can be expressed as

$$E_{xc}^{B3LYP} = E_{xc}^{LDA} + \alpha_0(E_x^{KS} - E_x^{LDA}) + \alpha_x(E_x^{GGA} - E_x^{LDA}) + \alpha_c(E_c^{GGA} - E_c^{LDA}). \quad (2.17)$$

The values of α_0, α_x and α_c are obtained by fitting the expected values to a set of experimental data [97]. M062X is one of the most used Minnesota functional that depends on meta-GGA approximation [98]. Hybrid-exchange correlation for M062X can be expressed as

$$E_{XC}^{hyb} = \frac{X}{100}E_X^{HF} + \left(1 - \frac{X}{100}\right)E_X^{DFT} + E_C^{DFT}. \quad (2.18)$$

The errors of atomization energies that resulted from LDA functional are decreased by GGA and hybrid functional. Hybride functionals can handle with some problems that cannot be solved by LDA and GGA functionals such as highly localized f electrons in transition metals.

2.3. Basis Sets

Atomic orbitals are described by basis sets functionals and molecular orbitals are constructed by linear combination of basis sets functionals. Wave functions for electronic states are built by molecular orbitals [99]. The linear combination of atomic orbitals (LCAO) can be expressed as

$$\psi_i = \sum_j c_{ij}\varphi_j \quad (2.19)$$

where i refers to number of molecular orbitals, φ_j is the number of atomic orbitals and c_{ij} is the coefficient. Constant coefficients can be provided by applying variational method.

The main classes of basis sets contain Slater Type Orbitals (STO) and Gaus-

sian Type Orbitals (GTO). The electron density around the nucleus can be explained and more accurate solutions to Schrödinger's equation of hydrogen-like atoms can be obtained by STOs. On the other hand, electron-state correlations are not explained precisely via STOs because of the absence of many-electron interactions in hydrogen-like atoms. In addition, there is computational difficulty for calculation of integral with STOs. This difficulty resulted in development of GTOs by S. Francis Boys. It is known that STOs are the linear combination of GTOs [100].

The electrons will be restricted to a particular region of space by basis set. The larger basis set resulted in fewer constraints on electrons and thus more precise approximations of real molecular orbitals or electron density are obtained. The core functions are represented by the first number at basis set while valence functions are represented by number after dash. Diffuse and polarization functions can also be added to increase the accuracy of calculation. There is proportional relationship between accuracy and computational cost. Flexibility is applied to the orbital for better representation of electron density in bonding regions by polarization functions. The diffuse functions are used for increasing electronic radius at places that can have electrons.

The basis set 6-311+G(d,p) in Pople notation denotes a split-valence triple zeta basis set with 6 d-type basis functions for heavy atoms, 3 p-type basis functions for H atoms, and the "+" denoting the addition of diffuse function for heavy atoms while "(++)" refers to addition of diffuse functions for hydrogen. Polarization function can be represented as (d) or * for heavy atoms while (d,p) or ** represent the applying polarization function for hydrogen atoms.

2.4. Polarizable Continuum Model

To get more realistic calculations, solvent environment is important. Solvent can be applied to the calculations explicitly and implicitly. Each of the solvent molecule is treated individually at explicit solvation models and this resulted in high computational cost. For that reason, the usage of implicit, continuum, solvation model becomes desirable [101]. Solvent is treated as a continuous medium covering the solute. The overall

solvation process of continuum solvation model consists of several physical effects and total solvation free energy can be described as

$$\Delta G_{solvation} = \Delta G_{cavity} + \Delta G_{dispersion} + \Delta G_{electrostatic} + \Delta G_{repulsion}. \quad (2.20)$$

The terms in Equation (2.20) represent addition of solute to the system, interaction between solvent and solute, electrostatic interaction energy between solvent and solute and exchange solute-solvent interactions.

The Polarizable Continuum Model (PCM) was first reported by Tomasi et al [102]. Solute cavity that is constructed by covering spheres around the atoms of the solute molecule is used at PCM. The radii of these spheres are determined by the van der Waals radius of the atoms multiplied by a predefined factor. To simulate solvation effects, the solute cavity is overlapped by a continuous dielectric medium. The reaction field is expressed by the point charges on the cavity surface. There are several methods to apply PCM. Dielectric PCM (D-PCM), Conductor-like PCM (C-PCM), and Integral Equation Formalism PCM (IEF-PCM) can be given as example for these methods [103]. The medium is constructed as a conductor instead of dielectric at C-PCM [104]. The IEF-PCM model is used as solvation model in this thesis.

2.5. Time-Dependent Density Functional Theory (TD-DFT)

DFT has inherent limitations, while being a fairly successful theory. The static ground-state density and static DFT are insufficient to explain the dynamics and excitation of a system in reaction to a time-dependent external perturbation. Time-dependent density-functional theory (TD-DFT) is a variation of DFT that deals with excited-state characteristics, dynamics, and spectroscopy. TD-DFT was established by Runge and Gross, who extended the Hohenberg-Kohn theorem to time-dependent densities and potentials. The primary idea of TD-DFT is to represent systems using

the many-body Schrodinger equation as

$$i\frac{\partial}{\partial t}\psi(\{r\},t) = \widehat{H}(\{r\},t)\Psi(\{r\},t). \tag{2.21}$$

The Hamiltonian operator is denoted by $\widehat{H}$, while the coordinates of N electrons are denoted by r. The Hamiltonian operator can be expressed as

$$\widehat{H}(\{r\},t) = \hat{T}(\{r\},t) + \widehat{W}(\{r\},t) + \hat{V}_{ext}(\{r\},t). \tag{2.22}$$

The first term which is the kinetic energy function $\hat{T}(\{r\},t)$ can be described as

$$\hat{T}(\{r\}) = -\frac{1}{2}\sum_{i=1}^{N}\nabla i^2. \tag{2.23}$$

The electron-electron repulsion term and the external potential term can be written as

$$\widehat{W}(\{r\},t) = -\frac{1}{2}\sum_{i,j=1\, i\neq j}^{N}\frac{1}{\mid r_i - r_j \mid} \tag{2.24}$$

$$\hat{V}_{ext}(\{r\},t) = \sum_{i=1}^{N}\upsilon_{ext}(r_i,t). \tag{2.25}$$

The Coulomb interaction of electrons with a group of nuclei is also described as

$$\upsilon_{ext}(r,t) = -\sum_{\upsilon=1}^{N_n}\frac{Z_\upsilon}{\mid r - R_\upsilon(t) \mid}. \tag{2.26}$$

The charge and location of the nucleus are represented by Z_υ and R_υ, respectively, where υ and N_n denote the total number of nuclei in the system.

The chance of detecting one electron at r_1 and another at r_2 at a given time t is the absolute square of the wave function $\psi\ (\{r\},t)$ and can be expressed as

$$p(r,t) = N\int d^3r_2...d^3r_N \mid \Psi(r,r_2...r_N,t) \mid^2 . \tag{2.27}$$

When comparison is done between DFT and TD-DFT, both show a direct relationship between density and external potentials. In both cases, density is the most critical factor. The density in DFT is only determined by the space coordinate, but the density in TDDFT is determined by both the time and space coordinates. The potentials have the same distinction. The static Schrodinger equation that is used in DFT is a second order differential equation in spatial coordinate, so it's possible to express it as an eigenvalue problem. On the other hand, a first order differential equation in the time coordinate constitutes the time-dependent Schrodinger equation in TD-DFT.

2.6. Tamm-Dancoff Approximation (TDA)

The failure of TD-DFT, the extended version of DFT, in certain areas, such as precisely anticipating charge-transfer state excitation energies and providing the exact long-range 1/R dependence on donor-acceptor distance, is linked to triplet instability problems [105–107]. Problems resulting from triplet instabilities are solved and computationally more workable response equations are provided by introducing Tamm–Dancoff approximation (TDA) to TD-DFT for calculation of triplet excitation energy [108]. As a result of solving triplet instability problems, more accurate results are obtained. TDA considers only positive energy electron-hole pairs and the interaction between positive and negative charge electron-hole pairs are ignored. As a consequence, one electron-hole pair is supposed to raises at any time interval.

To determine linear optical characteristics and express polarization functions, the Bethe-Salpeter equation (BSE) is used. However, the system that has large amount of electron-hole pair resulted in complex non-Hermitian BS that is hard to solve [109]. The solvable Hermitian BS is obtained from reducing non-Hermitian BS by applying TDA [110]. The reduced equation can be expressed as

$$\tilde{M}X_p = \omega_p X_p. \tag{2.28}$$

X_p represents amplitude vector while ω_p represents the excitation energy term and ω_p

can be expressed as

$$\omega_p = \sum_{ai}(\epsilon_a - \epsilon_i)X_{ai}^2 + \sum_{abij}\left[\left\langle ib \,\|\, aj\right\rangle + B_{a_i,b_j}\right]X_{ai}X_{bj}. \tag{2.29}$$

The total energy for the excited state of p when the effects of the solvent are considered as

$$G_p^{TDA} = G_{gs}^{HF} + \omega_p. \tag{2.30}$$

The first term represents the ground state energy while second term represents the TDA excitation energy.

2.7. Wigner Distribution

Quantum mechanics contains operators and wave functions (or,more generally, density operators) as opposed to classical physics. Distribution function was used to formulate quantum mechanics by Wigner in 1932 [111]. It allows quantum mechanics to be re-stated in terms of classical ideas, with quantum mechanical expectation values now being expressed as averages over phase-space distribution functions. In other words, statistical data from the density operator is converted to a quasi-classical (distribution) function. The Wigner distribution can be constructed using either coordinate-space or momentum-space wave functions. By using coordinate-space function, Wigner transform for a one-dimensional system can be stated as

$$W(x,p) = \frac{1}{2\pi}\int_{-\infty}^{\infty}\psi^*\Big(x+\frac{s}{2}\Big)\psi\Big(x-\frac{s}{2}\Big)e^{ips}ds \tag{2.31}$$

where ψ denotes the wavefunction, p represents momentum, and x indicates position. The term $\psi^*\Big(x+\frac{s}{2}\Big)$ can be rewritten as

$$\psi^*\Big(x+\frac{s}{2}\Big) = \Big\langle \psi \mid x+\frac{s}{2}\Big\rangle. \tag{2.32}$$

Equation (2.31) also has a term $\psi\Big(x-\frac{s}{2}\Big)$ that can be written as

$$\psi\Big(x-\frac{s}{2}\Big)=\Big\langle x-\frac{s}{2}\mid\psi\Big\rangle. \tag{2.33}$$

The third term e^{ips} in Equation (2.31) is multiplied by 1/2 in the following equation, and the third term becomes:

$$\frac{1}{2\pi}e^{ips}=\frac{1}{\sqrt{2\pi}}e^{ip(x+\frac{s}{2})}\frac{1}{\sqrt{2\pi}}e^{-ip(x-\frac{s}{2})}. \tag{2.34}$$

It is possible to rewrite Equation (2.34) in a different way:

$$\frac{1}{\sqrt{2\pi}}e^{ip(x+\frac{s}{2})}\frac{1}{\sqrt{2\pi}}e^{-ip(x-\frac{s}{2})}=\Big\langle x+\frac{s}{2}\mid p\Big\rangle\Big\langle x-\frac{s}{2}\mid\psi\Big\rangle ds. \tag{2.35}$$

Equation (2.31) is expanded using the expressions from Equation (2.32), (2.33), and (2.34), yielding the following equation:

$$W(x,p)=\int_{-\infty}^{\infty}\Big\langle\psi\mid x+\frac{s}{2}\Big\rangle\Big\langle x+\frac{s}{2}\mid p\Big\rangle\Big\langle p\mid x-\frac{s}{2}\Big\rangle\Big\langle x-\frac{s}{2}\mid\psi\Big\rangle ds. \tag{2.36}$$

The first term is the amplitude of a particle in the state ψ with the $\Big(x-\frac{s}{2}\Big)$ position while the amplitude of a particle with a location of $\Big(x-\frac{s}{2}\Big)$ and momentum p represent the second term. The amplitude of a particle with a location of $\Big(x+\frac{s}{2}\Big)$ and momentum p is the third term and the amplitude of a particle in the state ψ with the position of $\Big(x+\frac{s}{2}\Big)$ represents the last term. Integration over s can be used to create a superposition of potential trajectories, which finally leads to a quasi-probability distribution in phase space [112].

The Wigner function was first used in statistical mechanics, but more recently, it has been discovered to be beneficial in a variety of fields, including hydrodynamics, plasmas, quantum corrections for transport coefficients, collision theory, signal analysis and optical systems and devices [113]. However, the W function has restrictions, particularly for particles with spin and relativistic particles.

2.8. Φ_s Index

Evaluation of the charge-separation property of compounds is important to understand the charge transfer efficiency. A quantum mechanical descriptor, Φ_s, which is the measurement of the overlap between attachment and detachment densities is used to get rationale about charge transfer ability [114]. As mentioned before, Φ_s is related to the density matrices and density matrices related to ground state (P_0) and excited state (P_x) can be obtained from excited state calculations. The difference density matrix Δ is expressed as

$$\Delta = P_x - P_0 \Rightarrow \sum_{k=1}^{K} (\Delta S)_{kk} = 0. \tag{2.37}$$

If there is no electron exchange in the system, the entropy change ΔS is equal to zero. The eigenvalues of Δ in the diagonal matrix δ can be obtained via unitary similarity transformation:

$$\exists U | \delta = U^{\dagger} \Delta U;\ \delta_{ij} = 0 \ \forall\ i \neq j. \tag{2.38}$$

Two novel diagonal matrices that have positive and negative eigenvalues obtained from diagonalizing Δ are used to provide Detachment Γ and Attachment Λ density matrices. These density matrices can be explained in the space of K atomic orbitals as

$$\sum_{\mu=1}^{K} (\Gamma S)_{\mu\mu} = \sum_{\mu=1}^{K} (\Lambda S)_{\mu\mu}. \tag{2.39}$$

Then, detachment/attachment densities can be expressed in 3D space as

$$\varrho_{\tau}(\xi_1, \xi_2, \xi_3) = \sum_{\mu=1}^{K} \sum_{\upsilon=1}^{K} (\tau)_{\mu\upsilon} \varphi_{\mu}(\xi_1, \xi_2, \xi_3) \varphi_{\upsilon}(\xi_1, \xi_2, \xi_3) \tag{2.40}$$

$$\tau = \Gamma, \Lambda. \tag{2.41}$$

ξ_1, ξ_2, ξ_3 represent the three spatial coordinates. The detachment from the ground state and attachment in excited states are described by two aforementioned functions. The detached/attached charged can be expressed as

$$\vartheta_\tau = \int_R d\xi_1 \int_R d\xi_2 \int_R d\xi_3 \varrho_\tau(\xi_1, \xi_2, \xi_3) \equiv \int_{R^3} d^3\xi \varrho_\tau(\xi). \tag{2.42}$$

Finally, the measurement of overlap between attachment and detachment densities, Φ_s, can be written as

$$\Phi_s = \vartheta^{-1} \int_{R^3} d^3\xi \sqrt{\varrho\Gamma(\xi)\varrho\Lambda(\xi)}. \tag{2.43}$$

Φ_s indices that are reported in this thesis are based on Lowdin and Mulliken charge distributions. The equal separation of overlap population between two atoms of a bond in Mulliken analysis resulted in values that are far from reality in some cases. Atomic orbitals are transformed to an orthogonal basis set in Lowdin charge distribution and this resulted in advanced population analysis [115]. The values of Φ_s indices change from 0 to 1. Values close to 0 mean small overlap between densities and thus charge transfer (CT) character while values close to 1 represent high overlap between densities and locally excited (LE) character.

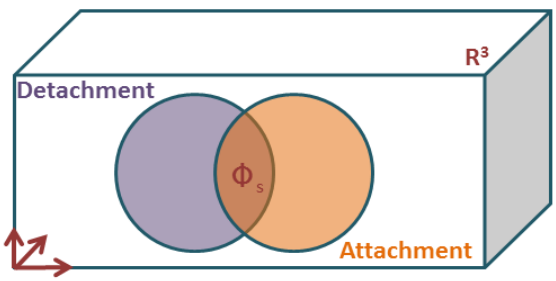

Figure 2.1. Descripton of the Φ_s index as the overlap between the attachment and detachment densities.

2.9. Spin-Orbit Coupling

Spin-orbit coupling (SOC) that is the interaction of the magnetic moment of an electron under the effective magnetic field was reported by Thomas [116]. The relativistic quantum electron theory was used to further explain the SOC by Dirac [117]. SOC that gives rise to change in the atomic energy levels of electron can be expressed as interaction between magnetic moments of nucleus and electron.

Summation of spin angular momentum and orbital angular momentum gives the total angular momentum $\vec{j}$ of electron as

$$\vec{j} = \vec{l} + \vec{s}. \tag{2.44}$$

The magnetic moment of an electron can be described as

$$\mu = -\frac{e}{2M}L \tag{2.45}$$

where M represents the electron's mass while L represents the electron's angular momentum. Equation (2.45) can be written with quantum case as

$$\hat{\mu}_z = -\frac{1}{2M}\hat{L}_Z. \tag{2.46}$$

The term $\hat{\mu}_z$ can be expressed in open form as

$$\hat{\mu}_z = -\frac{e\hbar}{2M}m_l \equiv -\mu_B m_l. \tag{2.47}$$

Bohn magneton term is described by μ_B term. Then, the Hamiltonian can be written as

$$\hat{H}_{SO} = f(r)\hat{L}\hat{S}. \tag{2.48}$$

The open form of f(r) can be expressed as

$$f(r) = \frac{1}{2M^2c^2r}\frac{dV(r)}{dr}. \tag{2.49}$$

The reformed version of Equation (2.48) can be written by application of the square of the total momentum ($\hat{J}^2 = \hat{L}^2 - \hat{S}^2$) as

$$H_{S-O} = \frac{1}{2}f(r)\hat{J}^2 - \hat{L}^2 - \hat{S}^2. \tag{2.50}$$

Finally, f(r) term can be written as

$$\left\langle f(r)\right\rangle = \frac{Z^3}{8\pi\epsilon_0 M^2C^2}\int_0^\infty \frac{1}{r^3} \mid R_{nl}(r) \mid^2 r^2dr. \tag{2.51}$$

Z represents the atomic number. As described in introduction part, high H_{SO} value is required for effective RISC process. Increase in atomic number resulted in increase at H_{SO} value as shown in Equation (2.51). For that reason, heavy atom containing compounds have high SOC constants. In TADF mechanism, the spin angular momentum changes when electron transfer from T_1 excited state to S_1 excited state while orbital angular momentum remains unchanged and SOC becomes zero or close to zero.

3. RESULTS

Important parameters for efficient TADF mechanism were explained in introduction part. TADF efficiency of studied compounds which can be found in Figure1.6–1.11 was examined with different descriptors and reported in this chapter. Results chapter consists of three main sections. Firstly, computational procedure is explained. Descriptor analysis section which contains subsections (dihedral angles and geometries, nature of states, ΔE_{ST}, SOC constants and NTO analysis and Φ_s indices) follows the computational procedure. Lastly, theoretical spectra analysis is discussed.

3.1. Computational Procedure

Density Functional Theory (DFT) calculations have been conducted with Gaussian 16 program package [118]. 6-31+G(d,p) basis set and 6-311++G(3df,3pd) extrabasis set are used at all of the ground and excited state calculations except for the SOC calculations [119]. Extrabasis set is used to increase the accuracy of calculations because molecules under investigation contain sulfur atoms. To include solvent effects, the integral equation formalism polarizable continuum model (IEF-PCM) has been applied implicitly.

Ground state and excited state optimizations were done with M062X functional because it is known that M062X is good at generating ground state geometries of aromatic rings [98]. Optimized geometries of ground and excited states were obtained by the CYLview software package. Firstly, a comprehensive conformer search was done and experimental absorption spectra solvents were used for optimizations. The dihedral angles and differences in geometries were discussed.

Excited state calculations were conducted with the lowest energy conformer that is provided from the conformer search.Tamm-Dancoff Approximation (TDA) was applied to the excited state calculation. S_1 and T_1 excited state energies were obtained with B3LYP/6-31+G(d,p), M062X/6-31+G(d,p) and PBE0/6-31+G(d,p). Theoretical

ΔE_{ST} values were generated in experimental solvent and compared with experimental ΔE_{ST} values.

Spin-orbit coupling (SOC) constants were obtained with B3LYP, M062X and PBE0 functionals with DZP basis set for RISC while ISC SOC constants were obtained with M062X functional. T_1 geometries were used for RISC SOC constants while S_1 geometries were used for ISC SOC constants because RISC occurs from T_1 to S_1 excited state and ISC occurs from S_1 to T_1 excited state. Amsterdam Density Functional (ADF) program was used for the calculation of SOC constants [120].

Natural transition orbital (NTO) analysis was done for $S_0 \rightarrow S_1$ and $S_0 \rightarrow T_1$ excitations at both S_0 and T_1 geometries with NancyEX code to visualize the distribution of frontier molecular orbitals [121]. B3LYP, M062X, PBE0 functionals with 6-31+G(d,p) were used for NTO analysis. Visualization and nature of excited states were obtained by Avogadro program package [122]. Φ_s indice which is the measurement of overlap between HOMO and LUMO was calculated with NancyEX software package in Lowdin and Mulliken charge distribution [123].

UV-Vis absorption spectra and emission spectra were reproduced in experimental spectra solvent for all of the studied compounds. B3LYP, M062X, PBE0 and BLYP functionals and 6-31+G(d,p) basis set were used for reproducing absorption spectra while M062X functional was used for generating emission spectra with 6-31+G(d,p) basis set. The vertical electronic excitations $S_0 \rightarrow S_1$, $S_1 \rightarrow S_0$ and $T_1 \rightarrow S_0$ were used to obtain absorption, fluorescence and phosphorescence spectra, respectively. The absorption spectra were obtained from 40 different initial conditions (conformations) that are generated with Wigner distribution to include dynamic effect by Newton-X software package [124]. The comparison between experimental and theoretical spectra was done and the effect of functionals was examined.

3.2. Descriptor Analysis

3.2.1. Dihedral Angles and Geometries

The geometries of ground and excited states are important for understanding the TADF mechanism. For that reason, the optimizations at the ground state (S_0) and excited states (S_1 and T_1) were done at M062X/6-31+G(d,p) level. Besides geometries, the dihedral angle between the donor and adjacent units is one of the descriptors that were analyzed to provide rationale for effective structural design of TADF emitters. The studied compounds have five different donor units that are called Cz, DMAC, PXZ, PTZ and DPA and these donor units are combined with different sulfone-based acceptor units.

The comparison between ground and excited states was done to examine differences between geometries. First of all, the angle between phenyl units that construct DPS acceptor structure at S_1 and T_1 geometries shows differences from ground state geometries as shown in Table 3.1-3.2. Donor units DMAC, PXZ and PTZ can show folded structure property at ground state geometries while these structures can become planar at S_1 and T_1 geometries. PXZ-DBTO2, PXZ-TTR and PXZDSO2 have folded PXZ donors at S_0 geometry while S_1 and T_1 geometries have planar donor units. Compounds 4 and PTZ-Ph-TTR have one folded donor unit at S_0, S_1 and T_1 geometries. The S_0 geometries of compound 2, PXZ-DPS and PTSOPT have two folded donor units while S_1 and T_1 geometries have one folded and one planar donor structure. Compounds 3, 1a and DPO-TXO2 have two folded donor units at S_0, one folded donor unit at S_1 and T_1 geometry has 2 planar donor units while DMAC-TTR and PTZ-TTR have one folded donor unit at S_0 and T_1 geometries and donor becomes planar at S_1 geometry. The optimized geometries of ground and excited states are shown in Table 3.1-3.6.

Table 3.1. Optimized geometries of Group 1 compounds at S_0, S_1 and T_1 energy levels.

Compounds	S_0 Level	S_1 Level	T_1 Level
1	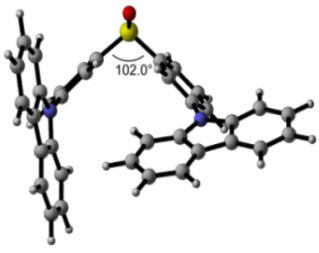	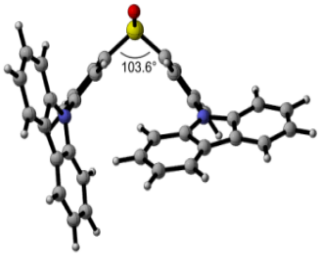	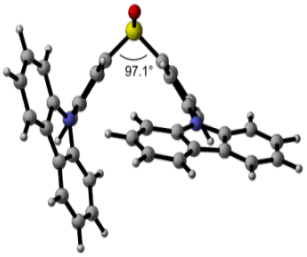
2	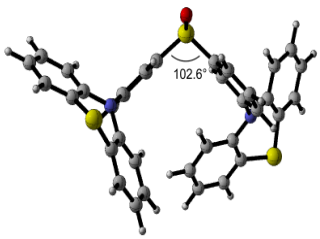	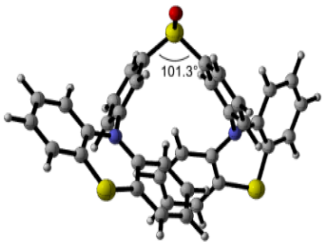	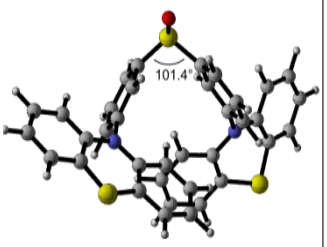
3	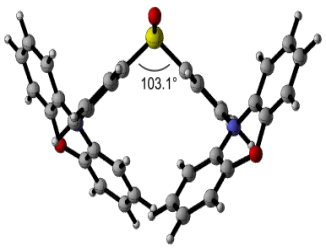	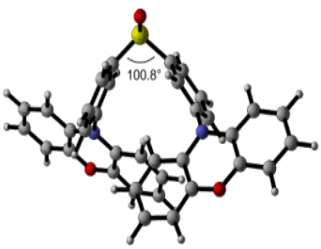	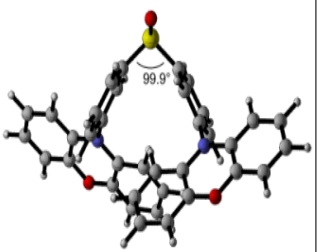
4	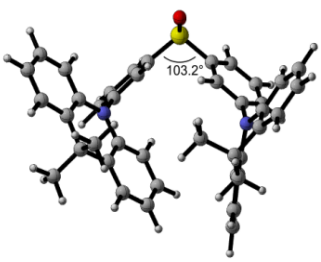	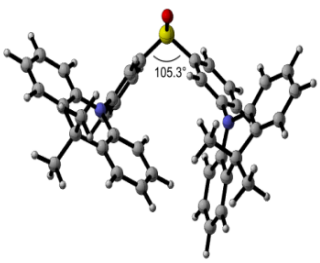	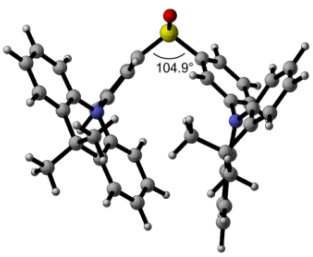
5	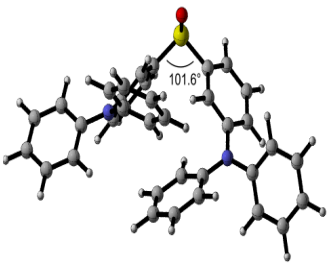	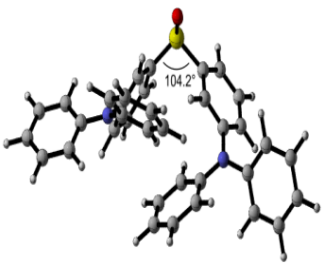	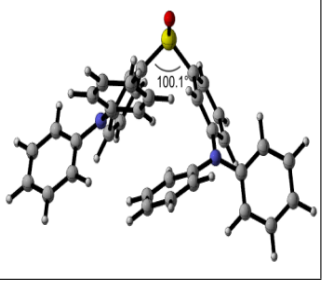

Table 3.2. Optimized geometries of Group 2 compounds at S_0, S_1 and T_1 energy levels.

Compounds	S_0 Level	S_1 Level	T_1 Level
SF2C	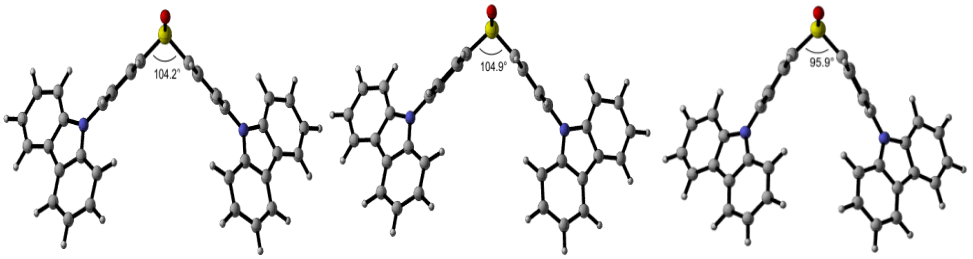		
PTSOPT	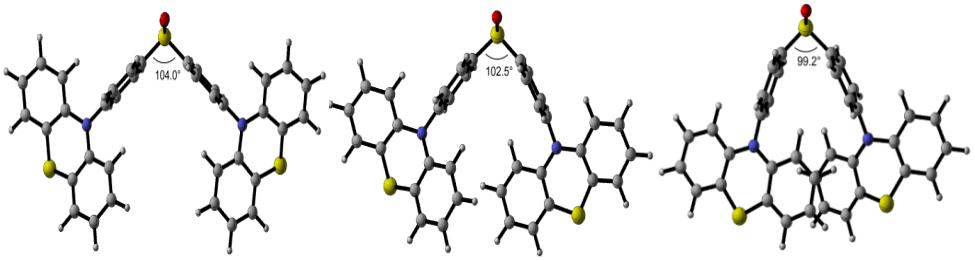		
PXZ-DPS	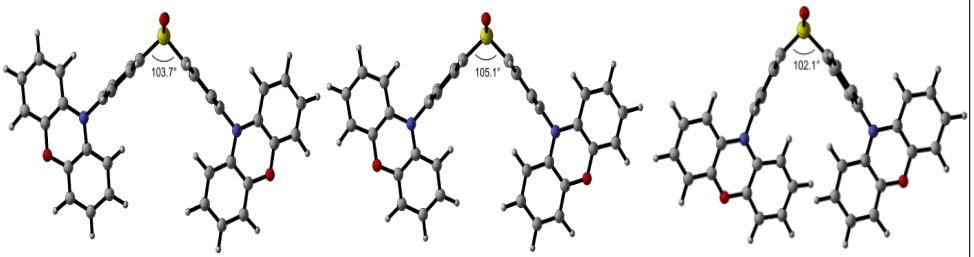		
DMAC-DPS	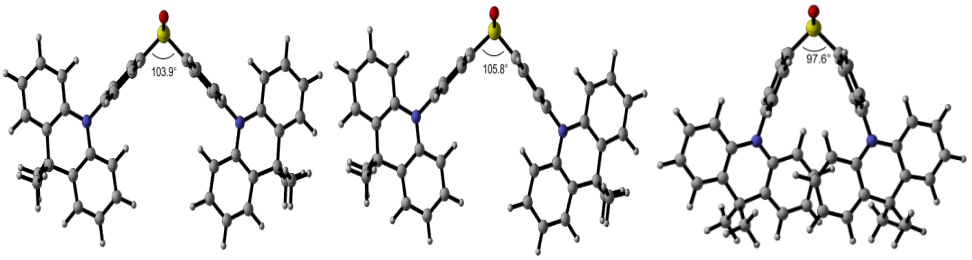		
DPA-DPS	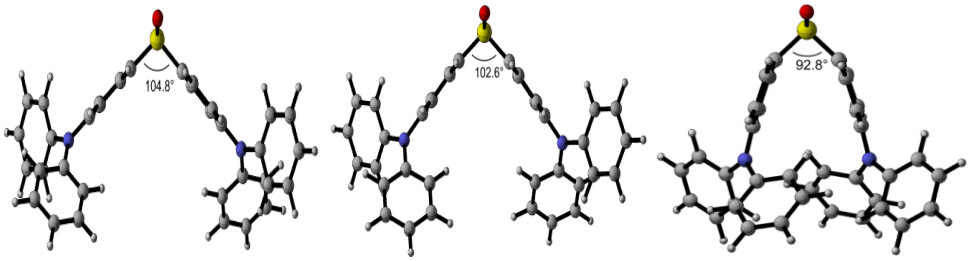		

Table 3.3. Optimized geometries of Group 3 compounds at S_0, S_1 and T_1 energy levels.

Compounds	S_0 Level	S_1 Level	T_1 Level
1a	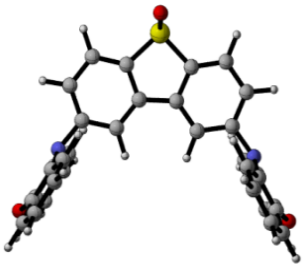	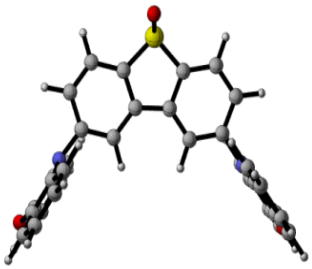	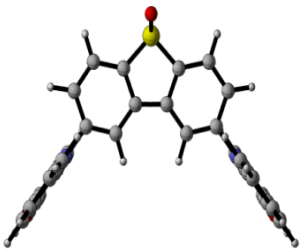
4ASOA	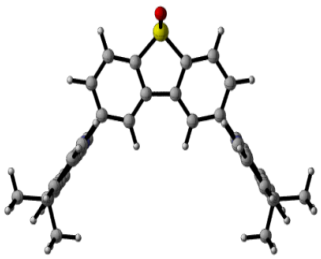	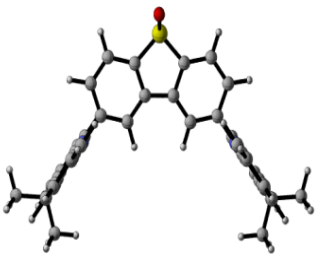	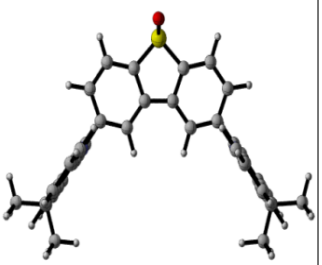
PXZ-DBTO2	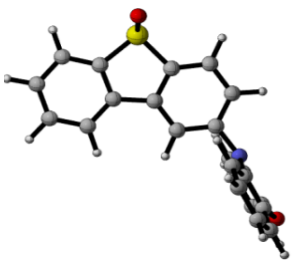	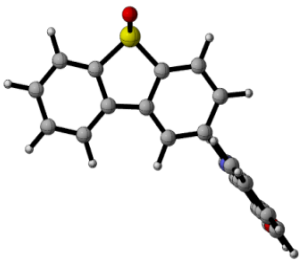	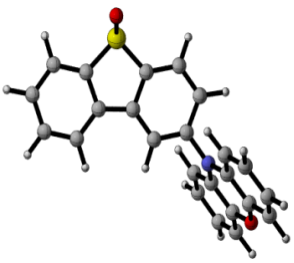
DPO-TXO2	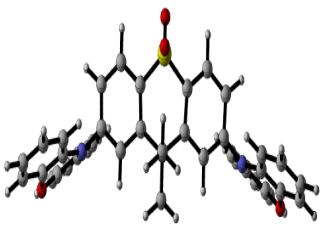	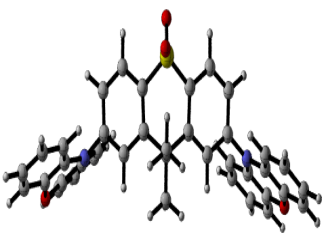	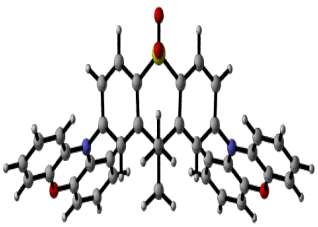
DDMA-TXO2	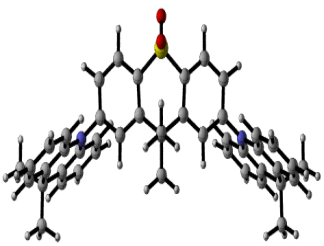	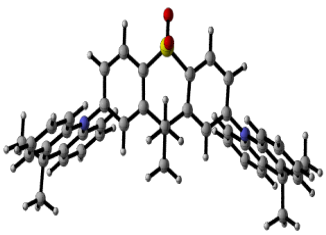	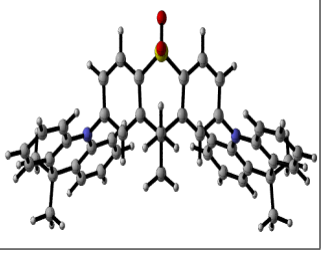

Table 3.4. Optimized geometries of Group 4 compounds at S_0, S_1 and T_1 energy levels.

Compounds	**S_0 Level**	**S_1 Level**	**T_1 Level**
Cz-TTR	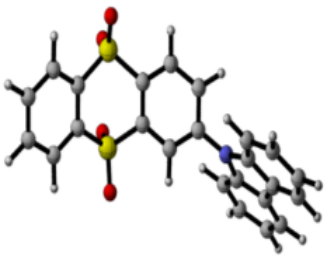	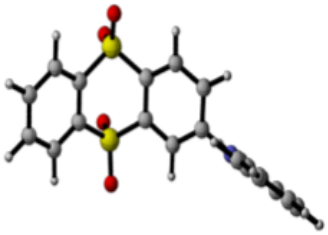	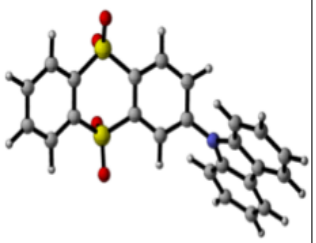
DMAC-TTR	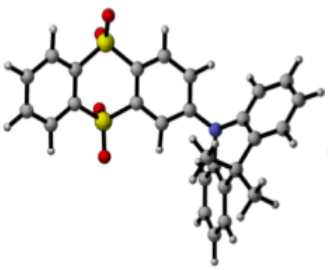		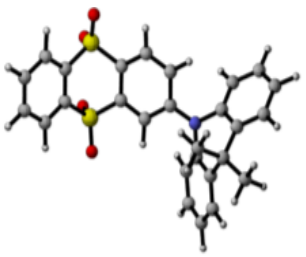
PXZ-TTR	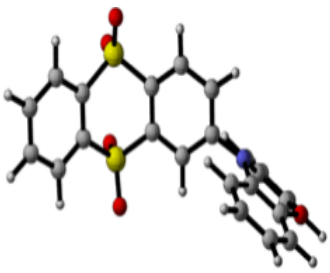	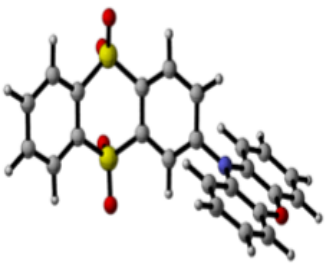	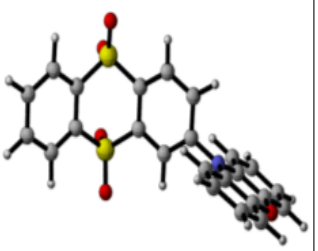
PTZ-TTR	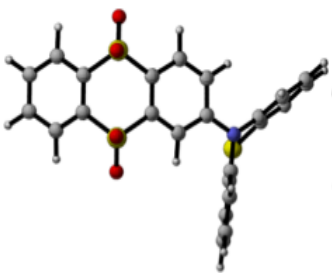	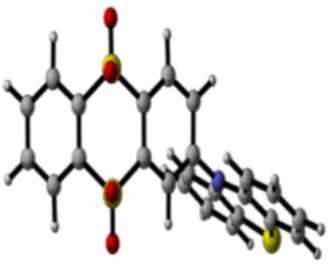	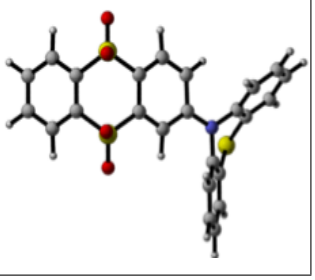

Table 3.5. Optimized geometries of Group 5 compounds at S_0, S_1 and T_1 energy levels.

Compounds	**S_0 Level**	**S_1 Level**	**T_1 Level**
CzPhDSO2	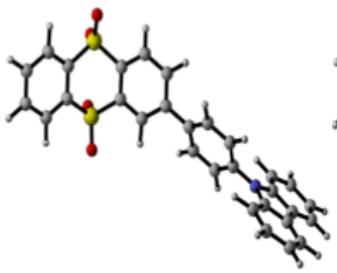	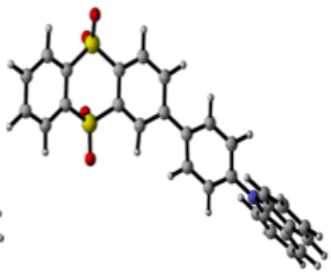	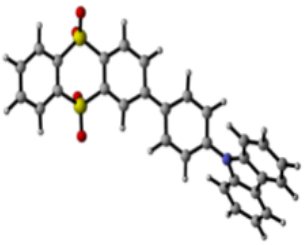
ACRDSO2	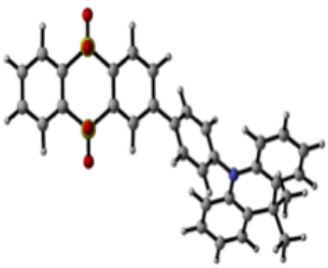	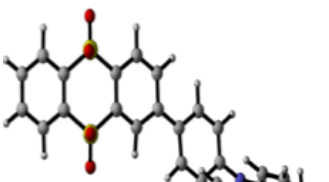	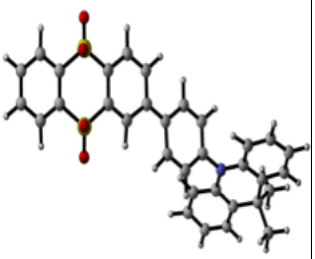
PXZDSO2	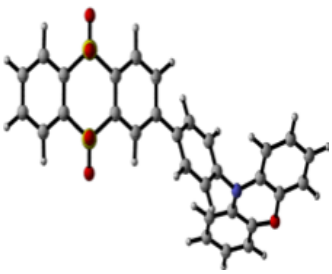	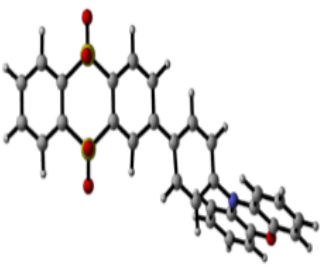	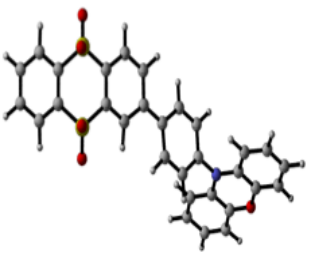
PTZ-Ph-TTR	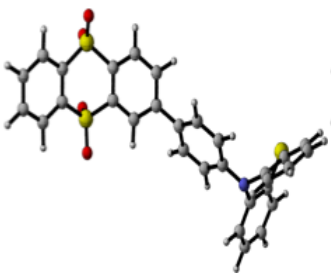	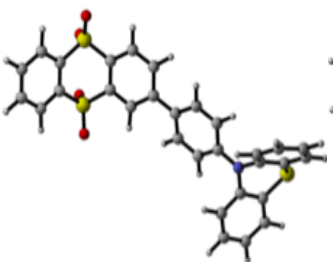	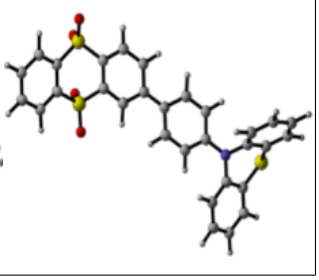

Table 3.6. Optimized geometries of Group 6 compounds at S_0, S_1 and T_1 energy levels.

Compounds	S_0 Level	S_1 Level	T_1 Level
Ac-OSO	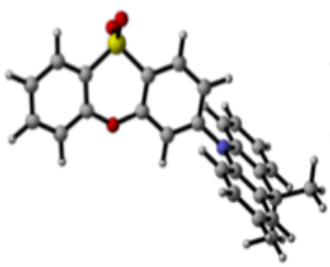	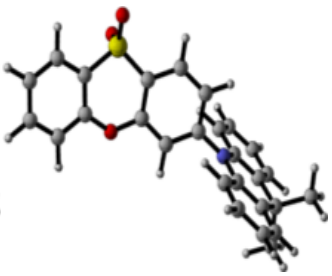	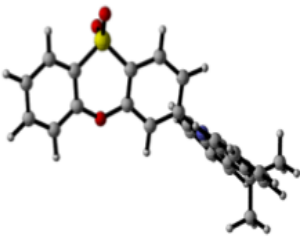
CzSOXO	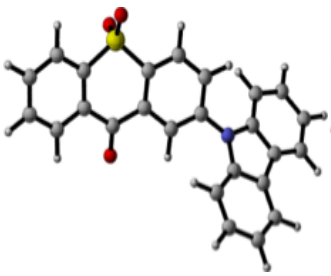	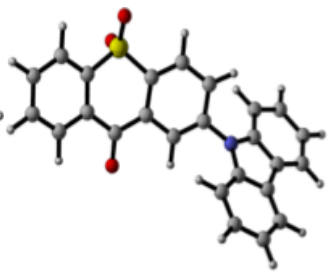	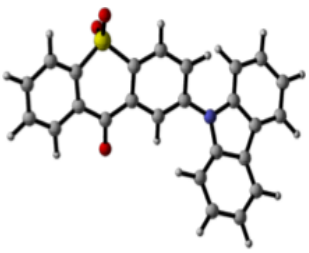
TXO-PhCz	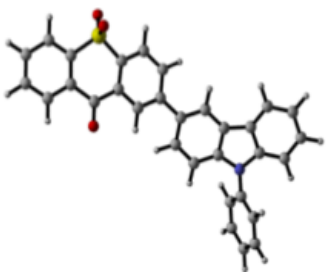	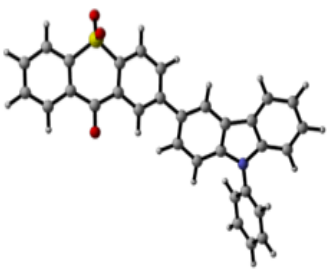	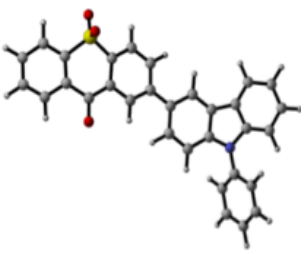

Besides the differences between structures, the dihedral angles between donor-acceptor and donor adjacent units (bridge) are different for S_0, S_1 and T_1 geometries. Dihedral angle affects the efficiency of the TADF mechanism and perpendicular positioning of donor unit to the acceptor unit resulted in small ΔE_{ST} and small overlap between HOMO and LUMO which are required for effective TADF mechanism. Firstly, ground state (S_0) geometries are examined and the relationship between dihedral angles and ΔE_{ST} values is reported.

The dihedral angle between donor-acceptor and donor-bridge is $\sim 50°$ for Cz donor unit. The less rigid structure and more freely move of Cz unit are responsible for low dihedral angle. Deviation from ideal dihedral angle which is the 90° resulted in high ΔE_{ST} values $\geqslant 0.1$ eV for both experimental and theoretical results except

for the compounds CzSOXO and TXO-PhCz. We can say that Cz unit gives the approximately same dihedral angle as all of the studied sulfone-based acceptor units. Carbazole unit in TXO-PhCz has different substitution position and additional phenyl unit which is resulted in lower dihedral angle $< 50°$ between acceptor and donor units while dihedral angle between phenyl and carbazole is close to 50°.

DMAC is the most rigid donor unit among all studied donor units. For that reason, we expect to get ideal dihedral angle with DMAC. As expected, DMAC has ideal dihedral angle and located to the adjacent units perpendicularly. Compound DMAC-TTR that has TTR as an acceptor unit is an outlier compound. The dihedral angle between donor-acceptor units is $\sim 10°$ with folded shaped DMAC and DMAC-TTR has planar conformation which is not desired structure for TADF emitters. DMAC containing compounds have small ΔE_{ST} values $\leqslant 0.09$ eV except for DMAC-TTR.

PXZ donor unit creates dihedral angle between $\sim 70° - 100°$ and all of the PXZ containing compounds have small ΔE_{ST} values. PXZ has the highest dihedral angle value with DMTD and para substituted DPS acceptor units. The addition of bridge at compound PXZDSO2 resulted in higher dihedral angle between bridge-donor when compared to non-bridge form PXZ-TTR. PTZ containing compounds at Group 1 and 2 with DPS acceptor have approximately 75° dihedral angle while the compounds at Group 4 and 5 with PTZ donor units have low $\sim 15°$ dihedral angle with planar conformation. As expected, the planar conformation and lower dihedral angle resulted in higher ΔE_{ST} values.

The least rigid donor unit DPA consists of two phenyl units that are not linked to each other can move freely without sterical restriction. As a result of dihedral angle approximately lower than 40°, compounds that have DPA donor units have high ΔE_{ST} values. According to dihedral angles, DMAC and PXZ are the ideal donor units for the TADF mechanism. This idea should be supported with other descriptor analyses. The dihedral angles of investigated compounds at S_0, S_1 and T_1 levels are reported in Figure 3.1–3.6.

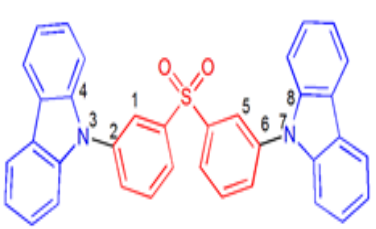

1

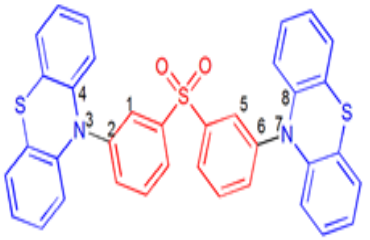

2

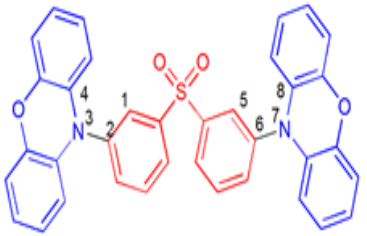

3

4

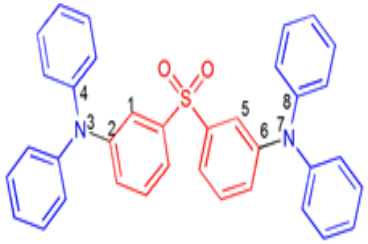

5

Compounds	$\theta(D\text{-}A)_1$ ($S_0/S_1/T_1$)	$\theta(D\text{-}A)_2$ ($S_0/S_1/T_1$)
1	52.45/59.74/55.72	53.17/60.72/44.73
2	-99.76/-88.74/-89.89	-75.03/-77.68/-78.82
3	73.63/88.17/84.75	73.63/87.71/84.75
4	-92.38/-89.71/-104.21	108.04/106.61/113.13
5	-25.20/-41.88/-22.79	41.79/53.01/53.02

Figure 3.1. Dihedral angles (Θ) for the Group 1 emitters measured from the S_0, S_1 and T_1 geometries (M062X/6-31+G(d,p)).

SF2C

PTSOPT

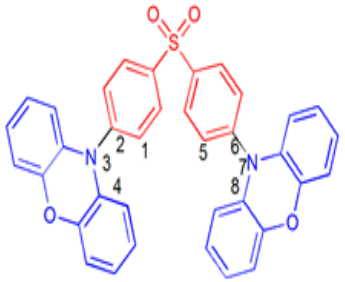

PXZ-DPS

DMAC-DPS

DPA-DPS

Compounds	$\theta(D\text{-}A)_1$ ($S_0/S_1/T_1$)	$\theta(D\text{-}A)_2$ ($S_0/S_1/T_1$)
SF2C	-51.39/-53.88/-45.78	51.40/63.11/46.54
PTSOPT	-74.86/-74.47/-71.45	77.11/88.05/96.55
PXZ-DPS	-104.20/-105.73/-106.21	102.17/89.53/69.12
DMAC-DPS	-91.08/-92.03/-105.44	89.23/89.55/72.95
DPA-DPS	-30.48/-43.11/-34.82	-30.40/-43.18/-32.57

Figure 3.2. Dihedral angles (Θ) for the Group 2 emitters measured from the S_0, S_1 and T_1 geometries (M062X/6-31+G(d,p)).

1a

4ASOA

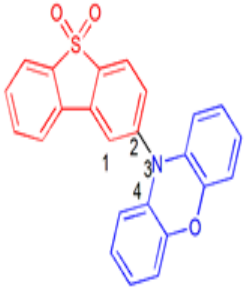

PXZ-DBTO2

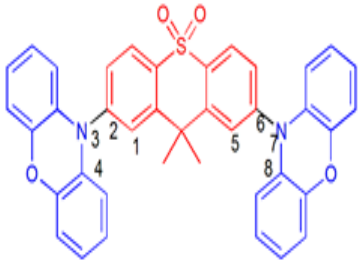

DPO-TXO2

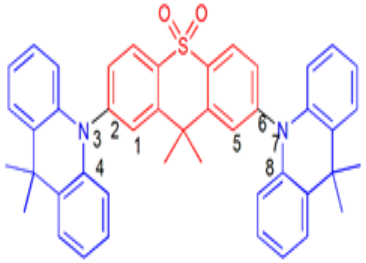

DDMA-TXO2

Compounds	$\theta(D\text{-}A)_1$ ($S_0/S_1/T_1$)	$\theta(D\text{-}A)_2$ ($S_0/S_1/T_1$)
1a	75.80/89.64/90.06	-75.83/-78.61/-90.08
4ASOA	90.15/91.23/90.62	-90.16/-91.50/-90.63
PXZ-DBTO2	-76.00/-91.63/-109.80	-
DPO-TXO2	102.26/102.74/105.58	-102.27/-90.17/-105.58
DDMA-TXO2	89.07/90.14/101.81	-89.07/-89.30/-101.81

Figure 3.3. Dihedral angles (Θ) for the Group 3 emitters measured from the S_0, S_1 and T_1 geometries (M062X/6-31+G(d,p)).

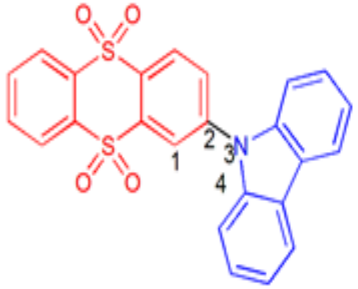

Cz-TTR

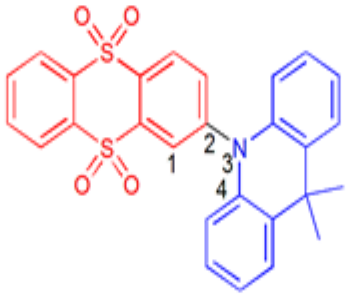

DMAC-TTR

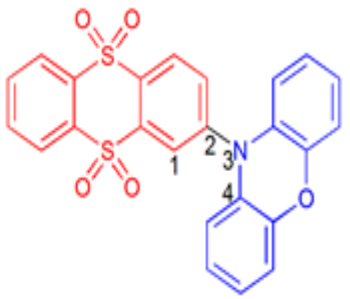

PXZ-TTR

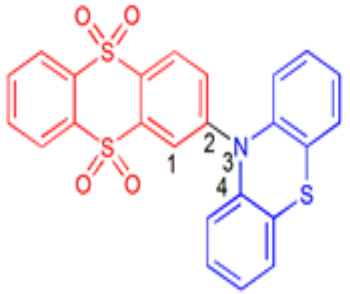

PTZ-TTR

Compounds	$\theta(D\text{-}A)_1$ ($S_0/S_1/T_1$)
Cz-TTR	49.02/65.43/45.36
DMAC-TTR	-9.57/-90.38/-5.43
PXZ-TTR	-83.98/-92.63/-102.05
PTZ-TTR	15.11/-90.76/5.53

Figure 3.4. Dihedral angles (Θ) for the Group 4 emitters measured from the S_0, S_1 and T_1 geometries (M062X/6-31+G(d,p)).

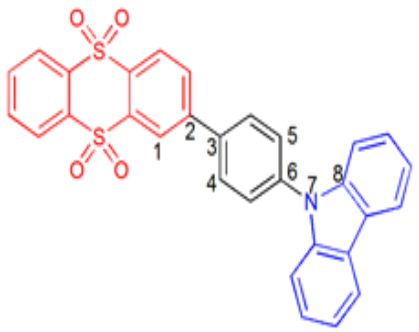

CzPhDSO2

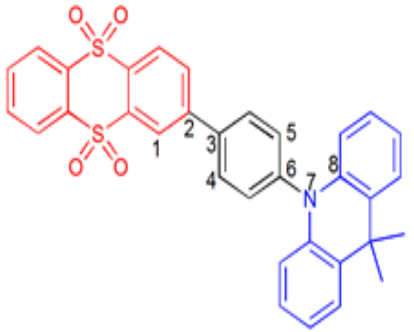

ACRDSO2

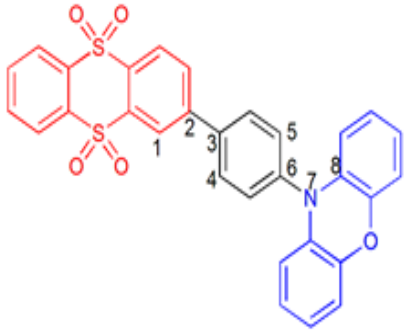

PXZDSO2

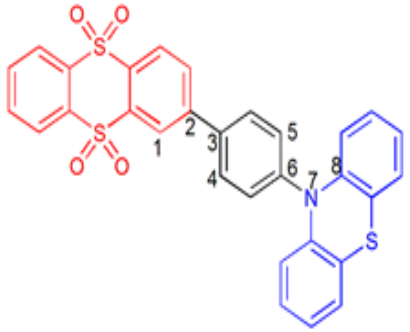

PTZ-Ph-TTR

Compounds	$\theta(D\text{-}A)_1$ ($S_0/S_1/T_1$)	$\theta(D\text{-}A)_2$ ($S_0/S_1/T_1$)
CzPhDSO2	37.70/13.59/-1.93	53.36/46.33/42.18
ACRDSO2	-38.58/-10.41/-8.05	90.40/92.63/62.57
PXZDSO2	-39.45/-10.79/-12.91	102.92/92.30/72.00
PTZ-Ph-TTR	36.08/20.08/2.63	17.34/-1.56/2.32

Figure 3.5. Dihedral angles (Θ) for the Group 5 emitters measured from the S_0, S_1 and T_1 geometries (M062X/6-31+G(d,p)).

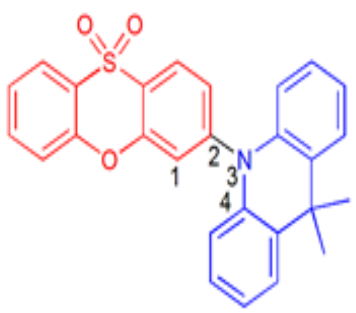

Ac-OSO

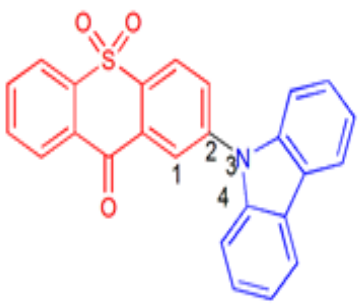

CzSOXO

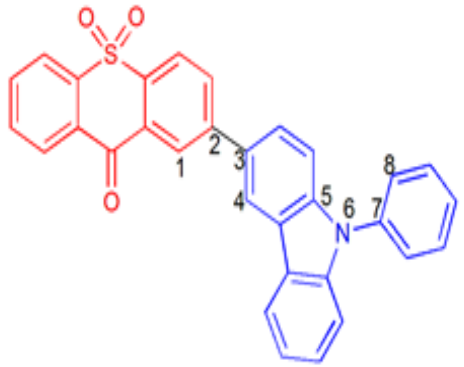

TXO-PhCz

Compounds	$\theta(D\text{-}A)_1$ ($S_0/S_1/T_1$)	$\theta(D\text{-}A)_2$ ($S_0/S_1/T_1$)
Ac-OSO	89.29/89.38/66.90	-
CzSOXO	-53.24/-55.65/-41.96	-
TXO-PhCz	37.32/38.35/15.45	56.92/57.01/58.96

Figure 3.6. Dihedral angles (Θ) for the Group 6 emitters measured from the S_0, S_1 and T_1 geometries (M062X/6-31+G(d,p)).

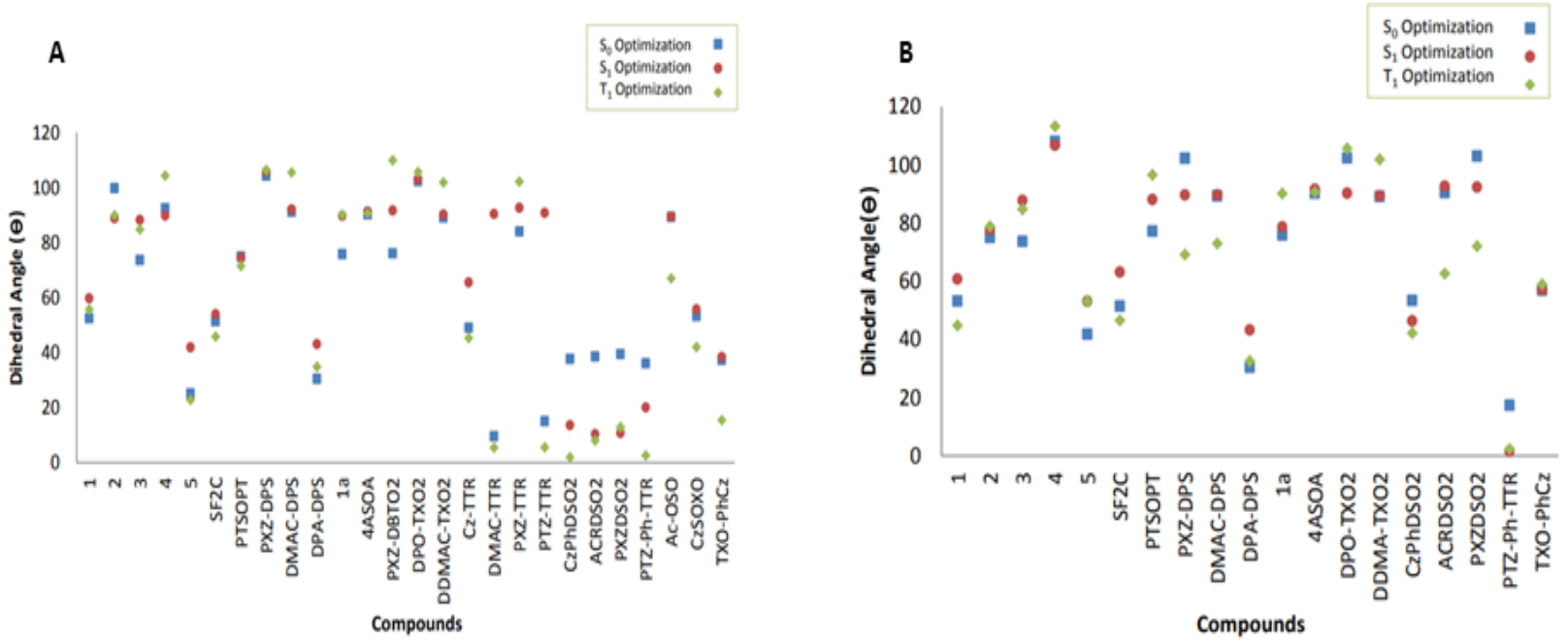

Figure 3.7. The dihedral angles A) $\Theta(D-A)_1$ and B) $\Theta(D-A)_2$ of the investigated compounds at S_0, S_1 and T_1 optimized geometries (M062X/6-31+G(d,p)).

The comparison between dihedral angles at S_0, S_1 and T_1 geometries was done via Figure 3.7. $\Theta(D-A)_1$ and $\Theta(D-A)_2$ are represented in A and B respectively. The changes in dihedral angles for S_0, S_1 and T_1 levels are different for $\Theta(D-A)_1$ and $\Theta(D-A)_2$. Generally, dihedral angles of different levels are close to each other. The higher differences resulted from change in conformation. For example, the dihedral angle differences between S_1 and other levels (S_0 and T_1) of DMAC-TTR and PTZ-TTR are high and these compounds have planar conformation with folded donor units at S_0 and T_1 geometries. However, folded donor structure becomes planar at S_1 geometry and dihedral angle shows change when compared to other levels.

3.2.2. Nature of States

Nature of states is important descriptor for TADF mechanism and it mostly depends on CT character. However, Penfold and Monkman suggest the TADF mechanism based on S_{CT}, T_{CT} and T_{LE}. According to mechanism, k_{RISC} has higher value because of the mixed character (^{3}CT and ^{3}LE) of triplet states that are coupled by non-adiabatic (vibronic) coupling. Higher k_{RISC} resulted in more efficient TADF mechanism, so nature of states takes important role in the TADF mechanism. The nature of singlet and triplet excited states were obtained from NTO analysis and analyzed with B3LYP, M062X and PBE0 functionals for both S_0 and T_1 geometries.

The natures obtained by B3LYP and PBE0 functionals are similar while M062X functional shows difference and gives the highest LE nature among all of functionals. CT character is dominant at singlet excitations for both S_0 and T_1 geometries. B3LYP and PBE0 give CT character for singlet excitations at all of the compounds. On the other hand, M062X gives increased LE character for singlet excitations especially at low dihedral angle donor containing compounds. Besides low dihedral angle compounds, PTZ containing compound 2 has CT-LE character with M062X functional. We can say that all of the functionals give correct character (CT) for singlet excited states except for outliers. According to TADF mechanism proposed by Penfold and Monkman, addition of LE character to the triplet state increases the efficiency of mechanism, so triplet excited states should have LE character. All of the compounds have increased

LE nature at triplet excitations when compared to singlet excitations especially with M062X functional while B3LYP and PBE0 almost give CT character for all compounds. DMAC and PXZ containing compounds DMAC-DPS, 1a, 4ASOA, DDMA-TXO2 and PXZ-TTR are prone to generate CT character at both singlet and triplet excitations for S_0 and T_1 geometries. The rigidity of building moieties and ideal dihedral angles of these compounds can be responsible for CT nature and absence of LE character at triplet excited states can decrease the efficiency of mechanism. Despite of low dihedral angle, compounds SF2C and DPA-DPS have CT nature for singlet and triplet excitations at both S_0 and T_1 geometries. Differences at S_0 and T_1 geometries as explained before resulted in changes of nature at some of the compounds. As mentioned before, we expect to get CT character at singlet excitations while LE character at triplet excitations. M062X is the only functional that gives correct character for triplet excited states while B3LYP and PBE0 give wrong character for triplet excited states. Table 3.7-3.12 consist of the nature of excited states for all of the studied compounds and contain nature of the second triplet excited states if T_2 state has lower energy than S_1 excited state.

Table 3.7. Natures of different excited states for Group 1 with B3LYP, M062X and PBE0 functionals.

Group 1							
Compound	**Method**	**S_0 Geometry**	**T_1 Geometry**	**S_0 Geometry**		**T_1 Geometry**	
		$S_0 \rightarrow S_1$	**$S_0 \rightarrow S_1$**	**$S_0 \rightarrow T_1$**	**$S_0 \rightarrow T_2$**	**$S_0 \rightarrow T_1$**	**$S_0 \rightarrow T_2$**
		CT vs LE	**CT vs LE**	**CT vs LE**		**CT vs LE**	
1	B3LYP	CT	CT	CT	CT	CT	CT
	M062X	CT	CT	LE	LE	CT	CT
	PBE0	CT	CT	CT	CT	CT	CT
2	B3LYP	CT	CT	CT	CT	CT	CT
	M062X	CT-LE	CT	CT-LE	LE	CT-LE	CT-LE
	PBE0	CT	CT	CT	CT	CT	CT-LE
3	B3LYP	CT	CT	CT	CT	CT	CT
	M062X	CT	CT	CT-LE	CT-LE	CT	CT
	PBE0	CT	CT	CT	CT	CT	CT
4	B3LYP	CT	CT	CT	-	CT	-
	M062X	CT	CT	CT-LE	-	CT	-
	PBE0	CT	CT	CT	-	CT	-
5	B3LYP	CT	CT	CT-LE	CT	CT	CT
	M062X	CT-LE	CT	CT-LE	CT-LE	CT	CT
	PBE0	CT	CT	CT-LE	CT	CT	CT

Table 3.8. Natures of different excited states for Group 2 with B3LYP, M062X and PBE0 functionals.

Group 2							
Compound	**Method**	**S_0 Geometry**	**T_1 Geometry**	**S_0 Geometry**		**T_1 Geometry**	
		$S_0 \rightarrow S_1$	**$S_0 \rightarrow S_1$**	**$S_0 \rightarrow T_1$**	**$S_0 \rightarrow T_2$**	**$S_0 \rightarrow T_1$**	**$S_0 \rightarrow T_2$**
		CT vs LE	**CT vs LE**	**CT vs LE**		**CT vs LE**	
SF2C	B3LYP	CT	CT	CT	CT	CT	CT
	M062X	CT	CT	CT	CT	CT	CT
	PBE0	CT	CT	CT	CT	CT	CT
PTSOPT	B3LYP	CT	CT	CT	CT	CT	CT
	M062X	CT	CT	LE	LE	CT	LE
	PBE0	CT	CT	CT	CT	CT	CT
PXZ-DPS	B3LYP	CT	CT	CT	CT	CT	CT
	M062X	CT	CT	CT-LE	CT-LE	CT	LE
	PBE0	CT	CT	CT	CT	CT	CT
DMAC-DPS	B3LYP	CT	CT	CT	CT	CT	CT
	M062X	CT	CT	CT	CT	CT	CT
	PBE0	CT	CT	CT	CT	CT	CT
DPA-DPS	B3LYP	CT	CT	CT	CT	CT	CT
	M062X	CT	CT	CT	CT	CT	CT
	PBE0	CT	CT	CT	CT	CT	CT

Table 3.9. Natures of different excited states for Group 3 with B3LYP, M062X and PBE0 functionals.

Group 3							
Compound	**Method**	**S_0 Geometry**	**T_1 Geometry**	**S_0 Geometry**		**T_1 Geometry**	
		$S_0 \rightarrow S_1$	**$S_0 \rightarrow S_1$**	**$S_0 \rightarrow T_1$**	**$S_0 \rightarrow T_2$**	**$S_0 \rightarrow T_1$**	**$S_0 \rightarrow T_2$**
		CT vs LE	**CT vs LE**	**CT vs LE**		**CT vs LE**	
1a	B3LYP	CT	CT	CT	CT	CT	CT
	M062X	CT	CT	CT	CT	CT	CT
	PBE0	CT	CT	CT	CT	CT	CT
4ASOA	B3LYP	CT	CT	CT	CT	CT	CT
	M062X	CT	CT	CT	CT	CT	CT
	PBE0	CT	CT	CT	CT	CT	CT
PXZ-DBTO2	B3LYP	CT	CT	CT	-	CT	-
	M062X	CT	CT	CT-LE	CT-LE	CT	LE
	PBE0	CT	CT	CT	-	CT	-
DPO-TXO2	B3LYP	CT	CT	CT	CT	CT	CT
	M062X	CT	CT	LE	LE	CT	CT
	PBE0	CT	CT	CT	CT	CT	CT
DDMA-TXO2	B3LYP	CT	CT	CT	CT	CT	CT
	M062X	CT	CT	CT	CT	CT	CT
	PBE0	CT	CT	CT	CT	CT	CT

Table 3.10. Natures of different excited states for Group 4 with B3LYP, M062X and PBE0 functionals.

GROUP 4							
Compound	**Method**	**S_0 Geometry**	**T_1 Geometry**	**S_0 Geometry**		**T_1 Geometry**	
		$S_0 \rightarrow S_1$	**$S_0 \rightarrow S_1$**	**$S_0 \rightarrow T_1$**	**$S_0 \rightarrow T_2$**	**$S_0 \rightarrow T_1$**	**$S_0 \rightarrow T_2$**
		CT vs LE	**CT vs LE**	**CT vs LE**		**CT vs LE**	
Cz-TTR	B3LYP	CT	CT	CT	-	CT-LE	-
	M062X	CT	CT-LE	CT	-	LE	-
	PBE0	CT	CT	CT	-	LE	-
DMAC-TTR	B3LYP	CT	CT	CT	-	CT	-
	M062X	CT	CT	CT	CT-LE	CT	CT-LE
	PBE0	CT	CT	CT	-	CT	-
PXZ-TTR	B3LYP	CT	CT	CT	-	CT	-
	M062X	CT	CT	CT	-	CT	-
	PBE0	CT	CT	CT	-	CT	-
PTZ-TTR	B3LYP	CT	CT	CT	-	CT	-
	M062X	CT	CT	CT	CT-LE	CT	CT-LE
	PBE0	CT	CT	CT	-	CT	-

Table 3.11. Natures of different excited states for Group 5 with B3LYP, M062X and PBE0 functionals.

GROUP 5							
Compound	**Method**	**S_0 Geometry**	**T_1 Geometry**	**S_0 Geometry**		**T_1 Geometry**	
		$S_0 \rightarrow S_1$	**$S_0 \rightarrow S_1$**	**$S_0 \rightarrow T_1$**	**$S_0 \rightarrow T_2$**	**$S_0 \rightarrow T_1$**	**$S_0 \rightarrow T_2$**
		CT vs LE	**CT vs LE**	**CT vs LE**		**CT vs LE**	
CzPhDSO2	B3LYP	CT	CT	CT	-	CT-LE	-
	M062X	CT	CT-LE	CT-LE	LE	CT-LE	CT-LE
	PBE0	CT	CT	CT	-	CT-LE	-
ACRDSO2	B3LYP	CT	CT	CT	-	CT	-
	M062X	CT	CT-LE	CT	-	CT-LE	-
	PBE0	CT	CT	CT	-	CT	-
PXZDSO2	B3LYP	CT	CT	CT	-	CT	-
	M062X	CT	CT-LE	CT-LE	CT-LE	CT-LE	LE
	PBE0	CT	CT	CT	-	CT	-
PTZ-Ph-TTR	B3LYP	CT	CT	CT	-	CT	-
	M062X	CT	CT	CT-LE	-	CT-LE	-
	PBE0	CT	CT	CT	-	CT	-

Table 3.12. Natures of different excited states for Group 6 with B3LYP, M062X and PBE0 functionals.

GROUP 6							
Compound	**Method**	**S_0 Geometry**	**T_1 Geometry**	**S_0 Geometry**		**T_1 Geometry**	
		$S_0 \rightarrow S_1$	**$S_0 \rightarrow S_1$**	**$S_0 \rightarrow T_1$**	**$S_0 \rightarrow T_2$**	**$S_0 \rightarrow T_1$**	**$S_0 \rightarrow T_2$**
		CT vs LE	**CT vs LE**	**CT vs LE**		**CT vs LE**	
Ac-OSO	B3LYP	CT	CT	CT	-	CT	-
	M062X	CT	CT	CT	LE	CT	LE
	PBE0	CT	CT	CT	-	CT	-
CzSOXO	B3LYP	CT	CT	CT	-	CT	-
	M062X	CT	CT	CT	CT	CT	LE
	PBE0	CT	CT	CT	-	CT	-
TXO-PhCz	B3LYP	CT	CT	CT	-	CT	-
	M062X	LE	CT	LE	CT-LE	CT-LE	LE
	PBE0	CT	CT	CT	-	CT	-

3.2.3. ΔE_{ST} Values

To provide design strategies for TADF emitters, ΔE_{ST} is one of the primary descriptors that are analyzed. Triplet excitons are harvested by RISC and small energy difference between S_1 and T_1 excited states, ΔE_{ST}, is required for effective RISC. Ideal dihedral angle and small overlap between HOMO and LUMO is the most known strategy to obtain small ΔE_{ST} values. According to studies, the value of ΔE_{ST} should be < 0.3 eV for successful RISC. However, there are examples of TADF emitters that have ΔE_{ST} values > 0.3 eV. Calculated ΔE_{ST} values were obtained for all of the studied compounds with B3LYP, M062X and PBE0 functional.

Most of the compounds have calculated ΔE_{ST} values that are in good correlation with experimental values. However, the calculated ΔE_{ST} values of compounds PTSOPT, Cz-TTR, ACRDSO2 and PXZDSO2 show deviations from experimental values. The deviation of Cz-TTR, PXZDSO2 and ACRDSO2 can result from differences in experimental and theoretical conditions. The experimental values of Cz-TTR, ACRDSO2 and PXZDSO2 are obtained in film while ΔE_{ST} values are calculated in absorption spectra solvent. As mentioned, Cz and DPA donor units create low dihedral angles which is not ideal situation for getting small ΔE_{ST}. For that reason, Cz and DPA donor units containing compounds 1, SF2C, CzPhDSO2, 5 and DPA-DPS have

high ΔE_{ST} values. In contrast to other Cz containing compounds, CzSOXO and TXO-PhCz have small ΔE_{ST} because TXO that is located as an acceptor unit has special conjugation break property that resulted from twisted carbonyl group. As mentioned before, orthogonality is desired structure for TADF emitters. DMAC and PXZ containing compounds that have dihedral angle ideal or close to ideal dihedral angle have small ΔE_{ST} values as expected. In contrast to orthogonality, DMAC-TTR, PTZ-TTR and PTZ-Ph-TTR have planar conformation, low dihedral angle, which is resulted in high ΔE_{ST} values. According to ΔE_{ST} values ($\leqslant$ 0.1 eV), DMAC and PXZ are the best options for donor unit selection. The experimental and calculated ΔE_{ST} values are shown in Table 3.13.

The calculated ΔE_{ST} values show that all of the functionals can be used to generate ΔE_{ST} values because of their good correlations with experimental values. Generally, B3LYP and PBE0 give similar results while M062X gives the higher results among all functionals. This result is consistent with the nature of states because higher LE character resulted in higher HOMO-LUMO overlap and ΔE_{ST} values. Besides focusing on the results, we also examine the trends between experimental and calculated results. The graphs are generated for each group of emitters to decide which functional generate the similar trend to the experimental results. Generated graphs are shown in Figure 3.8. Generally, generated trends are consistent with experimental trends. All functionals generate similar trends at Group 4 and 5. When we look at the graphs, we can see the similar trends between B3LYP and PBE0 except for Group 3. B3LYP functional creates the most similar trend to the experimental graph at Group 1, 3, 4 and 6 while M062X and PBE0 are the best functionals for Group 2 and 5, respectively. However, B3LYP and PBE0 give wrong nature of states as mentioned before and this means that they will also give wrong energies for excited states. It is known that B3LYP and PBE0 functionals underestimate CT energies with respect to LE energies. B3LYP and PBE0 accidentally give ΔE_{ST} values close to experimental data and this is the reason of widely usage of these functionals at literature.

Table 3.13. Calculated and experimental ΔE_{ST} values of studied compounds with 6-31+G(d,p) basis set.

GROUP 1				
	B3LYP	**M062X**	**PBE0**	**Exp. ΔE_{ST}**
1	0.15	0.42	0.20	0.44
2	0.03	0.30	0.05	0.01
3	0.03	0.20	0.04	0.06
4	0.03	0.10	0.04	0.05
5	0.38	0.58	0.46	-
GROUP 2				
	B3LYP	**M062X**	**PBE0**	**Exp. ΔE_{ST}**
SF2C	0.24	0.41	0.31	0.28±0.03
PTSOPT	0.02	0.20	0.02	0.41
PXZ-DPS	0.01	0.02	0.02	0.08
DMAC-DPS	0.01	0.00	0.01	0.09
DPA-DPS	0.46	0.58	0.54	0.54
GROUP 3				
	B3LYP	**M062X**	**PBE0**	**Exp. ΔE_{ST}**
1a	0.01	0.04	0.02	0.06
4ASOA	0.02	0.01	0.02	0.09
PXZ-DBTO2	0.014	0.057	0.020	0.068
DPO-TXO2	0.01	0.10	0.01	0.07±0.03
DDMA-TXO2	0.01	0.00	0.01	0.00
GROUP 4				
	B3LYP	**M062X**	**PBE0**	**Exp. ΔE_{ST}**
Cz-TTR	0.23	0.41	0.29	0.10
DMAC-TTR	0.51	0.78	0.60	0.45
PXZ-TTR	0.03	0.04	0.03	-
PTZ-TTR	0.45	0.80	0.56	0.38
GROUP 5				
	B3LYP	**M062X**	**PBE0**	**Exp.ΔE_{ST}**
CzPhDSO2	0.13	0.45	0.18	0.30
ACRDSO2	0.002	0.004	0.004	0.058
PXZDSO2	0.003	0.019	0.005	0.048
PTZ-Ph-TTR	0.30	0.65	0.40	0.57
GROUP 6				
	B3LYP	**M062X**	**PBE0**	**Exp.ΔE_{ST}**
Ac-OSO	0.02	0.01	0.02	0.06
CzSOXO	0.13	0.29	0.16	0.05
TXO-PhCz	0.121	0.397	0.162	0.073

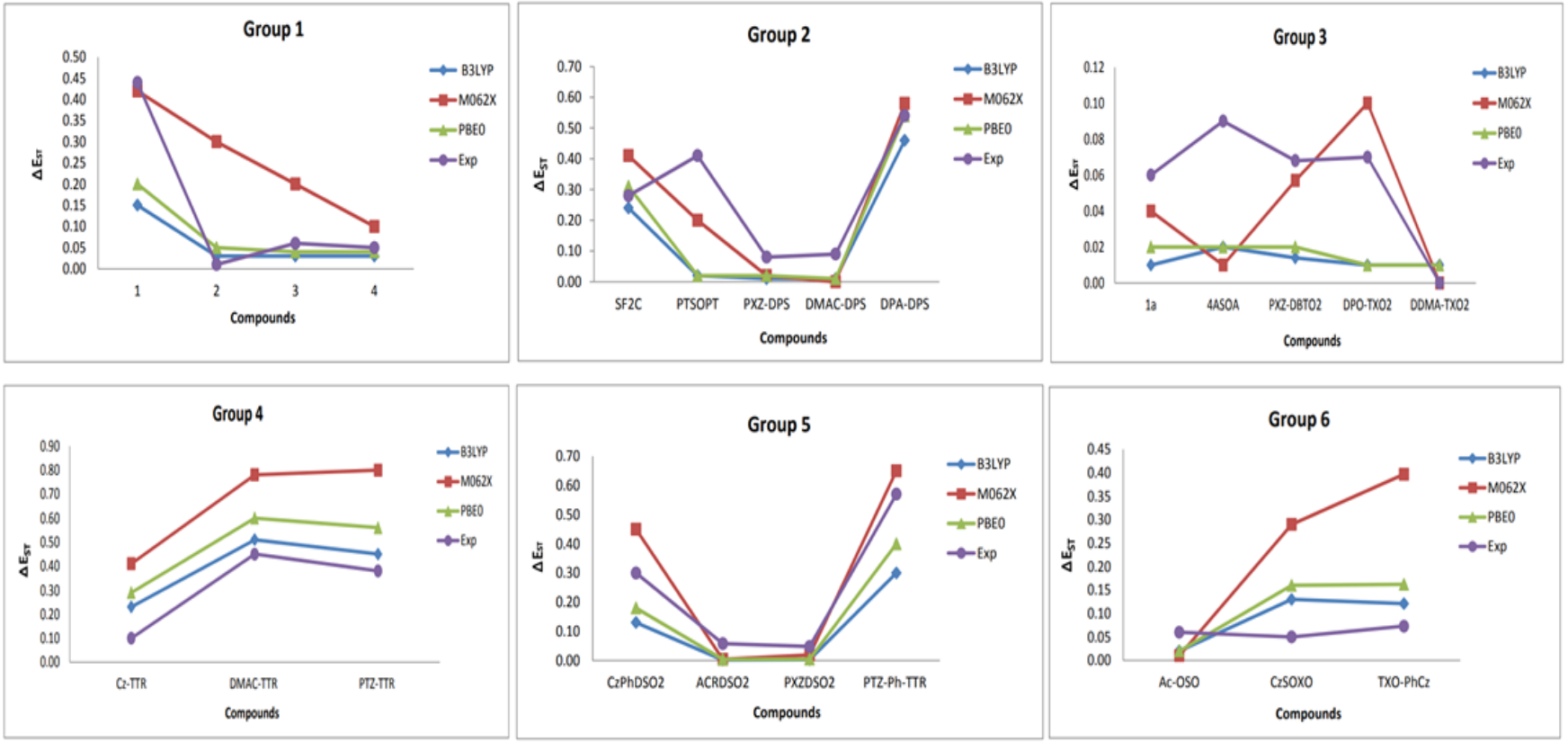

Figure 3.8. Comparison trend between calculated and experimental ΔE_{ST} values.

The value of ΔE_{ST} affects k_{RISC} constant and relationship between k_{RISC} and ΔE_{ST} is shown in Equation 1.6. The experimental k_{RISC} values of ten compounds that are 4, DMAC-DPS, PXZ-DPS, 4ASOA, PXZ-DBTO2, DPO-TXO2, DDMA-TXO2, Cz-TTR, Ac-OSO and CzSOXO are available in literature. The experimental and calculated ΔE_{ST} values and the relationship between k_{RISC}-$1/\Delta E_{ST}$ of these compounds generated by three different functionals are expressed in Figure 3.9. As shown in Figure 3.9.A, B3LYP and PBE0 give similar results and M062X gives higher values when compared to other functionals. We cannot say that functionals generate the trend same as experimental trend. However, B3LYP generates the most similar trend to the experimental data for selected group of compounds as similar to the assessment of all compounds in Figure 3.8. According to Equation (1.6), proportional relationship between k_{RISC} and $1/\Delta E_{ST}$ is expected and Figure 3.9.B shows that all of the functionals generate proportional relationship between k_{RISC} and $1/\Delta E_{ST}$. The comparison between functionals was done via R^2 factor. B3LYP gives the highest R^2=0,63 factor while PBE0 and M062X follow B3LYP with R^2 factors 0,3536 and 0,0516. To sum up, B3LYP is the best functional to generate ΔE_{ST} values. However, we know that it accidentally gives ΔE_{ST} values close to experimental data as mentioned before.

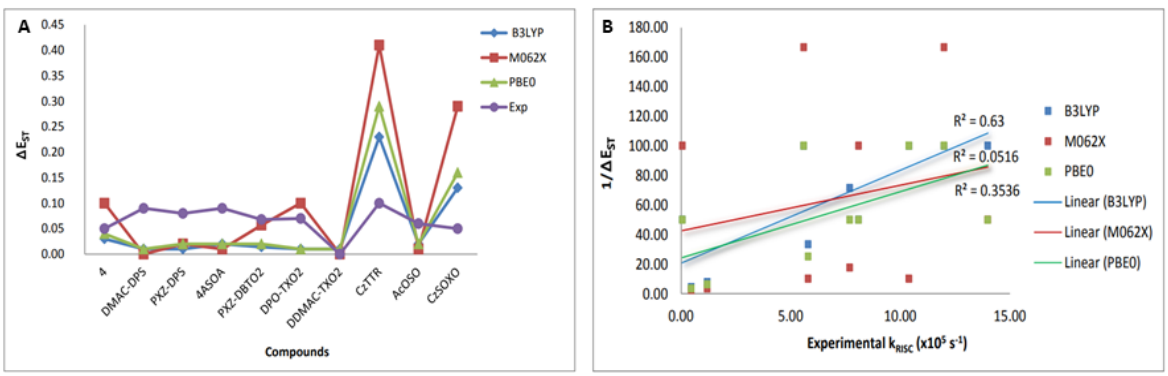

Figure 3.9. Graph representing relationship between calculated-experimental ΔE_{ST} and k_{RISC}-$1/\Delta E_{ST}$.

3.2.4. SOC Constants

Spin-orbit coupling (SOC) is one of the important descriptors required for RISC process. We know that SOC value is proportional to the atomic number so heavy atom containing compounds have higher SOC constants compared to organic compounds. In addition, SOC has property which is that when S_1 and T_1 states have same nature such as CT vs CT or LE vs LE, SOC constants are prone to be smaller while S_1 and T_1 states have different nature such as CT vs LE or LE vs CT, SOC constants are prone to be higher values. According to mathematical description of Equation 1.6, high SOC constant and small ΔE_{ST} values are required to obtain high k_{RISC}. SOC constants were generated with B3LYP, M062X and PBE0 functionals with DZP basis set. The usage of T_1 geometries to calculate SOC constants is more rationale because RISC occurs from T_1 excited state to S_1 excited state.

According to Table 3.14 and Figure 3.10, B3LYP and PBE0 functionals give similar SOC constants. M062X gives the highest LE nature among all functionals in triplet state and addition of LE character resulted in higher SOC constant as mentioned above, so compounds should have the highest SOC values with M062X functional. However, compounds CzPhDSO2 and PTZ-Ph-TTR do not obey this correlation and two sulfone groups located on TTR acceptor unit may be the reason for that situation, so additional functional ωB97XD was used to calculate SOC constants of compounds at Group 4 and 5 to solve this conflict. The nature of states that are generated with ωB97XD are similar to the M062X functional. However, SOC constants that are generated with ωB97XD functional are almost the same with M062X as can be seen from Figure 3.10. As a result, the addition of ωB97XD functional is not effective solution to solve the problem of stated compounds.

Table 3.14. SOC constants of studied compounds with different functionals (B3LYP, M062X, PBE0 and ωB97XD) and DZP basis set.

GROUP 1				
	B3LYP	**M062X**	**PBE0**	
1	0.268	0.485	0.298	
2	0.021	0.255	0.030	
3	0.001	0.191	0.000	
4	0.078	0.374	0.090	
5	0.108	0.231	0.121	
GROUP 2				
	B3LYP	**M062X**	**PBE0**	
SF2C	0.159	0.233	0.169	
PTSOPT	0.020	0.978	0.022	
PXZ-DPS	0.098	0.444	0.107	
DMAC-DPS	0.078	0.509	0.094	
DPA-DPS	0.091	0.102	0.090	
GROUP 3				
	B3LYP	**M062X**	**PBE0**	
1a	0.002	0.614	0.002	
4ASOA	0.000	0.620	0.000	
PXZ-DBTO2	0.096	0.489	0.107	
DPO-TXO2	0.067	0.668	0.082	
DDMA-TXO2	0.079	0.634	0.098	
GROUP 4				
	B3LYP	**M062X**	**PBE0**	**ωB97XD**
Cz-TTR	0.437	0.103	0.438	0.070
DMAC-TTR	0.344	0.289	0.343	0.228
PXZ-TTR	0.076	0.205	0.077	0.191
PTZ-TTR	0.512	0.441	0.537	0.350
GROUP 5				
	B3LYP	**M062X**	**PBE0**	**ωB97XD**
CzPhDSO2	0.269	0.193	0.257	0.147
ACRDSO2	0.179	0.442	0.206	0.412
PXZDSO2	0.070	0.500	0.082	0.532
PTZ-Ph-TTR	0.100	0.034	0.090	0.029
GROUP 6				
	B3LYP	**M062X**	**PBE0**	
Ac-OSO	0.177	0.510	0.192	
CzSOXO	0.140	0.518	0.152	
TXO-PhCz	0.055	0.210	0.051	

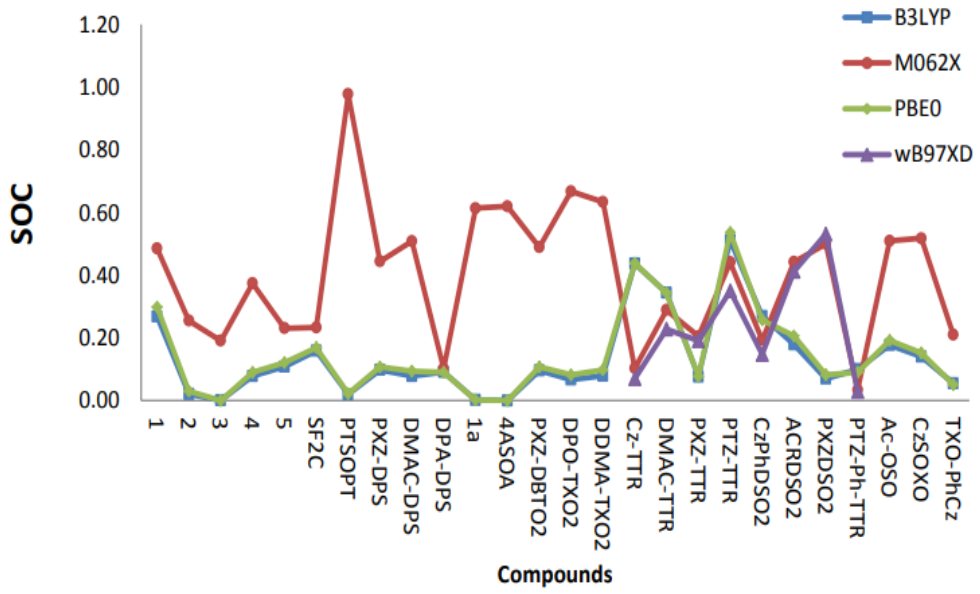

Figure 3.10. The comparison between different functionals for generating SOC constants.

SOC constants have proportional relationship with k_{RISC} as mentioned in Equation (1.6). To provide rationale between experimental results and our calculated results, comparison between experimental k_{RISC} and SOC constants was done. Figure 3.11. shows that M062X is the best functional to generate SOC constants while B3LYP and PBE0 show almost the same trend and have reverse relationship with k_{RISC}.

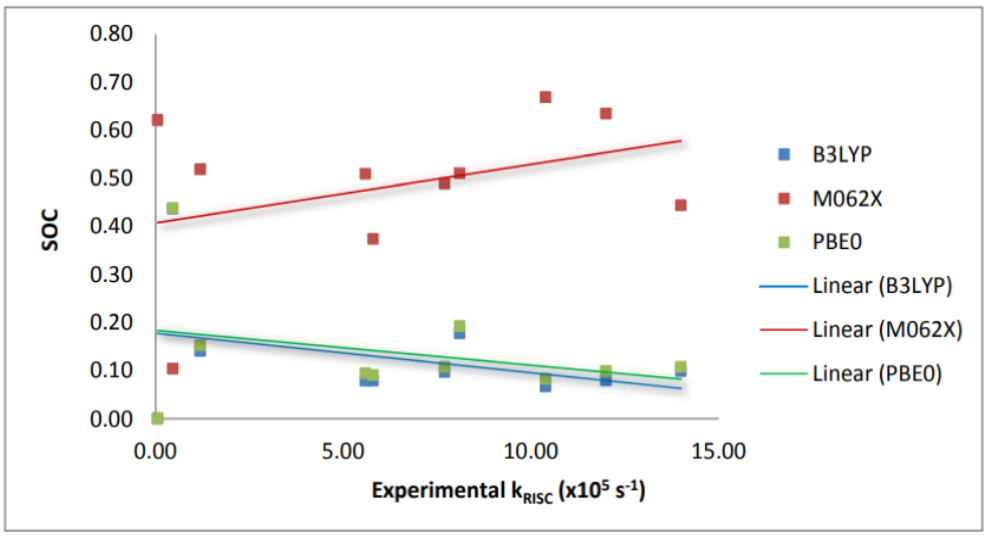

Figure 3.11. Relationship between k_{RISC} and calculated SOC constants with B3LYP, M062X and PBE0 functionals and DZP basis set.

We obtained calculated ΔE_{ST} and SOC constants, so we can provide the theoretical χ term. The theoretical χ term is compared with experimental k_{RISC} values in Figure 3.12. All of the functionals have proportional relationship between experimental k_{RISC} values and theoretical χ terms. B3LYP has the highest R^2 factor when compared to other functionals. However, we know that B3LYP and PBE0 generate reverse relationship between SOC constants and experimental k_{RISC}. As a result, theoretical χ terms are also compared with SOC constants and $1/\Delta E_{ST}$ values. M062X gives the best results and Figure 3.13. contains the relationship between χ terms and other descriptors that constitute χ terms with M062X functional for experimental k_{RISC} available compounds. Linear correlation between χ-SOC and χ-$1/\Delta E_{ST}$ is obtained as expected from Equation (1.6). with 0.2244 and 0.9767 R^2 factors. In addition, the relationship between χ terms and other descriptors that constitute χ terms with B3LYP and PBE0 functionals can be found in appendix part. Despites of M062X, there is reverse relationship between χ-SOC with B3LYP and PBE0 functionals.

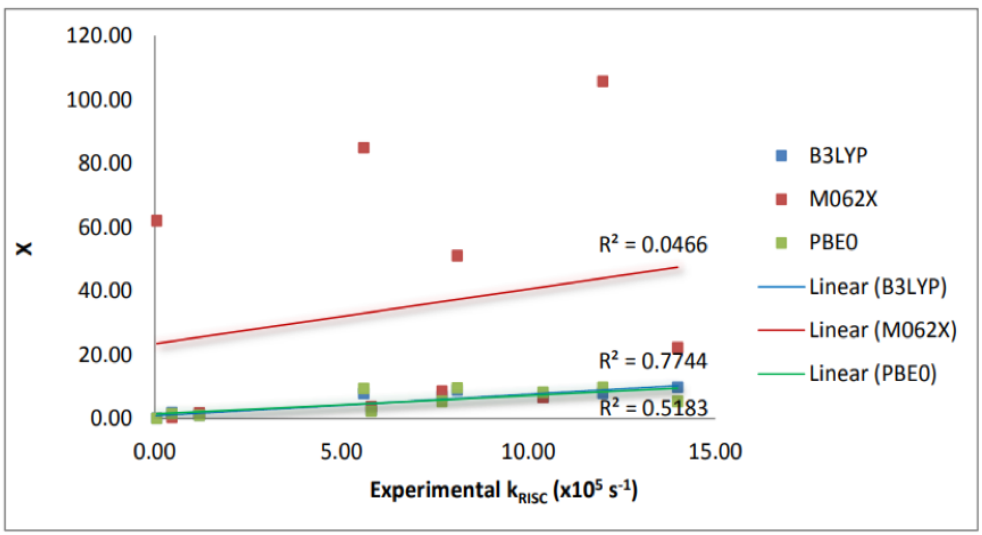

Figure 3.12. The comparison between experimental k_{RISC} values and theoretical χ terms that generated via B3LYP, M062X and PBE0 functionals.

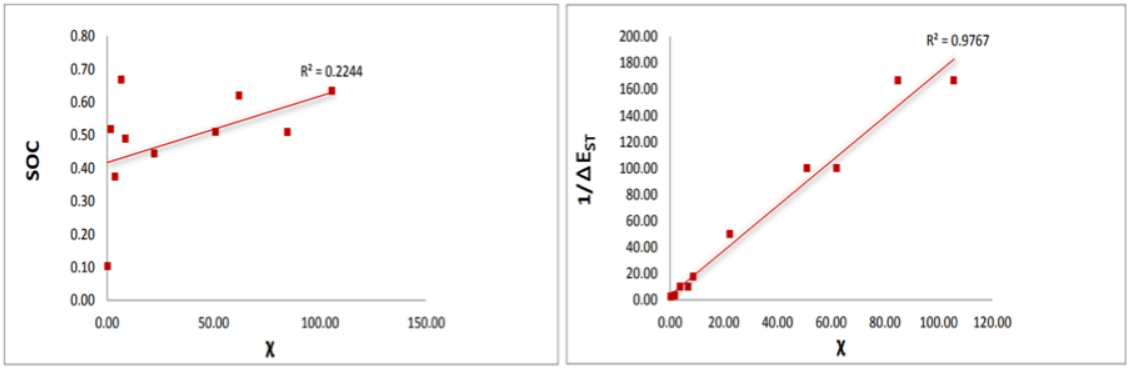

Figure 3.13. The relationship between χ-SOC and χ-$1/\Delta E_{ST}$ with M062X functional.

In addition to RISC SOC constants, we also calculated SOC constants for ISC process with M062X functional because M062X is the best option for calculating SOC constants. S_1 geometries are used for ISC SOC calculation because ISC occurs from S_1 to T_1 state. Singlet excited state has higher energy when compared to triplet excited state and transition from higher energy level to the lower energy level is easier, so we expect to get higher ISC SOC than RISC SOC values. Most of the compounds have higher ISC SOC values while compounds 4, 4ASOA, DMAC-TTR, PXZ-TTR, PTZ-TTR and TXO-PhCz have higher RISC SOC values when compared to ISC SOC values. The reason is that the mutual spin-orbit coupling is rather small for these compounds and vibronic effects may have to be considered [125].

Table 3.15. RISC and ISC SOC constants of Group 1 compounds with different M062X functional and DZP basis set.

GROUP 1		
Compounds	**ISC**	**RISC**
1	0.611	0.485
2	0.260	0.255
3	0.304	0.191
4	0.224	0.374
5	0.603	0.231

Table 3.16. RISC and ISC SOC constants of Group 2 compounds with M062X functional and DZP basis set.

GROUP 2		
Compounds	**ISC**	**RISC**
SF2C	0.667	0.233
PTSOPT	1.115	0.978
PXZ-DPS	1.259	0.444
DMAC-DPS	0.989	0.509
DPA-DPS	0.121	0.102

Table 3.17. RISC and ISC SOC constants of Group 3 compounds with M062X functional and DZP basis set.

GROUP 3		
Compounds	**ISC**	**RISC**
1a	0.869	0.614
4ASOA	0.580	0.620
PXZ-DBTO2	0.992	0.489
DPO-TXO2	1.180	0.668
DDMA-TXO2	0.943	0.634

Table 3.18. RISC and ISC SOC constants of Group 4 compounds with M062X functional and DZP basis set.

GROUP 4		
Compounds	**ISC**	**RISC**
Cz-TTR	0.668	0.103
DMAC-TTR	0.064	0.289
PXZ-TTR	0.143	0.205
PTZ-TTR	0.293	0.441

Table 3.19. RISC and ISC SOC constants of Group 5 compounds with M062X functional and DZP basis set.

GROUP 5		
Compounds	**ISC**	**RISC**
CzPhDSO2	0.295	0.193
ACRDSO2	0.784	0.442
PXZDSO2	0.755	0.500
PTZ-Ph-TTR	0.111	0.034

Table 3.20. RISC and ISC SOC constants of Group 6 compounds with M062X functional and DZP basis set.

GROUP 6		
Compounds	**ISC**	**RISC**
Ac-OSO	0.668	0.510
CzSOXO	1.265	0.518
TXO-PhCz	0.170	0.210

3.2.5. NTO Analysis and Φ_s Indices

To visualize overlap between HOMO and LUMO, natural transition orbital (NTO) analysis was done for singlet and triplet excitations. B3LYP, M062X and PBE0 functionals were used to visualize frontier molecular orbitals at both S_0 and T_1 geometries. Φ_s indice is the measurement of overlap between frontier molecular orbitals, so we expect good correlation between frontier molecular orbitals visualization and Φ_s indices. Lowdin and mulliken charge distributions are used to obtain Φ_s indices. Higher overlap resulted in higher Φ_s indices while smaller overlap resulted in smaller Φ_s indices. Φ_s indices increase with the increase at LE character because overlap between HOMO and LUMO increases with LE character. As previous results, B3LYP and PBE0 almost give same results while M062X shows more delocalized distribution (higher overlap). According to TADF mechanism, singlet excitations have good charge separation, CT, character and HOMO is located on donor unit while LUMO is located on acceptor unit. The distribution of frontier molecular orbitals and Φ_s indices of compounds with B3LYP, M062X and PBE0 functionals are shown in appendix part.

Cz and DPA donor units have low dihedral angles that resulted in high delocalization and planarization of the compounds. As a result, Cz and DPA containing compounds show high overlap between HOMO and LUMO that is not the desired situation. DMAC and PXZ containing compounds that have ideal or close to ideal dihedral angle have small overlap between HOMO and LUMO. PTZ containing compounds have small overlap with DPS acceptor unit when compared to TTR acceptor unit. The compounds that have planar conformation DMAC-TTR, PTZ-TTR and PTZ-Ph-TTR have high overlap between frontier molecular orbitals. Acceptor units TTR is prone to generate high overlap while DPS, DBSO, DMTD and TXO are prone to generate small overlap between frontier molecular orbitals. The addition of bridge resulted in better charge separation at compounds ACRDSO2 and PXZDSO2 while addition of bridge is not effective for better charge separation at CzPhDSO2 and PTZ-Ph-TTR. Table 3.21-3.22 contain HOMO-LUMO distribution of some compounds at S_0 and T_1 geometries with M062X functional for both $S_0 \rightarrow S_1$ excitation and $S_0 \rightarrow T_1$ excitation.

There is good correlation between distribution of frontier molecular orbitals and Φ_s indices. M062X gives the highest Φ_s indices among all of the studied functionals as expected and reported Φ_s indices are consistent with dihedral angles and overlap between frontier molecular orbitals. Cz and DPA that generate low dihedral angles resulted in high Φ_s indices while DMAC and PXZ that generate perpendicular or close to perpendicular dihedral angles give low Φ_s indices. Table 3.23-3.24 show Φ_s indices in Lowdin and Mulliken charge distributions for $S_0 \rightarrow S_1$ and $S_0 \rightarrow T_1$ excitations with M062X functional.

Table 3.21. Distribution of frontier molecular orbitals for compounds SF2C, DPA-DPS, PXZ-TTR and PXZDS02 at $S_0 \rightarrow S_1$ excitation and $S_0 \rightarrow T_1$ excitation.

Molecule	**M062X/6-31+G(d,p)**			
SF2C	$S_0 \rightarrow S_1$ Excitation		$S_0 \rightarrow T_1$ Excitation	
	HOMO	LUMO	HOMO	LUMO
	S_0 Optimization		S_0 Optimization	
	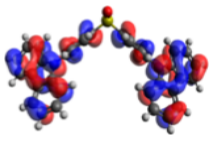	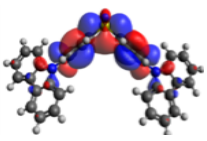	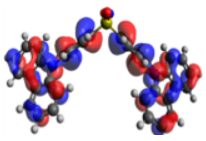	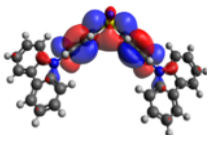
	T_1 Optimization		T_1 Optimization	
	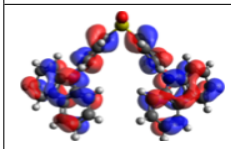	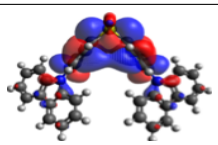	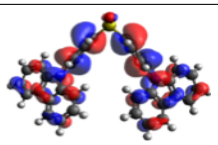	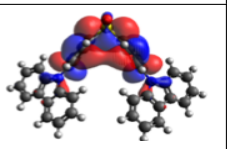
DPA-DPS	S_0 Optimization		S_0 Optimization	
	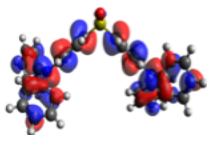	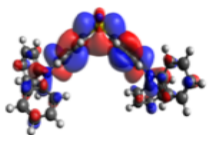	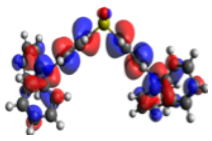	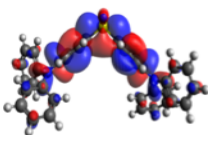
	T_1 Optimization		T_1 Optimization	
	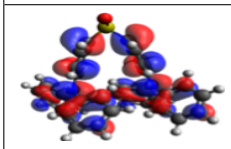	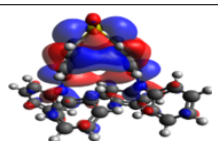	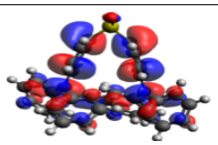	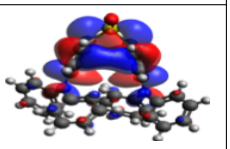
PXZ-TTR	S_0 Optimization		S_0 Optimization	
	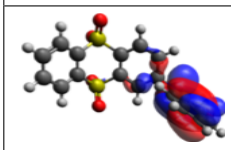	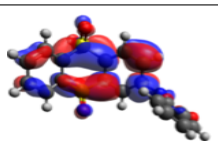	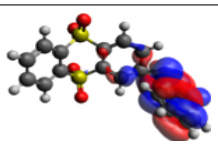	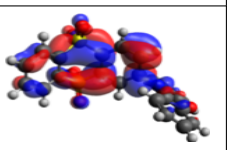
	T_1 Optimization		T_1 Optimization	
	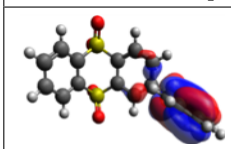	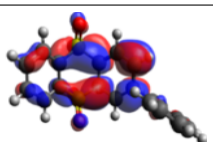	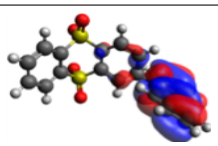	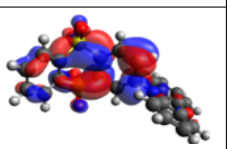
PXZDSO2	S_0 Optimization		S_0 Optimization	
	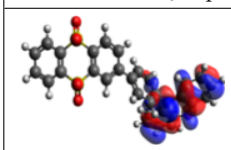	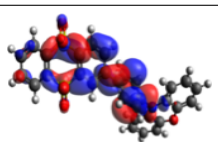	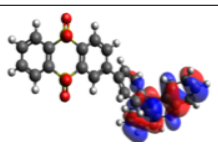	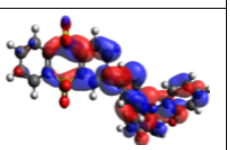
	T_1 Optimization		T_1 Optimization	
	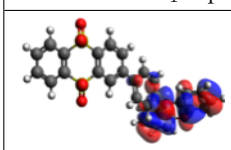	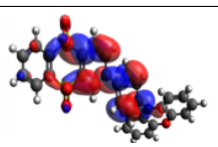	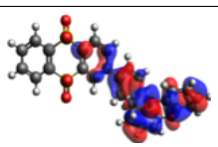	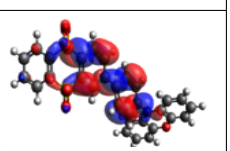

Table 3.22. Distribution of frontier molecular orbitals for compounds 4ASOA, DPO-TXO2, DMAC-TTR and Ac-OSO at $S_0 \rightarrow S_1$ excitation and $S_0 \rightarrow T_1$ excitation.

Molecule	**M062X/6-31+G(d,p)**			
4ASOA	$S_0 \rightarrow S_1$ Excitation		$S_0 \rightarrow T_1$ Excitation	
	HOMO	LUMO	HOMO	LUMO
	S_0 Optimization		S_0 Optimization	
	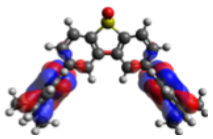			
	T_1 Optimization		T_1 Optimization	
				
DPO-TXO2	S_0 Optimization		S_0 Optimization	
	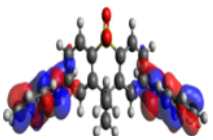		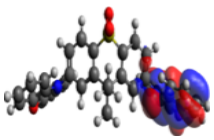	
	T_1 Optimization		T_1 Optimization	
	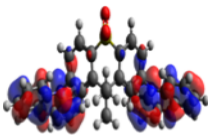		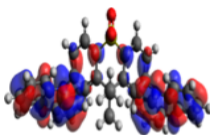	
DMAC-TTR	S_0 Optimization		S_0 Optimization	
	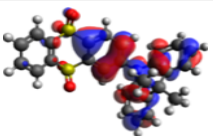		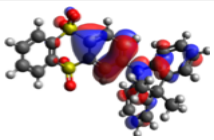	
	T_1 Optimization		T_1 Optimization	
	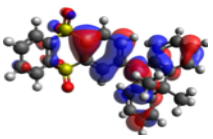		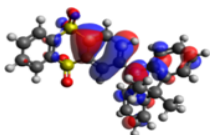	
Ac-OSO	S_0 Optimization		S_0 Optimization	
	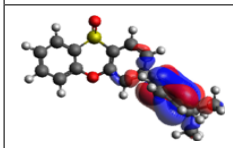		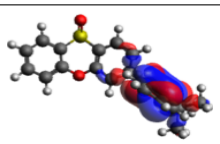	
	T_1 Optimization		T_1 Optimization	
	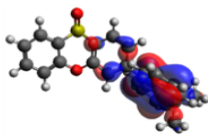		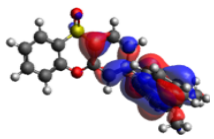	

Table 3.23. Φ_s indices for studied compounds in Lowdin (L) and Mulliken (M) charge distributions for the excitations from S_0 to S_1 (TDA:M062X/6-31+G(d,p)).

GROUP 1				
Compound	**S_0 Geometry**		**T_1 Geometry**	
	L	**M**	**L**	**M**
1	0.5570	0.6595	0.5968	0.7386
2	0.4703	0.5810	0.3306	0.4352
3	0.4383	0.5456	0.4230	0.5027
4	0.3939	0.4601	0.3352	0.4861
5	0.7416	0.8776	0.6402	0.8128
GROUP 2				
Compound	**S_0 Geometry**		**T_1 Geometry**	
	L	**M**	**L**	**M**
SF2C	0.7047	0.7487	0.7269	0.8004
PTSOPT	0.3310	0.4202	0.2434	0.3683
PXZ-DPS	0.2485	0.4401	0.5146	0.7627
DMAC-DPS	0.1642	0.2308	0.3938	0.5478
DPA-DPS	0.7594	0.8234	0.7631	0.8279
GROUP 3				
Compound	**S_0 Geometry**		**T_1 Geometry**	
	L	**M**	**L**	**M**
1a	0.1854	0.3092	0.1602	0.1786
4ASOA	0.1712	0.1825	0.1567	0.1668
PXZ-DBTO2	0.1435	0.2702	0.5615	0.6611
DPO-TXO2	0.2809	0.4708	0.4694	0.5873
DDMA-TXO2	0.3465	0.4097	0.4591	0.5519
GROUP 4				
Compound	**S_0 Geometry**		**T_1 Geometry**	
	L	**M**	**L**	**M**
Cz-TTR	0.5372	0.6048	0.6195	0.6939
DMAC-TTR	0.7150	0.8397	0.7653	0.8827
PXZ-TTR	0.5143	0.6580	0.6361	0.7622
PTZ-TTR	0.6951	0.8025	0.7249	0.8336
GROUP 5				
Compound	**S_0 Geometry**		**T_1 Geometry**	
	L	**M**	**L**	**M**
CzPhDSO2	0.7649	0.8196	0.7635	0.8161
ACRDSO2	0.4644	0.5488	0.5449	0.6122
PXZDSO2	0.2247	0.3882	0.7169	0.8632
PTZ-Ph-TTR	0.6631	0.7579	0.7470	0.7856
GROUP 6				
Compound	**S_0 Geometry**		**T_1 Geometry**	
	L	**M**	**L**	**M**
Ac-OSO	0.2870	0.3644	0.4516	0.5277
CzSOXO	0.5029	0.5709	0.5565	0.6294
TXO-PhCz	0.4630	0.4849	0.5933	0.6367

Table 3.24. Φ_s indices for studied compounds in Lowdin (L) and Mulliken (M) charge distributions for the excitations from S_0 to T_1 (TDA:M062X/6-31+G(d,p)).

GROUP 1				
Compound	**S_0 Geometry**		**T_1 Geometry**	
	L	**M**	**L**	**M**
1	0.7721	0.8781	0.8210	0.9206
2	0.7920	0.8824	0.5113	0.6086
3	0.7597	0.8619	0.4744	0.5660
4	0.6062	0.6792	0.4828	0.6695
5	0.8193	0.9671	0.7883	0.9065
GROUP 2				
Compound	**S_0 Geometry**		**T_1 Geometry**	
	L	**M**	**L**	**M**
SF2C	0.8405	0.8789	0.8563	0.9120
PTSOPT	0.7845	0.9099	0.2758	0.3985
PXZ-DPS	0.4301	0.5961	0.4778	0.7106
DMAC-DPS	0.1692	0.2371	0.5399	0.6931
DPA-DPS	0.8375	0.8890	0.8288	0.8957
GROUP 3				
Compound	**S_0 Geometry**		**T_1 Geometry**	
	L	**M**	**L**	**M**
1a	0.3842	0.4907	0.2250	0.2466
4ASOA	0.2102	0.2224	0.1627	0.1767
PXZ-DBTO2	0.5049	0.6072	0.5848	0.6788
DPO-TXO2	0.8393	0.8954	0.5074	0.6271
DDMA-TXO2	0.3422	0.4047	0.5383	0.6278
GROUP 4				
Compound	**S_0 Geometry**		**T_1 Geometry**	
	L	**M**	**L**	**M**
Cz-TTR	0.6815	0.7521	0.9528	0.9714
DMAC-TTR	0.7941	0.8950	0.8429	0.9354
PXZ-TTR	0.5156	0.6590	0.6152	0.7430
PTZ-TTR	0.8187	0.9002	0.8268	0.9242
GROUP 5				
Compound	**S_0 Geometry**		**T_1 Geometry**	
	L	**M**	**L**	**M**
CzPhDSO2	0.9017	0.9655	0.8941	0.9296
ACRDSO2	0.4545	0.5344	0.8311	0.9064
PXZDSO2	0.5210	0.6610	0.7065	0.8476
PTZ-Ph-TTR	0.8496	0.9997	0.8352	0.8776
GROUP 6				
Compound	**S_0 Geometry**		**T_1 Geometry**	
	L	**M**	**L**	**M**
Ac-OSO	0.3646	0.4385	0.5842	0.6816
CzSOXO	0.5258	0.5702	0.6481	0.7195
TXO-PhCz	0.4285	0.4437	0.7680	0.8301

Φ_s indices can increase or decrease at T_1 geometry when compared to S_0 geometry. This results from changes between S_0 and T_1 geometries. The comparison between S_0 and T_1 geometries of Φ_s indices is shown in Figure 3.14 for M062X functional. The Φ_s indices obtained from singlet excitations and Lowdin charge distribution are used in Figure 3.14. because Lowdin charge distribution generates more accurate results when compared to Mulliken charge distribution. As shown in Figure 3.14, Φ_s indices of S_0 and T_1 geometries are different. This is expected result because these geometries have different dihedral angles and different dihedral angles resulted in changes at overlap between HOMO and LUMO, so Φ_s indices.

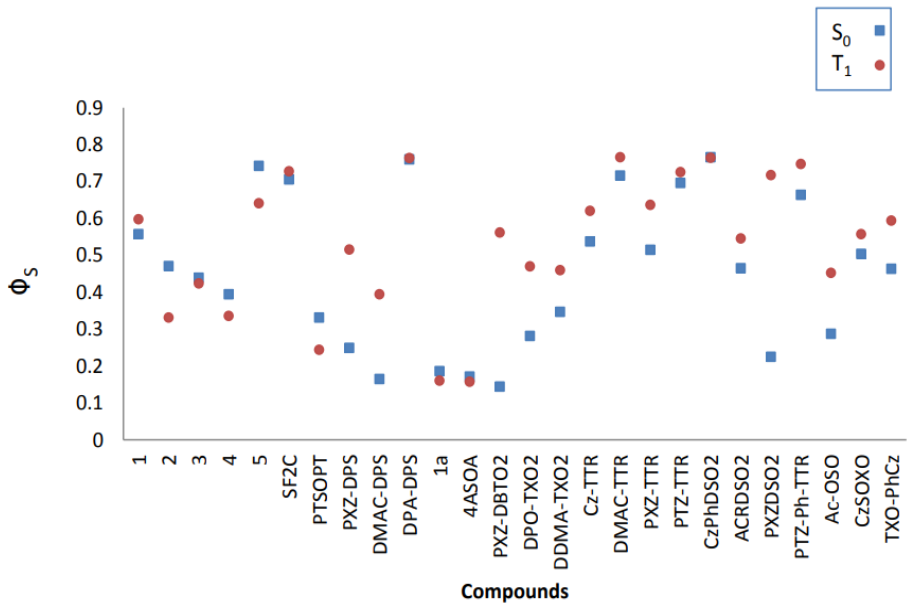

Figure 3.14. Φ_s indices of studied compounds at S_0 and T_1 geometries with M062X functional.

To obtain small ΔE_{ST}, small overlap between HOMO and LUMO is required and small overlap means small Φ_s indices, so the correlation between ΔE_{ST} and Φ_s indices is expected. To examine this relationship, the graph was generated in Figure 3.15. As expected, proportional relationship between Φ_s indices and ΔE_{ST} values is observed.

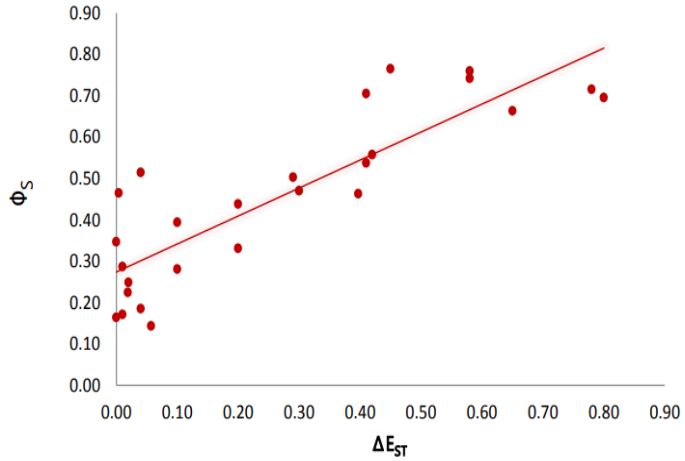

Figure 3.15. Relationship between Φ_s indices and ΔE_{ST} values for all of the studied compounds with M062X functional.

Finally, the relationship between SOC constants and Φ_s indices was examined and Figure 3.16 shows relationship between SOC constants and Φ_s indices for all of the studied compounds with M062X functional. S_1 and T_1 excited states Φ_s indices obtained from S_0 geometries are shown in Figure 3.16. There is reverse relationship between SOC constants and Φ_s indices. As mentioned in SOC constants section, the difference at the nature of S_1 and T_1 excited states has important effect on SOC constant, so it is not rationale to describe to relationship between SOC constants and Φ_s indices based on one excited state. S_1 and T_1 excited states should be treated together.

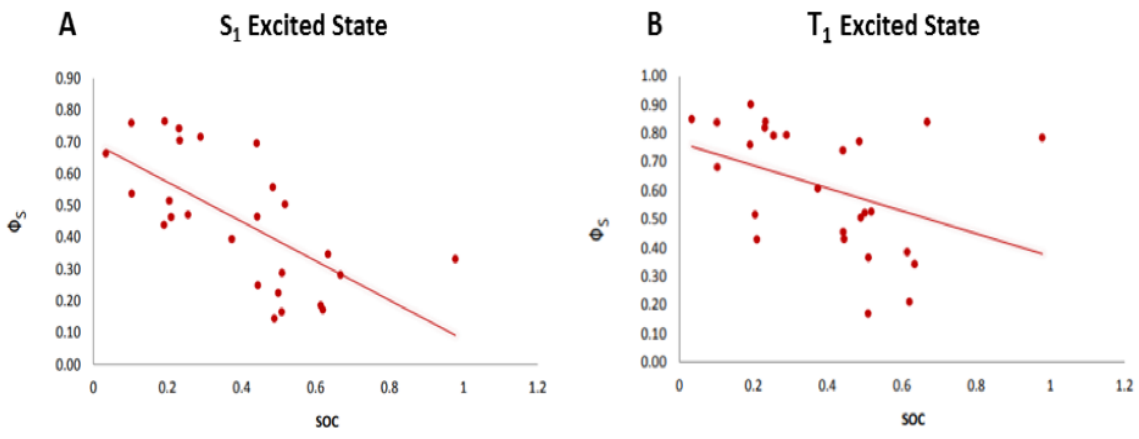

Figure 3.16. Relationship between SOC constants and Φ_s indices for all of the studied compounds with M062X functional.

3.3. Theoretical Spectra

UV-Vis absorption spectra of compounds were generated with B3LYP, M062X, PBE0 and BLYP functionals and 6-311++G(3df,3pd) was used as extrabasis set while 6-31+G(d,p) was used as basis set. In order to examine the $S_0 \rightarrow S_1$ excitation, 40 different initial coordinates, conformations, are provided by Wigner distribution and experimental spectra solvents were used at calculations. Almost all of the compounds have absorption spectra in toluene except for 1a and Cz-TTR. 1a has experimental absorption spectrum in DCM while Cz-TTR has experimental absorption spectrum in ethyl ethanoate. In addition, CzPhDSO2 has absorption spectrum in film, so theoretical spectra were generated in toluene. Compounds 5 and PXZ-TTR do not have experimental absorption spectra data.

According to comparison between experimental and theoretical spectra, B3LYP is the best functional to generate absorption spectra. However, there is same situation for B3LYP functional as explained in ΔE_{ST} section. B3LYP gives wrong natures of states and accidentally generates absorption spectra that similar to experimental absorption spectra. PBE0 follows the B3LYP functional and they generate similar absorption spectra at some of the compounds such as 2, 4, DMAC-DPS etc. M062X functional shows hypsochromic shift (blue shift) while BLYP shows bathochromic shift (red shift) when compared to other functionals. BLYP has the highest theoretical λ_{max} values while M062X has the lowest λ_{max} values as expected. Despite generating hypsochromic shift, M062X is the best functional to reproduce absorption spectra of PTSOPT, DPA-DPS, 1a, DDMA-TXO2 and PTZ-Ph-TTR. It is interesting for 1a and DDMA-TXO2 because these compounds have rigid acceptor and donor units that resulted in good charge separation CT character. Theoretical absorption spectra are reported in Figure 3.17–3.22. Experimental absorption spectra can be found in Appendix C.1-C.6.

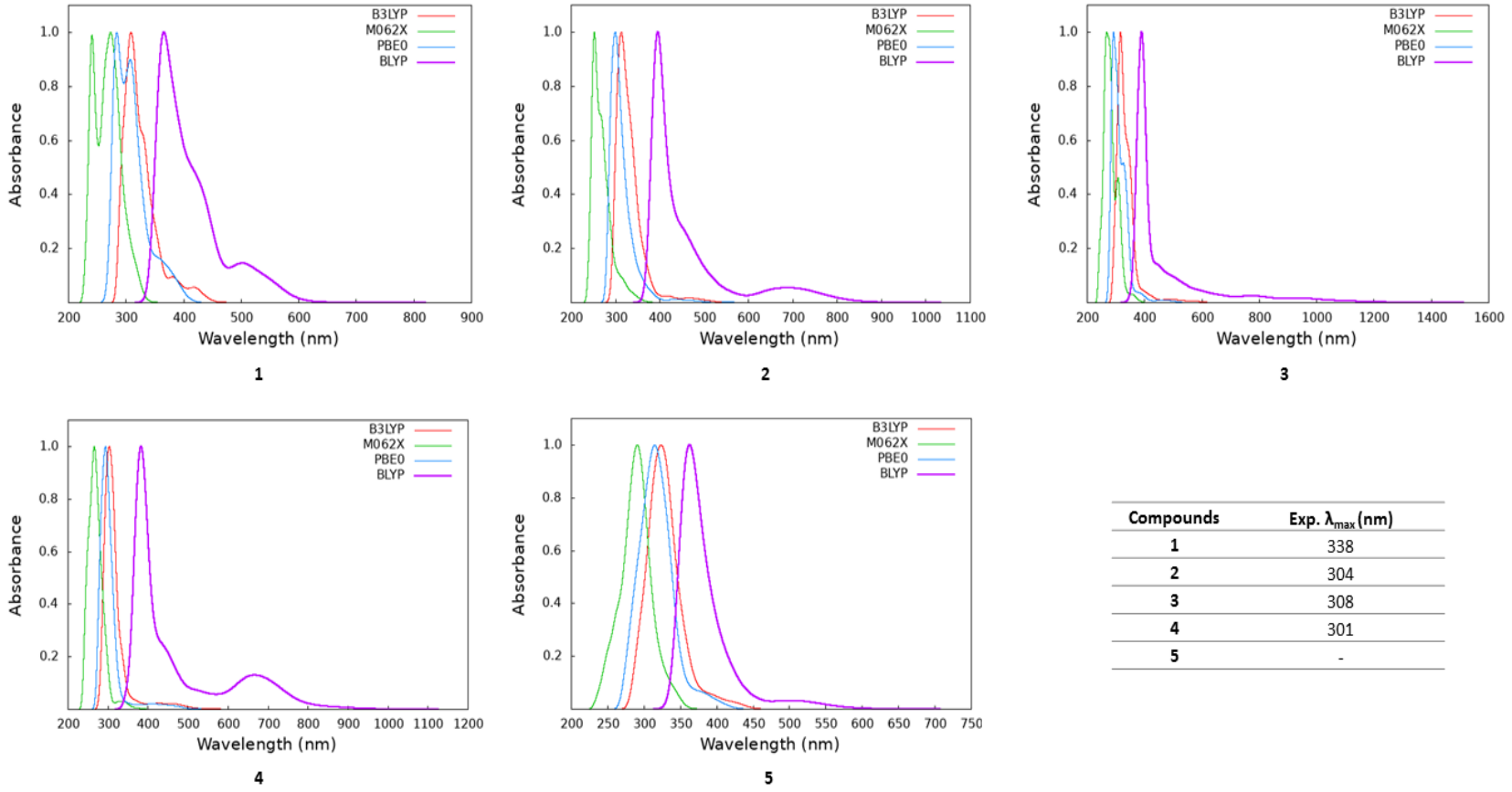

Compounds	Exp. λ_{max} (nm)
1	338
2	304
3	308
4	301
5	-

Figure 3.17. Absorption spectra for Group 1 TADF emitters calculated at different levels of theory and experimental λ_{max} values in nm 'see experimental spectra in Appendix C.1' [47].

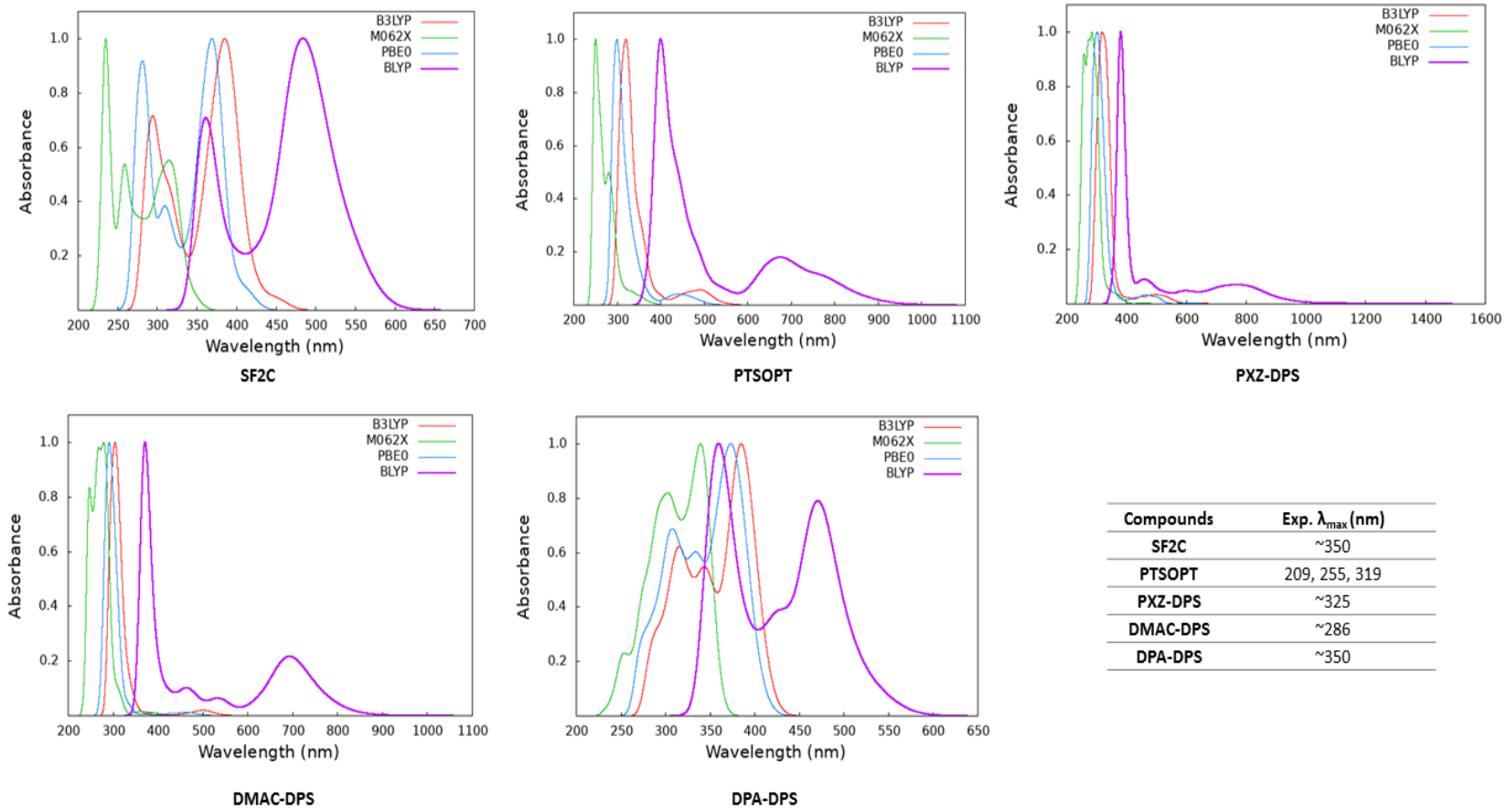

Compounds	Exp. λ_{max} (nm)
SF2C	~350
PTSOPT	209, 255, 319
PXZ-DPS	~325
DMAC-DPS	~286
DPA-DPS	~350

Figure 3.18. Absorption spectra for Group 2 TADF emitters calculated at different levels of theory and experimental λ_{max} values in nm 'see experimental spectra in Appendix C.2' [33,54-56].

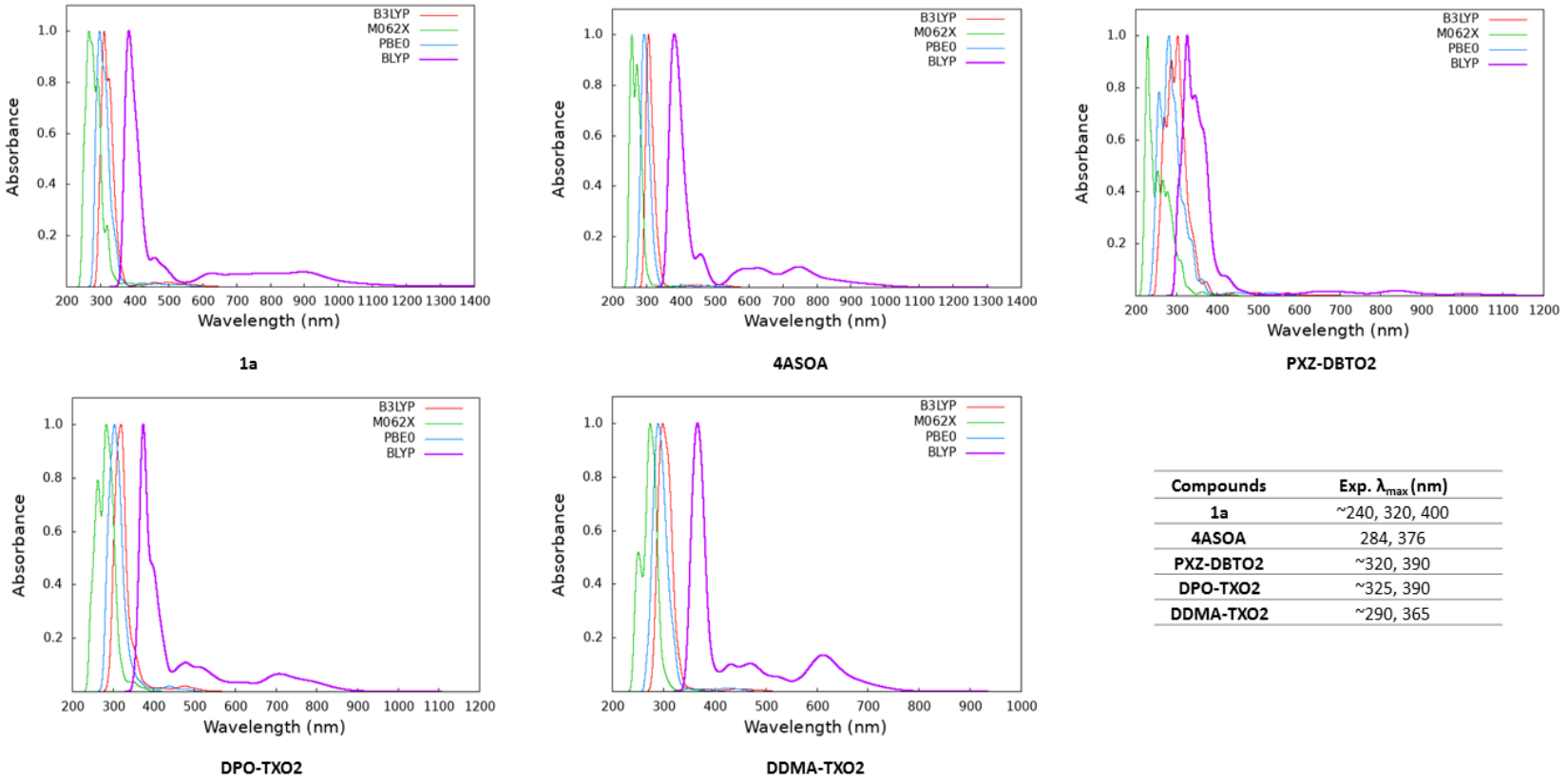

Compounds	Exp. λ_{max} (nm)
1a	~240, 320, 400
4ASOA	284, 376
PXZ-DBTO2	~320, 390
DPO-TXO2	~325, 390
DDMA-TXO2	~290, 365

Figure 3.19. Absorption spectra for Group 3 TADF emitters calculated at different levels of theory and experimental λ_{max} values in nm 'see experimental spectra in Appendix C.3' [20,22,71,81].

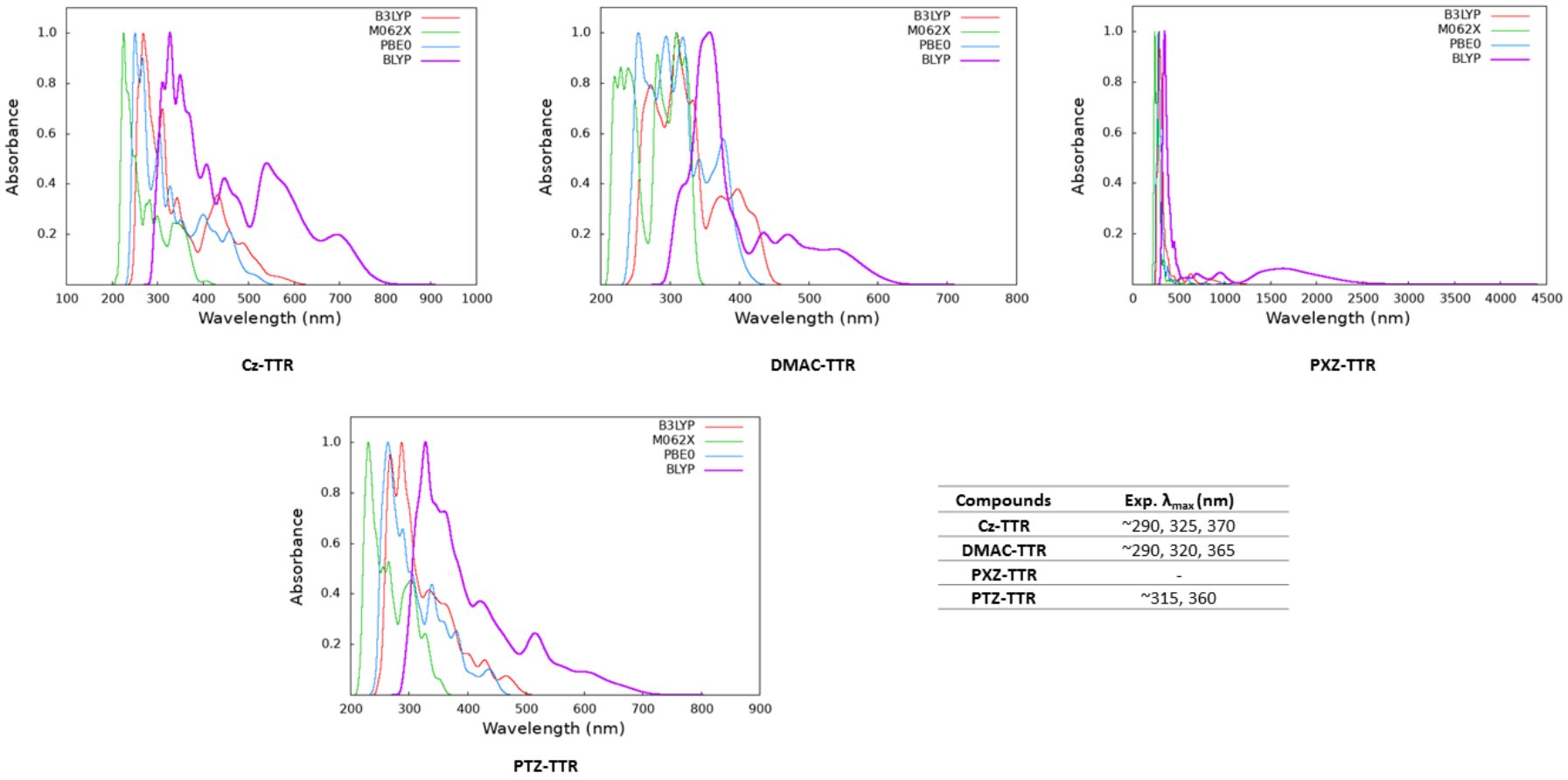

Compounds	Exp. λ_{max} (nm)
Cz-TTR	~290, 325, 370
DMAC-TTR	~290, 320, 365
PXZ-TTR	-
PTZ-TTR	~315, 360

Figure 3.20. Absorption spectra for Group 4 TADF emitters calculated at different levels of theory and experimental λ_{max} values in nm 'see experimental spectra in Appendix C.4' [36,84,85].

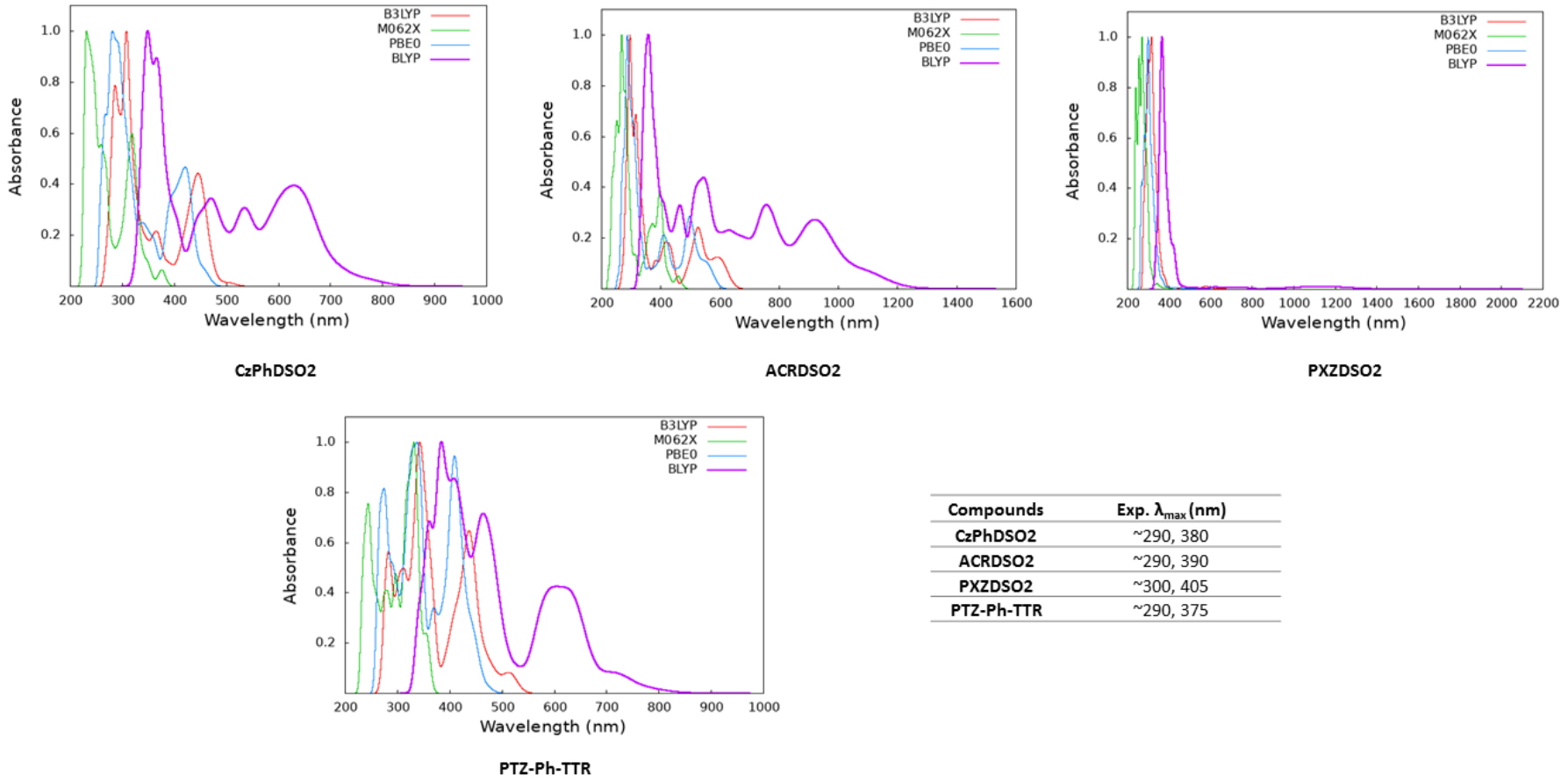

Compounds	Exp. λ_{max} (nm)
CzPhDSO2	~290, 380
ACRDSO2	~290, 390
PXZDSO2	~300, 405
PTZ-Ph-TTR	~290, 375

Figure 3.21. Absorption spectra for Group 5 TADF emitters calculated at different levels of theory and experimental λ_{max} values in nm 'see experimental spectra in Appendix C.5' [84,86,87].

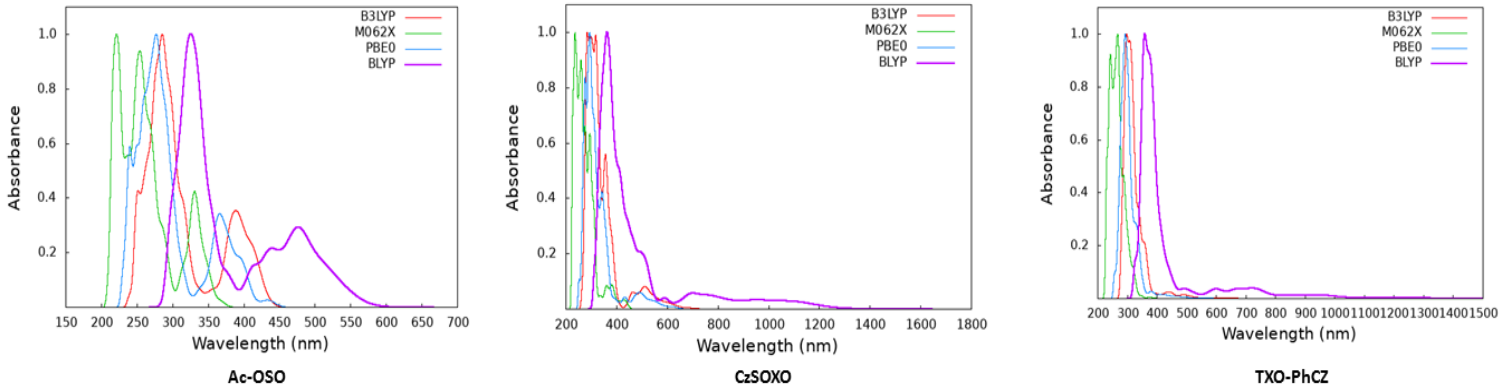

Compounds	Exp. λ_{max} (nm)
Ac-OSO	~360
CzSOXO	~330
TXO-PhCz	~300, 400

Figure 3.22. Absorption spectra for Group 6 TADF emitters calculated at different levels of theory and experimental λ_{max} values in nm 'see experimental spectra in Appendix C.6' [63,75,90].

4. CONCLUSION

Several descriptors were analyzed to get rationale for efficient TADF mechanism. Geometries and dihedral angles are one of the analyzed descriptors because of their impact on TADF efficiency. According to comparison between ground and excited states geometries, dihedral angles show deviations and some of the folded donor structures become planar at excited states. In addition, dihedral angles change with respect to donor unit and flexible donor units such as Cz and DPA resulted in low dihedral angle which is not the desired situation for TADF mechanism while rigid donor units resulted in ideal dihedral angles.

Natures of excited states were examined and M062X was shown to give the highest LE character while B3LYP and PBE0 functionals give similar natures. Generally, singlet excitations have CT character as expected from TADF mechanism with all of the functional while we can say that M062X is the only functional that gives correct nature of states (LE) for triplet excitations. Differences at S_0 and T_1 geometries resulted in changes at nature of states at some of the compounds.

Ideal dihedral angle and small overlap between HOMO and LUMO are the most known strategy to obtain low ΔE_{ST} values. According to calculated ΔE_{ST} values, M062X gives higher results among all of the functionals. This is expected because M062X gives the highest LE character which means higher overlap between HOMO and LUMO. Low dihedral angles resulted in high ΔE_{ST} values while high dihedral angles resulted in low ΔE_{ST} values. According to comparison between theoretical and experimental ΔE_{ST} values and relationship between experimental k_{RISC} and $1/\Delta E_{ST}$, B3LYP is the best functional. However, B3LYP generates wrong nature of states for triplet excitations and energies for excited states, so we can say that B3LYP accidentally gives the ΔE_{ST} values close to experimantal data.

SOC is important descriptor for RISC process and SOC constants obtained from M062X functional give the highest values in general. The proportional relationship

between k_{RISC} and SOC constants was obtained with M062X functional while other functionals give reverse relationship which is not correct. In addition, the relationship between (R)ISC probability (χ) and SOC-1/ΔE_{ST} is examined and M062X was obtained as the best functional. Lastly, ISC SOC values were obtained and ISC SOC values are higher than RISC SOC values at most of the compounds.

The results of NTO analysis are consistent with previous results and M062X gives the more delocalized distribution while B3LYP and PBE0 give localized distribution. Some of the acceptor groups are prone to generate high overlap such as TTR while DPS, DBSO, DMTD and TXO are prone to generate small overlap between frontier molecular orbitals. In addition, dihedral angle has effect on overlap and low dihedral angle resulted in high overlap. The Φ_s indices are in good correlation with distribution of frontier molecular orbitals and M062X gives the highest results among studied functionals. Because of the differences between dihedral angles, S_0 and T_1 states have different Φ_s indices. As expected, proportional relationship between Φ_s indices and ΔE_{ST} is obtained because the increase in Φ_s indices means an increase at overlap and this resulted in high ΔE_{ST} values.

According to comparison between theoretical and experimental absorption spectra, B3LYP is the best functional for generating absorption spectra. However, B3LYP is not reliable functional because of the wrong nature of states and energies as mentioned above. M062X shows hypsochromic shift while BLYP shows bathochromic shift. In contrast to absorption spectra, reproduced emission spectra are not successful when compared to colors of experimental and theoretical spectra. As is seen from generated spectra, PXZ and PTZ containing compounds are prone to generate higher emission wavelength and addition of bridge unit causes smaller emission wavelength.

To sum up, different sulfone-based TADF emitters were examined and effect of building moieties on the efficiency of TADF mechanism was discussed. According to ΔE_{ST} results, B3LYP accidentally generates the best results and this is the reason of mostly usage of B3LYP at literature. However, M062X is the only functional that gives the correct relationship with SOC and the relationship between χ and SOC-1/ΔE_{ST}

confirms the M062X as the most reliable functional. This study can give an idea about the design strategy of sulfone-based TADF emitters and correct functional for DFT studies.

REFERENCES

1. Tang, C. W. and S. A. Vanslyke, "Organic Electroluminescent Diodes", *Applied Physics Letters*, Vol. 51, No. 12, pp. 913–915, 1987.

2. Zhang, Q., H. Kuwabara, W. J. Potscavage, S. Huang, Y. Hatae, T. Shibata and C. Adachi, "Anthraquinone-Based Intramolecular Charge-Transfer Compounds: Computational Molecular Design, Thermally Activated Delayed Fluorescence, and Highly Efficient Red Electroluminescence", *Journal of the American Chemical Society*, Vol. 136, No. 52, pp. 18070–18081, 2014.

3. Uoyama, H., K. Goushi, K. Shizu, H. Nomura and C. Adachi, "Highly Efficient Organic Light-Emitting Diodes from Delayed Fluorescence", *Nature*, Vol. 492, No. 7428, pp. 234–238, 2012.

4. Li, Y., J. Y. Liu, Y. D. Zhao and Y. C. Cao, "Recent Advancements of High Efficient Donor–Acceptor Type Blue Small Molecule Applied for OLEDs", *Materials Today*, Vol. 20, No. 5, pp. 258–266, 2017.

5. Articles, F., "Element Made in Asia for the First Time", Vol. 26, No. 2, 2016.

6. Gadirov, R. M., R. R. Valiev, L. G. Samsonova, K. M. Degtyarenko, N. V. Izmailova, A. V. Odod, S. S. Krasnikova, I. K. Yakushchenko and T. N. Kopylova, "Thermally Activated Delayed Fluorescence in Dibenzothiophene Sulfone Derivatives: Theory and Experiment", *Chemical Physics Letters*, Vol. 717, pp. 53–58, 2019.

7. Chatterjee, T. and K. T. Wong, "Perspective on Host Materials for Thermally Activated Delayed Fluorescence Organic Light Emitting Diodes", *Advanced Optical Materials*, Vol. 7, pp. 1–34, 2019.

8. Alipour, M. and Z. Safari, "Photophysics of OLED Materials with Emitters Ex-

hibiting Thermally Activated Delayed Fluorescence and Used in Hole/Electron Transporting Layer from Optimally Tuned Range-Separated Density Functional Theory", *Journal of Physical Chemistry C*, Vol. 123, No. 1, pp. 746–761, 2019.

9. Im, Y., M. Kim, Y. J. Cho, J. A. Seo, K. S. Yook and J. Y. Lee, "Molecular Design Strategy of Organic Thermally Activated Delayed Fluorescence Emitters", *Chemistry of Materials*, Vol. 29, No. 5, pp. 1946–1963, 2017.

10. Adachi, C., M. A. Baldo, M. E. Thompson and S. R. Forrest, "Nearly 100% Internal Phosphorescence Efficiency in an Organic Light Emitting Device", *Journal of Applied Physics*, Vol. 90, No. 10, pp. 5048–5051, 2001.

11. Su, S. J., H. Sasabe, Y. J. Pu, K. I. Nakayama and J. Kido, "Tuning Energy Levels of Electron-Transport Materials by Nitrogen Orientation for Electrophosphorescent Devices with an Ideal Operating Voltage", *Advanced Materials*, Vol. 22, No. 30, pp. 3311–3316, 2010.

12. Kim, M. and J. Y. Lee, "Engineering the Substitution Position of Diphenylphosphine Oxide at Carbazole for Thermal Stability and High External Quantum Efficiency Above 30% in Blue Phosphorescent Organic Light-Emitting Diodes", *Advanced Functional Materials*, Vol. 24, No. 26, pp. 4164–4169, 2014.

13. Wang, Q., I. W. Oswald, X. Yang, G. Zhou, H. Jia, Q. Qiao, Y. Chen, J. Hoshikawa-Halbert and B. E. Gnade, "A Non-Doped Phosphorescent Organic Light-Emitting Device with Above 31% External Quantum Efficiency", *Advanced Materials*, Vol. 26, No. 48, pp. 8107–8113, 2014.

14. Udagawa, K., H. Sasabe, C. Cai and J. Kido, "Low-Driving-Voltage Blue Phosphorescent Organic Light-Emitting Devices with External Quantum Efficiency of 30%", *Advanced Materials*, Vol. 26, No. 29, pp. 5062–5066, 2014.

15. Lee, C. W. and J. Y. Lee, "Above 30% External Quantum Efficiency in Blue Phosphorescent Organic Light-Emitting Diodes Using Pyrido[2,3-b]indole Derivatives

as Host Materials", *Advanced Materials*, Vol. 25, No. 38, pp. 5450–5454, 2013.

16. Park, Y. S., S. Lee, K. H. Kim, S. Y. Kim, J. H. Lee and J. J. Kim, "Exciplex-Forming Co-Host for Organic Light-Emitting Diodes with Ultimate Efficiency", *Advanced Functional Materials*, Vol. 23, No. 39, pp. 4914–4920, 2013.

17. Nobuyasu, R. S., *Photophysics of TADF Emitters and Their Application in OLEDs Photophysics of TADF Emitters and Their Application in OLEDs*, Ph.D. Thesis, Durham University, 2018.

18. Sandanayaka, A. S., T. Matsushima and C. Adachi, "Degradation Mechanisms of Organic Light-Emitting Diodes Based on Thermally Activated Delayed Fluorescence Molecules", *Journal of Physical Chemistry C*, Vol. 119, No. 42, pp. 23845–23851, 2015.

19. Huang, R., J. Avó, T. Northey, E. Chaning-Pearce, P. L. D. Santos, J. S. Ward, P. Data, M. K. Etherington, M. A. Fox, T. J. Penfold, M. N. Berberan-Santos, J. C. Lima, M. R. Bryce and F. B. Dias, "The Contributions of Molecular Vibrations and Higher Triplet Levels to the Intersystem Crossing Mechanism in Metal-Free Organic Emitters", *Journal of Materials Chemistry C*, Vol. 5, pp. 6269–6280, 2017.

20. Ward, J. S., R. S. Nobuyasu, M. A. Fox, A. S. Batsanov, J. Santos, F. B. Dias and M. R. Bryce, "Bond Rotations and Heteroatom Effects in Donor-Acceptor-Donor Molecules: Implications for Thermally Activated Delayed Fluorescence and Room Temperature Phosphorescence", *Journal of Organic Chemistry*, Vol. 83, No. 23, pp. 14431–14442, 2018.

21. Grüne, J., N. Bunzmann, M. Meinecke, V. Dyakonov and A. Sperlich, "Kinetic Modeling of Transient Electroluminescence Reveals TTA as an Efficiency-Limiting Process in Exciplex-Based TADF OLEDs", *Journal of Physical Chemistry C*, Vol. 124, No. 47, pp. 25667–25674, 2020.

22. Higginbotham, H. F., C. L. Yi, A. P. Monkman and K. T. Wong, "Effects of Ortho-Phenyl Substitution on the rISC Rate of D-A Type TADF Molecules", *Journal of Physical Chemistry C*, Vol. 122, No. 14, pp. 7627–7634, 2018.

23. Haase, N., A. Danos, C. Pflumm, A. Morherr, P. Stachelek, A. Mekic, W. Brütting and A. P. Monkman, "Kinetic Modeling of Transient Photoluminescence from Thermally Activated Delayed Fluorescence", *Journal of Physical Chemistry C*, Vol. 122, No. 51, pp. 29173–29179, 2018.

24. Dias, F. B., K. N. Bourdakos, V. Jankus, K. C. Moss, K. T. Kamtekar, V. Bhalla, J. Santos, M. R. Bryce and A. P. Monkman, "Triplet Harvesting with 100% Efficiency by Way of Thermally Activated Delayed Fluorescence in Charge Transfer OLED Emitters", *Advanced Materials*, Vol. 25, No. 27, pp. 3707–3714, 2013.

25. Etherington, M. K., J. Gibson, H. F. Higginbotham, T. J. Penfold and A. P. Monkman, "Revealing the Spin-Vibronic Coupling Mechanism of Thermally Activated Delayed Fluorescence", *Nature Communications*, Vol. 7, pp. 1–7, 2016.

26. Dos Santos, P. L., M. K. Etherington and A. P. Monkman, "Chemical and Conformational Control of the Energy Gaps Involved in the Thermally Activated Delayed Fluorescence Mechanism", *Journal of Materials Chemistry C*, Vol. 6, No. 18, pp. 4842–4853, 2018.

27. Dias, F. B., J. Santos, D. R. Graves, P. Data, R. S. Nobuyasu, M. A. Fox, A. S. Batsanov, T. Palmeira, M. N. Berberan-Santos, M. R. Bryce and A. P. Monkman, "The Role of Local Triplet Excited States and D-A Relative Orientation in Thermally Activated Delayed Fluorescence: Photophysics and Devices", *Advanced Science*, Vol. 3, No. 12, pp. 1–10, 2016.

28. Ogiwara, T., Y. Wakikawa and T. Ikoma, "Mechanism of Intersystem Crossing of Thermally Activated Delayed Fluorescence Molecules", *Journal of Physical Chemistry A*, Vol. 119, No. 14, pp. 3415–3418, 2015.

29. Gibson, J., A. P. Monkman and T. J. Penfold, "The Importance of Vibronic Coupling for Efficient Reverse Intersystem Crossing in Thermally Activated Delayed Fluorescence Molecules", *ChemPhysChem*, Vol. 17, No. 1, pp. 2956–2961.

30. Marian, C. M., "Mechanism of the Triplet-to-Singlet Upconversion in the Assistant Dopant ACRXTN", *Journal of Physical Chemistry C*, Vol. 120, No. 7, pp. 3715–3721, 2016.

31. Ward, J. S., R. S. Nobuyasu, A. S. Batsanov, P. Data, A. P. Monkman, F. B. Dias and M. R. Bryce, "The Interplay of Thermally Activated Delayed Fluorescence (TADF) and Room Temperature Organic Phosphorescence in Sterically-Constrained Donor-Acceptor Charge-Transfer Molecules", *Chemical Communications*, Vol. 52, No. 12, pp. 2612–2615, 2016.

32. Gibson, J. and T. J. Penfold, "Nonadiabatic Coupling Reduces the Activation Energy in Thermally Activated Delayed Fluorescence", *Physical Chemistry Chemical Physics*, Vol. 19, No. 12, pp. 8428–8434, 2017.

33. Zhang, Q., J. Li, K. Shizu, S. Huang, S. Hirata, H. Miyazaki and C. Adachi, "Design of Efficient Thermally Activated Delayed Fluorescence Materials for Pure Blue Organic Light Emitting Diodes", *Journal of the American Chemical Society*, Vol. 134, No. 36, pp. 14706–14709, 2012.

34. Sohn, S., B. Hyun Koh, J. Y. Baek, H. Chan Byun, J. H. Lee, D. S. Shin, H. Ahn, H. K. Lee, J. Hwang, S. Jung and Y. H. Kim, "Synthesis and Characterization of Diphenylamine Derivative Containing Malononitrile for Thermally Activated Delayed Fluorescent Emitter", *Dyes and Pigments*, Vol. 140, pp. 14–21, 2017.

35. Gao, Y., Q. Q. Pan, L. Zhao, Y. Geng, T. Su, T. Gao and Z. M. Su, "Realizing Performance Improvement of Blue Thermally Activated Delayed Fluorescence Molecule DABNA by Introducing Substituents on the Para-Position of Boron Atom", *Chemical Physics Letters*, Vol. 701, pp. 98–102, 2018.

36. Wang, K., W. Liu, C. J. Zheng, Y. Z. Shi, K. Liang, M. Zhang, X. M. Ou and X. H. Zhang, "A Comparative Study of Carbazole-Based Thermally Activated Delayed Fluorescence Emitters with Different Steric Hindrance", *Journal of Materials Chemistry C*, Vol. 5, No. 19, pp. 4797–4803, 2017.

37. Feng, S., X. Guo and J. Zhang, "An Effective Strategy for Simply Varying Relative Position of Two Carbazole Groups in the Thermally Activated Delayed Fluorescence Emitters to Achieve Deep-Blue Emission", *Spectrochimica Acta - Part A: Molecular and Biomolecular Spectroscopy*, Vol. 226, 2020.

38. Gaj, M. P., C. Fuentes-Hernandez, Y. Zhang, S. R. Marder and B. Kippelen, "Highly Efficient Organic Light-Emitting Diodes from Thermally Activated Delayed Fluorescence Using a Sulfone-Carbazole Host Material", *Organic Electronics: Physics, Materials, Applications*, Vol. 16, pp. 109–112, 2015.

39. Hosokai, T., H. Nakanotani, S. Santou, H. Noda, Y. Nakayama and C. Adachi, "TADF Activation by Solvent Freezing: The Role of Nonradiative Triplet Decay and Spin-Orbit Coupling in Carbazole Benzonitrile Derivatives", *Synthetic Metals*, Vol. 252, pp. 62–68, 2019.

40. Serevičius, T., T. Nakagawa, M. C. Kuo, S. H. Cheng, K. T. Wong, C. H. Chang, R. C. Kwong, S. Xia and C. Adachi, "Enhanced Electroluminescence Based on Thermally Activated Delayed Fluorescence from a Carbazole-Triazine Derivative", *Physical Chemistry Chemical Physics*, Vol. 15, No. 38, pp. 15850–15855, 2013.

41. Huang, B., Q. Qi, W. Jiang, J. Tang, Y. Liu, W. Fan, Z. Yin, F. Shi, X. Ban, H. Xu and Y. Sun, "Thermally Activated Delayed Fluorescence Materials Based on 3,6-di-tert-butyl-9-((phenylsulfonyl)phenyl)-9H-carbazoles", *Dyes and Pigments*, Vol. 111, pp. 135–144, 2014.

42. Byeon, S. Y., J. H. Kim and J. Y. Lee, "CN-Modified Host Materials for Improved Efficiency and Lifetime in Blue Phosphorescent and Thermally Activated

Delayed Fluorescent Organic Light-Emitting Diodes", *ACS Applied Materials and Interfaces*, Vol. 9, No. 15, pp. 13339–13346, 2017.

43. Rajamalli, P., N. Senthilkumar, P. Gandeepan, P. Y. Huang, M. J. Huang, C. Z. Ren-Wu, C. Y. Yang, M. J. Chiu, L. K. Chu, H. W. Lin and C. H. Cheng, "A New Molecular Design Based on Thermally Activated Delayed Fluorescence for Highly Efficient Organic Light Emitting Diodes", *Journal of the American Chemical Society*, Vol. 138, No. 2, pp. 628–634, 2016.

44. Wang, L., J. Jin, W. Zhang, B. Pan, Z. Huang and S. Zhuang, "Toward High Efficiency Green Phosphorescent Organic Light-Emitting Diodes by Fine Tuning the Charge Transporting Properties of 1,2,4-thiadiazole Based Hosts", *Organic Electronics: Physics, Materials, Applications*, Vol. 16, pp. 177–185, 2015.

45. Yu, Y. J., X. Tang, H. T. Ge, Y. Yuan, Z. Q. Jiang and L. S. Liao, "Fluorenone-Based Thermally Activated Delayed Fluorescence Materials for Orange-Red Emission", *Organic Electronics: Physics, Materials, Applications*, Vol. 73, pp. 240–246, 2019.

46. Lien, Y. J., T. C. Lin, C. C. Yang, Y. C. Chiang, C. H. Chang, S. H. Liu, Y. T. Chen, G. H. Lee, P. T. Chou, C. W. Lu and Y. Chi, "First N-Borylated Emitters Displaying Highly Efficient Thermally Activated Delayed Fluorescence and High-Performance OLEDs", *ACS Applied Materials and Interfaces*, Vol. 9, No. 32, pp. 27090–27101, 2017.

47. Bezvikonnyi, O., D. Gudeika, D. Volyniuk, V. Mimaite, B. R. Sebastine and J. V. Grazulevicius, "Effect of Donor Substituents on Thermally Activated Delayed Fluorescence of Diphenylsulfone Derivatives", *Journal of Luminescence*, Vol. 206, pp. 250–259, 2019.

48. Tanaka, H., K. Shizu, H. Miyazaki and C. Adachi, "Efficient Green Thermally Activated Delayed Fluorescence (TADF) from a Phenoxazine-Triphenyltriazine (PXZ-TRZ) Derivative", *Chemical Communications*, Vol. 48, No. 93, pp. 11392–

11394, 2012.

49. Olivier, Y., M. Moral, L. Muccioli and J. C. Sancho-García, "Dynamic Nature of Excited States of Donor-Acceptor TADF Materials for OLEDs: How Theory Can Reveal Structure-Property Relationships", *Journal of Materials Chemistry C*, Vol. 5, No. 23, pp. 5718–5729, 2017.

50. Wu, K., T. Zhang, L. Zhan, C. Zhong, S. Gong, N. Jiang, Z. H. Lu and C. Yang, "Optimizing Optoelectronic Properties of Pyrimidine-Based TADF Emitters by Changing the Substituent for Organic Light-Emitting Diodes with External Quantum Efficiency Close to 25 % and Slow Efficiency Roll-Off", *Chemistry - A European Journal*, Vol. 22, No. 31, pp. 10860–10866, 2016.

51. Kitamoto, Y., T. Namikawa, D. Ikemizu, Y. Miyata, T. Suzuki, H. Kita, T. Sato and S. Oi, "Light Blue and Green Thermally Activated Delayed Fluorescence from 10H-Phenoxaborin-Derivatives and Their Application to Organic Light-Emitting Diodes", *Journal of Materials Chemistry C*, Vol. 3, No. 35, pp. 9122–9130, 2015.

52. Yang, Z., Z. Mao, Z. Xie, Y. Zhang, S. Liu, J. Zhao, J. Xu, Z. Chi and M. P. Aldred, "Recent Advances in Organic Thermally Activated Delayed Fluorescence Materials", *Chemical Society Reviews*, Vol. 46, No. 3, pp. 915–1016, 2017.

53. Tomkeviciene, A., T. Matulaitis, M. Guzauskas, V. Andruleviciene, D. Volyniuk and J. V. Grazulevicius, "Thianthrene and Acridan-Substituted Benzophenone or Diphenylsulfone: Effect of Triplet Harvesting via TADF and Phosphorescence on Efficiency of All-Organic OLEDS", *Organic Electronics*, Vol. 70, pp. 227–239, 2019.

54. Zhang, Q., B. Li, S. Huang, H. Nomura, H. Tanaka and C. Adachi, "Efficient Blue Organic Light-Emitting Diodes Employing Thermally Activated Delayed Fluorescence", *Nature Photonics*, Vol. 8, No. 4, pp. 326–332, 2014.

55. Lee, I. H., W. Song and J. Y. Lee, "Aggregation-Induced Emission Type Ther-

mally Activated Delayed Fluorescent Materials for High Efficiency in Non-Doped Organic Light-Emitting Diodes", *Organic Electronics*, Vol. 29, 2016.

56. Xie, Z., C. Chen, S. Xu, J. Li, Y. Zhang, S. Liu, J. Xu and Z. Chi, "White-Light Emission Strategy of a Single Organic Compound with Aggregation-Induced Emission and Delayed Fluorescence Properties", *Angewandte Chemie - International Edition*, Vol. 54, No. 24, pp. 7181–7184, 2015.

57. Xu, S., T. Liu, Y. Mu, Y. F. Wang, Z. Chi, C. C. Lo, S. Liu, Y. Zhang, A. Lien and J. Xu, "An Organic Molecule with Asymmetric Structure Exhibiting Aggregation-Induced Emission, Delayed Fluorescence, and Mechanoluminescence", *Angewandte Chemie - International Edition*, Vol. 54, No. 3, pp. 874–878, 2015.

58. Varathan, E. and A. Patnaik, "Oxidation State-Dependent Electronic Properties of Sulfur-Containing Thermally Activated Delayed Fluorescence Molecules", *Journal of Physical Chemistry A*, Vol. 123, No. 41, pp. 8755–8765, 2019.

59. Aydemir, M., S. Xu, C. Chen, M. R. Bryce, Z. Chi and A. P. Monkman, "Photophysics of an Asymmetric Donor-Acceptor-Donor′ TADF Molecule and Reinterpretation of Aggregation-Induced TADF Emission in These Materials", *Journal of Physical Chemistry C*, Vol. 121, No. 33, pp. 17764–17772, 2017.

60. Tsai, C. C., W. C. Huang, H. Y. Chih, Y. C. Hsh, C. W. Liao, C. H. Lin, Y. X. Kang, C. H. Chang, Y. J. Chang and C. W. Lu, "Efficient Donor-Acceptor-Donor Borylated Compounds with Extremely Small ΔEST for Thermally Activated Delayed Fluorescence OLEDs", *Organic Electronics*, Vol. 63, pp. 166–174, 2018.

61. Ou, C. J., J. Y. Lin, J. Mao, S. Q. Chu, Y. Zhao, L. H. Xie, H. T. Cao, X. W. Zhang, Y. Wei and W. Huang, "Friedel-Crafts Arylmethylation: A Simple Approach to Synthesize Bipolar Host Materials for Efficient Electroluminescence", *Organic Electronics*, Vol. 38, pp. 370–378, 2016.

62. Wei, Q., N. Fei, A. Islam, T. Lei, L. Hong, R. Peng, X. Fan, L. Chen, P. Gao and Z. Ge, "Small-Molecule Emitters with High Quantum Efficiency: Mechanisms, Structures, and Applications in OLED Devices", *Advanced Optical Materials*, Vol. 6, No. 20, pp. 1–31, 2018.

63. Lee, S. Y., C. Adachi and T. Yasuda, "High-Efficiency Blue Organic Light-Emitting Diodes Based on Thermally Activated Delayed Fluorescence from Phenoxaphosphine and Phenoxathiin Derivatives", *Advanced Materials*, Vol. 28, No. 23, pp. 4626–4631, 2016.

64. Jia, X., W. Han, T. Xue, D. Zhao, X. Li, J. Nie and T. Wang, "Diphenyl Sulfone-Based A-π-D-π-A Dyes as Efficient Initiators for One-Photon and Two-Photon Initiated Polymerization", *Polymer Chemistry*, Vol. 10, No. 17, pp. 2152–2161, 2019.

65. Hussain, A., H. Yuan, W. Li and J. Zhang, "Theoretical Investigations of the Realization of Sky-Blue to Blue TADF Materials: Via CH/N and H/CN Substitution at the Diphenylsulphone Acceptor", *Journal of Materials Chemistry C*, Vol. 7, No. 22, pp. 6685–6691, 2019.

66. Bezvikonnyi, O., D. Gudeika, D. Volyniuk, M. Rutkis and J. V. Grazulevicius, "Diphenylsulfone-Based Hosts for Electroluminescent Devices: Effect of Donor Substituents", *Dyes and Pigments*, Vol. 175, p. 108104, 2020.

67. Che, W., Y. Xie and Z. Li, "Structural Design of Blue-to-Red Thermally-Activated Delayed Fluorescence Molecules by Adjusting the Strength between Donor and Acceptor", *Asian Journal of Organic Chemistry*, Vol. 9, No. 9, pp. 1262–1276, 2020.

68. Bui, T. T., F. Goubard, M. Ibrahim-Ouali, D. Gigmes and F. Dumur, "Recent Advances on Organic Blue Thermally Activated Delayed Fluorescence (TADF) Emitters for Organic Light-Emitting Diodes (OLEDs)", *Beilstein Journal of Organic Chemistry*, Vol. 14, pp. 282–308, 2018.

69. Hatakeyama, T., K. Shiren, K. Nakajima, S. Nomura, S. Nakatsuka, K. Kinoshita, J. Ni, Y. Ono and T. Ikuta, "Ultrapure Blue Thermally Activated Delayed Fluorescence Molecules: Efficient HOMO-LUMO Separation by the Multiple Resonance Effect", *Advanced Materials*, Vol. 28, No. 14, pp. 2777–2781, 2016.

70. Im, Y., S. Y. Byun, J. H. Kim, D. R. Lee, C. S. Oh, K. S. Yook and J. Y. Lee, "Recent Progress in High-Efficiency Blue-Light-Emitting Materials for Organic Light-Emitting Diodes", *Advanced Functional Materials*, Vol. 27, No. 13, 2017.

71. Lee, I. and J. Y. Lee, "Molecular Design of Deep Blue Fluorescent Emitters with 20% External Quantum Efficiency and Narrow Emission Spectrum", *Organic Electronics*, Vol. 29, pp. 160–164, 2016.

72. Liang, X., Z. L. Tu and Y. X. Zheng, "Thermally Activated Delayed Fluorescence Materials: Towards Realization of High Efficiency through Strategic Small Molecular Design", *Chemistry - A European Journal*, Vol. 25, No. 22, pp. 5623–5642, 2019.

73. Bergmann, L., D. M. Zink, S. Bräse, T. Baumann and D. Volz, "Metal–Organic and Organic TADF-Materials: Status, Challenges and Characterization", *Topics in Current Chemistry*, Vol. 374, No. 3, 2016.

74. Jankus, V., P. Data, D. Graves, C. McGuinness, J. Santos, M. R. Bryce, F. B. Dias and A. P. Monkman, "Highly Efficient TADF OLEDs: How the Emitter-Host Interaction Controls both the Excited State Species and Electrical Properties of the Devices to Achieve Near 100% Triplet Harvesting and High Efficiency", *Advanced Functional Materials*, Vol. 24, No. 39, pp. 6178–6186, 2014.

75. Wang, H., L. Xie, Q. Peng, L. Meng, Y. Wang, Y. Yi and P. Wang, "Novel Thermally Activated Delayed Fluorescence Materials-Thioxanthone Derivatives and Their Applications for Highly Efficient OLEDs", *Advanced Materials*, Vol. 26, No. 30, pp. 5198–5204, 2014.

76. Xu, S., T. Liu, Y. Mu, Y. F. Wang, Z. Chi, C. C. Lo, S. Liu, Y. Zhang, A. Lien and J. Xu, "An Organic Molecule with Asymmetric Structure Exhibiting Aggregation-Induced Emission, Delayed Fluorescence, and Mechanoluminescence", *Angewandte Chemie - International Edition*, Vol. 54, No. 3, pp. 874–878, 2015.

77. Wang, C., C. Deng, D. Wang and Q. Zhang, "Prediction of Intramolecular Charge-Transfer Excitation for Thermally Activated Delayed Fluorescence Molecules from a Descriptor-Tuned Density Functional", *Journal of Physical Chemistry C*, Vol. 122, No. 14, pp. 7816–7823, 2018.

78. Dos Santos, P. L., D. Chen, P. Rajamalli, T. Matulaitis, D. B. Cordes, A. M. Slawin, D. Jacquemin, E. Zysman-Colman and I. D. Samuel, "Use of Pyrimidine and Pyrazine Bridges as a Design Strategy to Improve the Performance of Thermally Activated Delayed Fluorescence Organic Light Emitting Diodes", *ACS Applied Materials and Interfaces*, Vol. 11, No. 48, pp. 45171–45179, 2019.

79. Gan, S., W. Luo, B. He, L. Chen, H. Nie, R. Hu, A. Qin, Z. Zhao and B. Z. Tang, "Integration of Aggregation-Induced Emission and Delayed Fluorescence into Electronic Donor-Acceptor Conjugates", *Journal of Materials Chemistry C*, Vol. 4, No. 17, pp. 3705–3708, 2016.

80. Kim, J. H. and J. Y. Lee, "Dibenzothiophene-Dioxide Acceptor Based Thermally Activated Delayed Fluorescent Emitters for Color Tunable Organic Light-Emitting Diodes", *Journal of Industrial and Engineering Chemistry*, Vol. 50, pp. 111–114, 2017.

81. Kim, J. U., S. S. Reddy, L. S. Cui, H. Nomura, S. Hwang, D. H. Kim, H. Nakanotani, S. H. Jin and C. Adachi, "Thermally Activated Delayed Fluorescence of Bis(9,9-dimethyl-9,10-dihydroacridine) Dibenzo[b,d]thiophene 5,5-dioxide Derivatives for Organic Light-Emitting Diodes", *Journal of Luminescence*, Vol. 190, pp. 485–491, 2017.

82. Pereira, D. D. S., P. L. Dos Santos, J. S. Ward, P. Data, M. Okazaki, Y. Takeda, S. Minakata, M. R. Bryce and A. P. Monkman, "An Optical and Electrical Study of Full Thermally Activated Delayed Fluorescent White Organic Light-Emitting Diodes", *Scientific Reports*, Vol. 7, No. 1, pp. 1–8, 2017.

83. Dos Santos, P. L., J. S. Ward, M. R. Bryce and A. P. Monkman, "Using Guest-Host Interactions to Optimize the Efficiency of TADF OLEDs", *Journal of Physical Chemistry Letters*, Vol. 7, No. 17, pp. 3341–3346, 2016.

84. Wang, K., Y. Z. Shi, C. J. Zheng, W. Liu, K. Liang, X. Li, M. Zhang, H. Lin, S. L. Tao, C. S. Lee, X. M. Ou and X. H. Zhang, "Control of Dual Conformations: Developing Thermally Activated Delayed Fluorescence Emitters for Highly Efficient Single-Emitter White Organic Light-Emitting Diodes", *ACS Applied Materials and Interfaces*, Vol. 10, No. 37, pp. 31515–31525, 2018.

85. Wang, K., C. J. Zheng, W. Liu, K. Liang, Y. Z. Shi, S. L. Tao, C. S. Lee, X. M. Ou and X. H. Zhang, "Avoiding Energy Loss on TADF Emitters: Controlling the Dual Conformations of D–A Structure Molecules Based on the Pseudoplanar Segments", *Advanced Materials*, Vol. 29, No. 47, pp. 1–9, 2017.

86. Sun, K., Y. Sun, W. Jiang, S. Huang, W. Tian and Y. Sun, "Highly Efficient and Color Tunable Thermally Activated Delayed Fluorescent Emitters and Their Applications for the Solution-Processed OLEDs", *Dyes and Pigments*, Vol. 139, pp. 326–333, 2017.

87. Xie, G., X. Li, D. Chen, Z. Wang, X. Cai, D. Chen, Y. Li, K. Liu, Y. Cao and S. J. Su, "Evaporation- and Solution-Process-Feasible Highly Efficient Thianthrene-9,9′,10,10′-Tetraoxide-Based Thermally Activated Delayed Fluorescence Emitters with Reduced Efficiency Roll-Off", *Advanced Materials*, Vol. 28, No. 1, pp. 181–187, 2016.

88. Xu, S., Q. Yang, Y. Wan, R. Chen, S. Wang, Y. Si, B. Yang, D. Liu, C. Zheng and W. Huang, "Predicting Intersystem Crossing Efficiencies of Organic Molecules

for Efficient Thermally Activated Delayed Fluorescence", *Journal of Materials Chemistry C*, Vol. 7, No. 31, pp. 9523–9530, 2019.

89. Mu, Y., B. Xu, Z. Yang, H. Wen, Z. Yang, S. K. B. Mane, J. Zhao, Y. Zhang, Z. Chi and B. Z. Tang, "Reversible and Continuous Color-Tunable Persistent Luminescence of Metal-Free Organic Materials by "self"-Interface Energy Transfer", *ACS Applied Materials and Interfaces*, Vol. 12, No. 4, pp. 5073–5080, 2020.

90. Wang, Z., Y. Li, X. Cai, D. Chen, G. Xie, K. K. Liu, Y. C. Wu, C. C. Lo, A. Lien, Y. Cao and S. J. Su, "Structure-Performance Investigation of Thioxanthone Derivatives for Developing Color Tunable Highly Efficient Thermally Activated Delayed Fluorescence Emitters", *ACS Applied Materials and Interfaces*, Vol. 8, No. 13, pp. 8627–8636, 2016.

91. Sun, H., Z. Hu, C. Zhong, X. Chen, Z. Sun and J. L. Brédas, "Impact of Dielectric Constant on the Singlet-Triplet Gap in Thermally Activated Delayed Fluorescence Materials", *Journal of Physical Chemistry Letters*, Vol. 8, No. 11, pp. 2393–2398, 2017.

92. Engel, E. and R. Dreizler, "Density Functional Theory", *Springer*, 2013.

93. Becke, A. D., "A New Mixing of Hartree-Fock and Local Density-Functional Theories", *The Journal of Chemical Physics*, Vol. 98, No. 2, pp. 1372–1377, 1993.

94. Kohn, W. and L. J. Sham, "Self-Consistent Equations Including Exchange and Correlation Effects", *Physical Review*, Vol. 140, No. 4A, p. A1133, 1965.

95. Negele, J. W., "Structure of Finite Nuclei in the Local-Density Approximation", *Physical Review C*, Vol. 1, No. 4, p. 1260, 1970.

96. Perdew, J., K. Burke and M. Ernzerhof, "Generalized Gradient Approximation Made Simple", *Physical Review Letters*, Vol. 77, No. 18, p. 3865, 1996.

97. Lee, C., W. Yang and R. G. Parr, "Development of the Colle-Salvetti Correlation-Energy Formula into a Functional of the Electron Density", *Physical Review B*, Vol. 37, No. 2, p. 785, 1988.

98. Zhao, Y. and D. G. Truhlar, "The M06 Suite of Density Functionals for Main Group Thermochemistry, Thermochemical Kinetics, Noncovalent Interactions, Excited States, and Transition Elements:Two New Functionals and Systematic Testing of Four M06-Class Functionals and 12 Other Functionals", *Theoretical Chemistry Accounts*, Vol. 120, No. 1-3, pp. 215–241, 2008.

99. Slater, J. C., "Atomic Shielding Constants", *Physical Review*, Vol. 36, No. 1, p. 57, 1930.

100. Boys, S. F., "Electronic-Wave Functions-I. A General Method of Calculation for the Stationary States of Any Molecular System", *Proceedings of the Royal Society of London Series A Mathematical and Physical Sciences*, Vol. 200, No. 1063, pp. 542–554, 1950.

101. Cramer, C. J. and D. G. Truhlar, "Implicit Solvation Models: Equilibria, Structure, Spectra, and Dynamics", *Chemical Reviews*, Vol. 99, No. 8, pp. 2161–2200, 1999.

102. Miertuš, S., E. Scrocco and T. J, "Elecrostatic Interaction of a Solute with a Continuum. A Direct utilization of AB Initio Molecular Potentials for the Prevision of Solvent Effects", *Chemical Physics*, Vol. 55, No. 1, pp. 117–129, 1981.

103. Reineke, S., F. Lindner, G. Schwartz, N. Seidler, K. Walzer, N. Lüssem and K. Leo, "White Organic Light-Emitting Diodes with Fluorescent Tube Efficiency", *Nature*, Vol. 459, No. 7244, pp. 234–238, 2009.

104. Barone, V. and M. Cossi, "Quantum Calculation of Molecular Energies and Energy Gradients in Solution by a Conductor Solvent Model", *The Journal of Physical Chemistry A*, Vol. 102, No. 11, pp. 1995–2001, 1998.

105. Dreuw, A., J. L. Weisman and M. Head-Gordon, "Long-Range Charge-Transfer Excited States in Time-Dependent Density Functional Theory Require Non-Local Exchange", *The Journal of Chemical Physics*, Vol. 119, No. 6, p. 2943–2946, 2003.

106. Maitra, N. T., F. Zhang, R. J. Cave and K. Burke, "Double Excitations within Time-Dependent Density Functional Theory Linear Response", *The Journal of Chemical Physics*, Vol. 120, No. 13, p. 5932–5937, 2004.

107. Elliott, P., S. Goldson, C. Canahui and N. T. Maitra, "Perspectives on Double-Excitations in TDDFT", *Chemical Physics*, Vol. 391, No. 1, p. 110–119, 2011.

108. Cheng, C. Y., M. S. Ryley, M. J. Peach, D. J. Tozer, Helgaker and A. M. Teale, "Molecular Properties in the Tamm–Dancoff Approximation: Indirect Nuclear Spin–Spin Coupling Constants", *Molecular Physics*, Vol. 113, pp. 1937–1951, 2015.

109. Bai, Z., J. Demmel, J. Dongarra, A. Ruhe and H. von der Vorst, "Templates for the Solution of Algebraic Eigenvalue Problems: A Practical Guide", *Society for Industrial and Applied Mathematics*, 2000.

110. Grüning, M., A. Marini and X. Gonze, "Exciton-Plasmon States in Nanoscale Materials: Breakdown of the Tamm-Dancoff Approximation", *Nano Letters*, Vol. 9, No. 8, p. 2820–2824, 2009.

111. Wigner, E. P., "On the Quantum Correction for Thermodynamic Equilibrium", *Part I: Physcical Chemistry. Part II: Solid State Physics*, pp. 110–120, 1997.

112. Steuernagel, O., D. Kakofengitis and G. Ritter, "Wigner Flow Reveals Topological Order in Quantum Phase Space Dynamics", *Physical Review Letters*, Vol. 110, No. 3, p. 030401, 2013.

113. Dragoman, D., "Applications of the Wigner Distribution Function in Signal Processing", *Eurasip Journal on Applied Signal Processing*, Vol. 2005, No. 10, pp.

1520–1534, 2005.

114. Etienne, T., A. X and A. Monari, "Toward a Quantitative Assessment of Electronic Transitions'Charge-Transfer Character", *Journal of Chemical Theory and Computation*, Vol. 10, No. 9, pp. 3896–3905, 2014.

115. Gross, K. C., P. G. Seybold and C. M. Hadad, "Comparison of Different Atomic Charge Schemes for Predicting pKa Variations in Substituted Anilines and Phenols", *International Journal of Quantum Chemistry*, Vol. 90, No. 1, pp. 445–458, 2002.

116. Spavieri, G. and M. Mansuripur, "Origin of the Spin-Orbit Interaction", *Physica Scripta*, Vol. 90, No. 8, 2015.

117. Kholmetskii, A. L., O. V. Missevitch and T. Yarman, "On the Classical Analysis of Spin-Orbit Coupling in Hydrogenlike Atoms", *American Journal of Physics*, Vol. 78, No. 4, pp. 428–432, 2010.

118. Frisch, M. J., G. W. Trucks, H. B. Schlegel, G. E. Scuseria, M. A. Robb, J. R. Cheeseman, G. Scalmani, V. Barone, G. A. Petersson, H. Nakatsuji, X. Li, M. Caricato, A. V. Marenich, J. Bloino, B. G. Janesko, R. Gomperts, B. Mennucci, H. P. Hratchian, J. V. Ortiz, A. F. Izmaylov, J. L. Sonnenberg, D. Williams-Young, F. Ding, F. Lipparini, F. Egidi, J. Goings, B. Peng, A. Petrone, T. Henderson, D. Ranasinghe, V. G. Zakrzewski, J. Gao, N. Rega, G. Zheng, W. Liang, M. Hada, M. Ehara, K. Toyota, R. Fukuda, J. Hasegawa, M. Ishida, T. Nakajima, Y. Honda, O. Kitao, H. Nakai, T. Vreven, K. Throssell, J. A. Montgomery, J. E. Peralta, F. Ogliaro, M. J. Bearpark, J. J. Heyd, E. N. Brothers, K. N. Kudin, V. N. Staroverov, T. A. Keith, R. Kobayashi, J. Normand, K. Raghavachari, A. P. Rendell, J. C. Burant, S. S. Iyengar, J. Tomasi, M. Cossi, J. M. Millam, M. Klene, C. Adamo, R. Cammi, J. W. Ochterski, R. L. Martin, K. Morokuma, O. Farkas, J. B. Foresman and D. J. Fox, "Gaussian 16, Rev C 01", *Gaussian Inc Wallingford CT*, 2016.

119. Kolleth, A., S. Müller, A. Lumbroso, G. Tanriver, S. Catak, S. Sulzer-Mosse and A. De Mesmaeker, "Access to 3-Aminobenzothiophenes and 3-Aminothiophenes Fused to 5-Membered Heteroaromatic Rings Through 6-Electrocyclization Reaction of Keteniminium Salts", *Tetrahedron Letters*, Vol. 59, No. 34, p. 3242–3248, 2018.

120. Te Velde, G., F. M. Bickelhaupt, E. J. Baerends, C. Fonseca Guerra, S. J. van Gisbergen, J. G. Snijders and T. Ziegler, "Chemistry with ADF", *Journal of Computational Chemistry*, Vol. 22, No. 9, p. 931–967, 2001.

121. Etienne, T., X. Assfeld and A. Monari, "New Insight into the Topology of Excited States Through Detachment/Attachment Density Matrices-Based Centroids of Charge", *Journal of Chemical Theory and Computation*, Vol. 10, No. 9, p. 3906–3914, 2014.

122. Hanwell, M. D. and D. E. Curtis, "Avogadro: An Advanced Semantic Chemical Editor, Visualization, and Analysis Platform", *Advances in Mathematics*, Vol. 262, p. 476–483, 2014.

123. Etienne, T., X. Assfeld and A. Monari, "Toward a Quantitative Assessment of Electronic Transitions" Charge-Transfer Character", *Journal of Chemical Theory and Computation*, Vol. 10, No. 9, p. 3896–3905, 2014.

124. Barbatti, M., M. Ruckenbauer, F. Plasser, J. Pittner, G. Granucci, M. Persico and H. Lischka, "Newton-X: A Surface-Hopping Program for Nonadiabatic Molecular Dynamics", *Wiley Interdisciplinary Reviews: Computational Molecular Science*, Vol. 4, No. 1, p. 26–33, 2014.

125. Lv, L. L., K. Yuan and Y. C. Wang, "Theoretical Studying of Basic Photophysical Processes in a Thermally Activated Delayed Fluorescence Copper(I) Complex: Determination of Reverse Intersystem Crossing and Radiative Rate Constants", *Organic Electronics*, Vol. 51, pp. 207–219, 2017.

APPENDIX A: THE RELATIONSHIP BETWEEN χ-SOC and χ-1/ΔE_{ST}

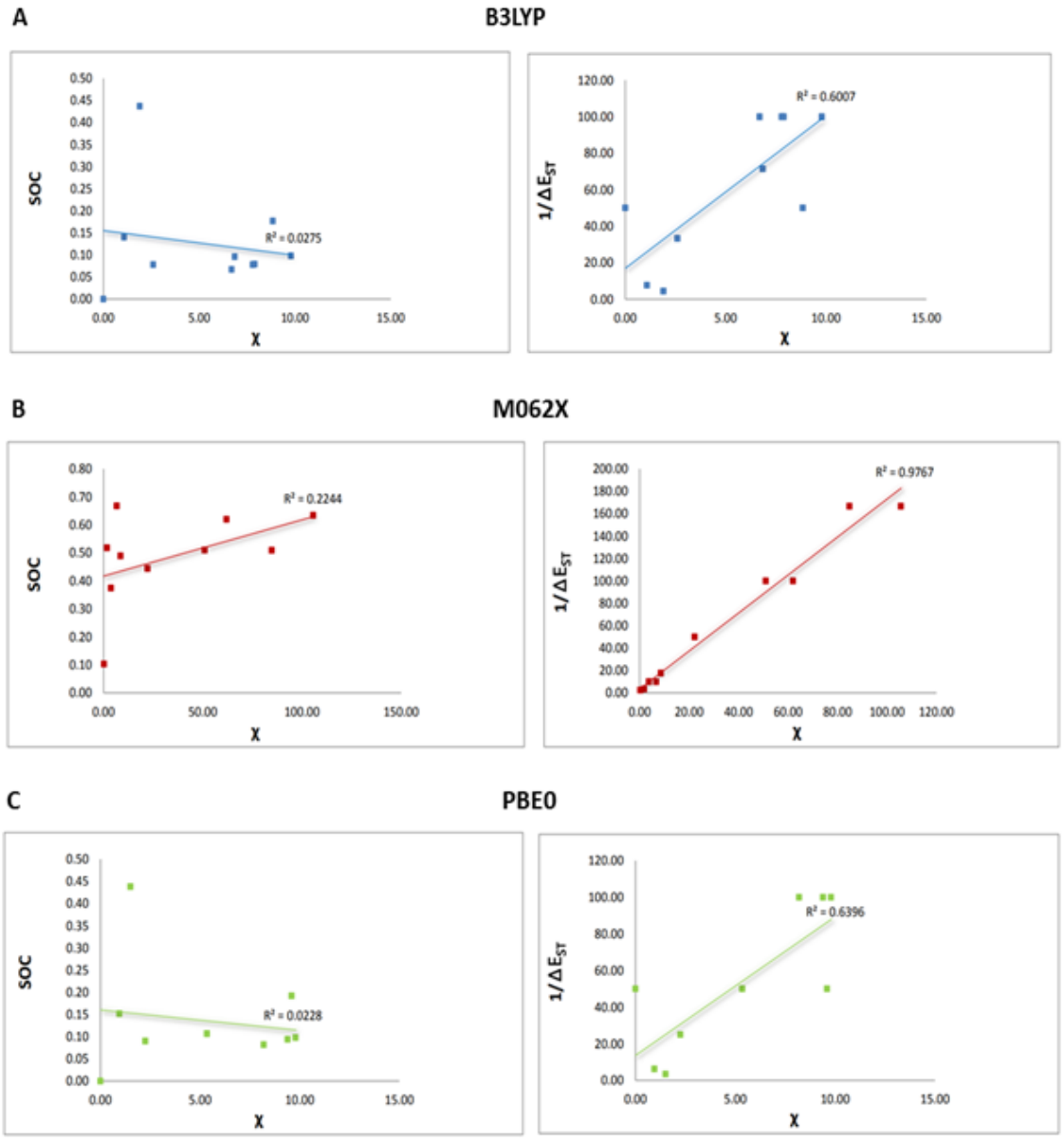

Figure A.1. The relationship between χ-SOC and χ-1/ΔE_{ST} with B3LYP, M062X and PBE0 functionals.

APPENDIX B: DISTRIBUTION OF FRONTIER MOLECULAR ORBITALS AND Φ_s INDICES

Table B.1. Distribution of frontier molecular orbitals for compounds 1, 2 and 3 at $S_0 \rightarrow S_1$ excitation and $S_0 \rightarrow T_1$ excitation (TDA: B3LYP/6-31+G(d,p)).

Molecule	**B3LYP/6-31+G(d,p)**			
1	$S_0 \rightarrow S_1$ Excitation		$S_0 \rightarrow T_1$ Excitation	
	HOMO	LUMO	HOMO	LUMO
	S_0 Optimization		S_0 Optimization	
	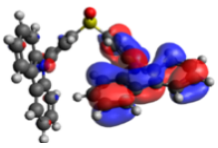	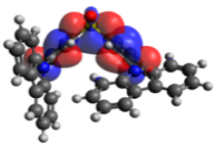	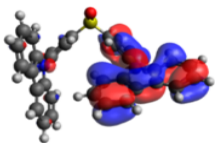	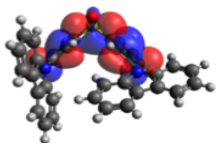
	T_1 Optimization		T_1 Optimization	
	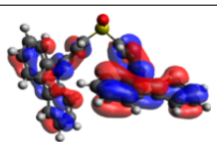	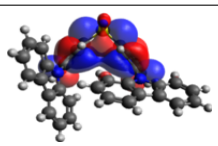	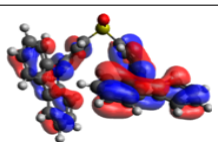	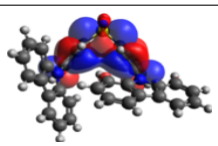
2	S_0 Optimization		S_0 Optimization	
		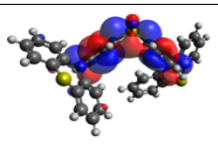	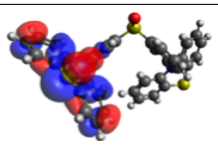	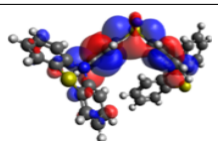
	T_1 Optimization		T_1 Optimization	
	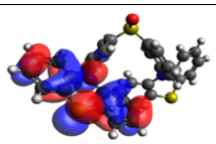	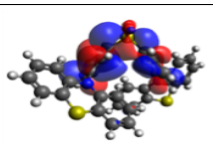	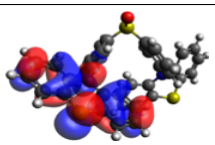	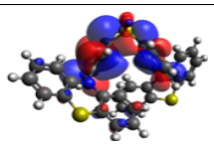
3	S_0 Optimization		S_0 Optimization	
	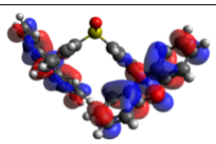	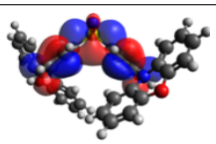	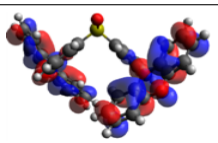	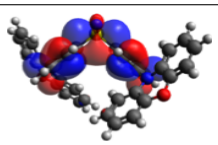
	T_1 Optimization		T_1 Optimization	
	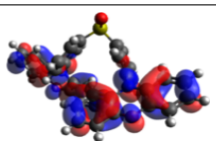	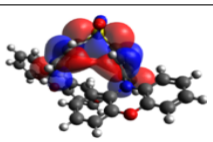	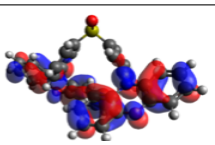	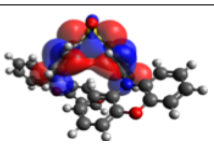

Table B.2. Distribution of frontier molecular orbitals for compounds 4 and 5 at $S_0 \rightarrow S_1$ excitation and $S_0 \rightarrow T_1$ excitation (TDA: B3LYP/6-31+G(d,p)).

Molecule	**B3LYP/6-31+G(d,p)**			
4	$S_0 \rightarrow S_1$ Excitation		$S_0 \rightarrow T_1$ Excitation	
	HOMO	LUMO	HOMO	LUMO
	S_0 Optimization		S_0 Optimization	
	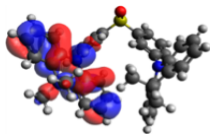		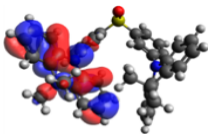	
	T_1 Optimization		T_1 Optimization	
	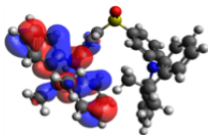		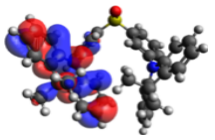	
5	S_0 Optimization		S_0 Optimization	
	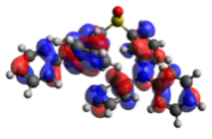		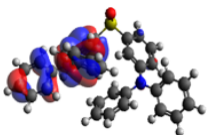	
	T_1 Optimization		T_1 Optimization	
	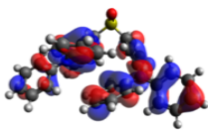		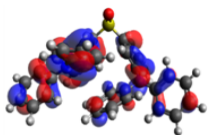	

Table B.3. Distribution of frontier molecular orbitals for compound 1 at $S_0 \rightarrow S_1$ excitation and $S_0 \rightarrow T_1$ excitation (TDA: M062X/6-31+G(d,p)).

Molecule	**M062X/6-31+G(d,p)**			
1	$S_0 \rightarrow S_1$ Excitation		$S_0 \rightarrow T_1$ Excitation	
	HOMO	LUMO	HOMO	LUMO
	S_0 Optimization		S_0 Optimization	
	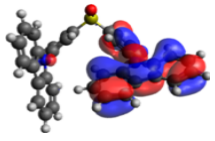		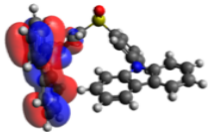	
	T_1 Optimization		T_1 Optimization	
	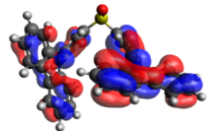		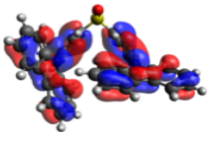	

Table B.4. Distribution of frontier molecular orbitals for compounds 2, 3, 4 and 5 at $S_0 \rightarrow S_1$ excitation and $S_0 \rightarrow T_1$ excitation (TDA: M062X/6-31+G(d,p)).

Molecule	**M062X/6-31+G(d,p)**			
2	$S_0 \rightarrow S_1$ Excitation		$S_0 \rightarrow T_1$ Excitation	
	HOMO	LUMO	HOMO	LUMO
	S_0 Optimization		S_0 Optimization	
	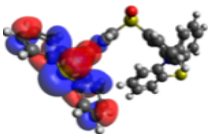		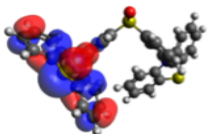	
	T_1 Optimization		T_1 Optimization	
	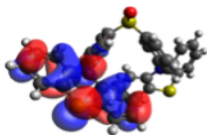		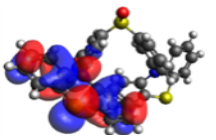	
3	S_0 Optimization		S_0 Optimization	
	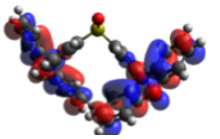		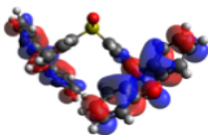	
	T_1 Optimization		T_1 Optimization	
	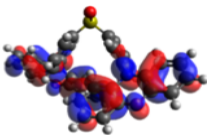		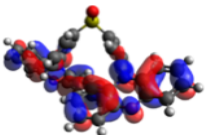	
4	S_0 Optimization		S_0 Optimization	
	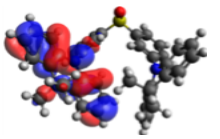		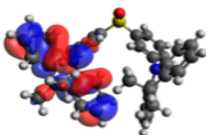	
	T_1 Optimization		T_1 Optimization	
	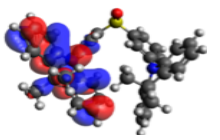		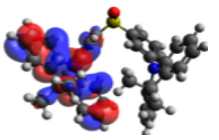	
5	S_0 Optimization		S_0 Optimization	
	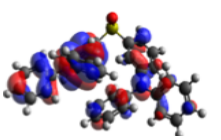		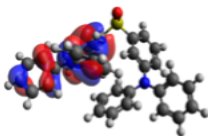	
	T_1 Optimization		T_1 Optimization	
	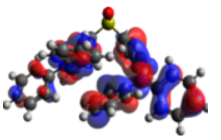		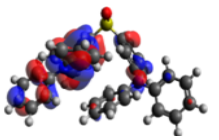	

Table B.5. Distribution of frontier molecular orbitals for compounds 1, 2 and 3 at S_0 → S_1 excitation and S_0 → T_1 excitation (TDA: PBE0/6-31+G(d,p)).

Molecule	**PBE0/6-31+G(d,p)**			
1	S_0 → S_1 Excitation		S_0 → T_1 Excitation	
	HOMO	LUMO	HOMO	LUMO
	S_0 Optimization		S_0 Optimization	
	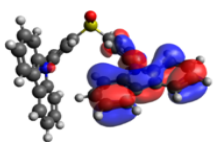	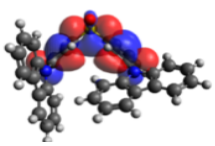	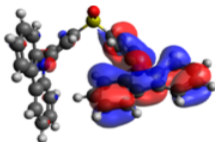	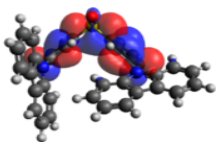
	T_1 Optimization		T_1 Optimization	
	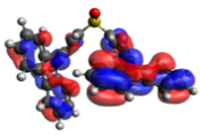	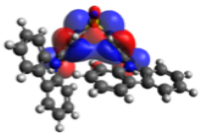	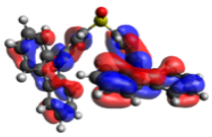	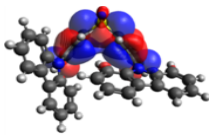
2	S_0 Optimization		S_0 Optimization	
		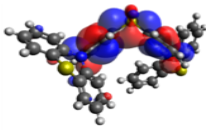		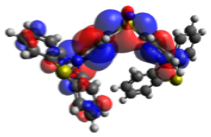
	T_1 Optimization		T_1 Optimization	
	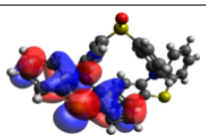	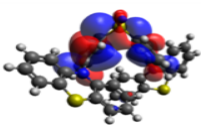	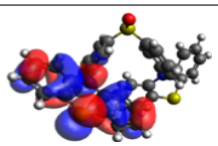	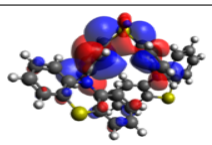
3	S_0 Optimization		S_0 Optimization	
	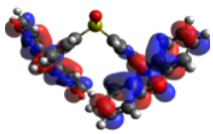	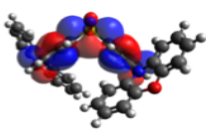	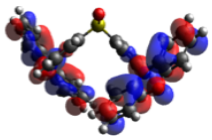	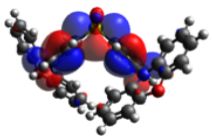
	T_1 Optimization		T_1 Optimization	
	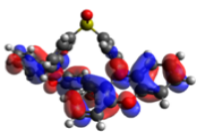		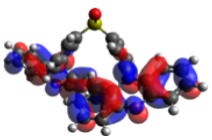	

Table B.6. Distribution of frontier molecular orbitals for compounds 4 and 5 at $S_0 \rightarrow S_1$ excitation and $S_0 \rightarrow T_1$ excitation (TDA: PBE0/6-31+G(d,p)).

Molecule	**PBE0/6-31+G(d,p)**			
4	$S_0 \rightarrow S_1$ Excitation		$S_0 \rightarrow T_1$ Excitation	
	HOMO	LUMO	HOMO	LUMO
	S_0 Optimization		S_0 Optimization	
	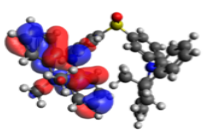	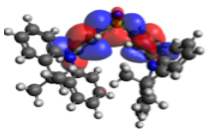		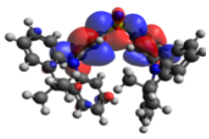
	T_1 Optimization		T_1 Optimization	
	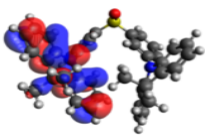	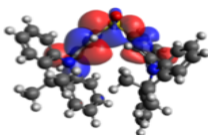		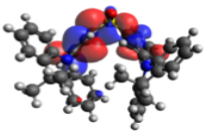
5	S_0 Optimization		S_0 Optimization	
	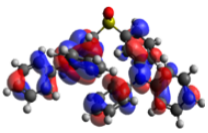	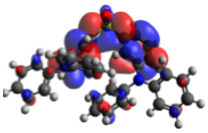	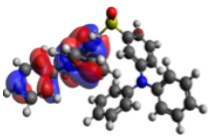	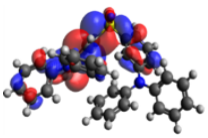
	T_1 Optimization		T_1 Optimization	
	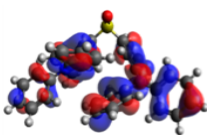	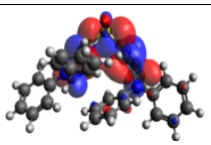	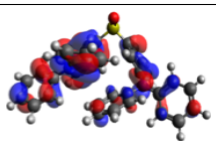	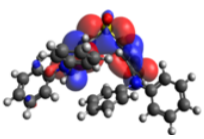

Table B.7. Distribution of frontier molecular orbitals for compounds SF2C, PTSOPT and PXZ-DPS at $S_0 \rightarrow S_1$ excitation and $S_0 \rightarrow T_1$ excitation (TDA: B3LYP/6-31+G(d,p)).

Molecule	**B3LYP/6-31+G(d,p)**			
SF2C	$S_0 \rightarrow S_1$ Excitation		$S_0 \rightarrow T_1$ Excitation	
	HOMO	LUMO	HOMO	LUMO
	S_0 Optimization		S_0 Optimization	
	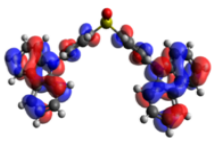	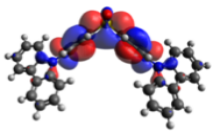	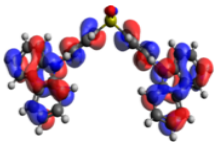	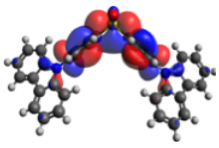
	T_1 Optimization		T_1 Optimization	
	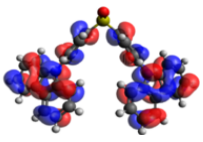	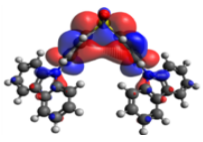	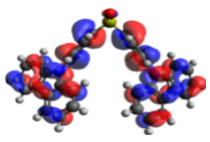	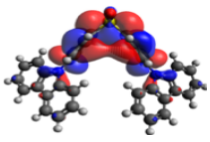
PTSOPT	S_0 Optimization		S_0 Optimization	
	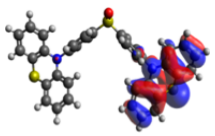	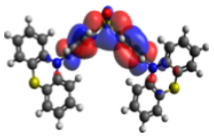	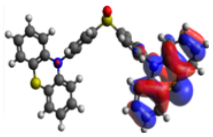	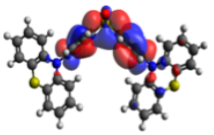
	T_1 Optimization		T_1 Optimization	
	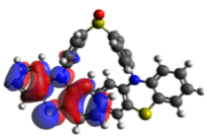	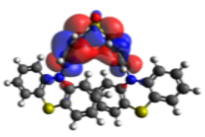		
PXZ-DPS	S_0 Optimization		S_0 Optimization	
	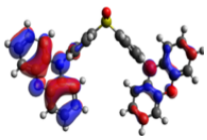	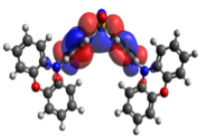	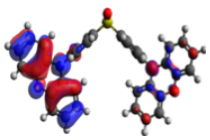	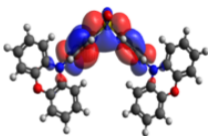
	T_1 Optimization		T_1 Optimization	
	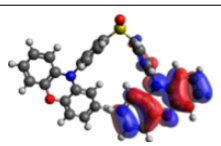	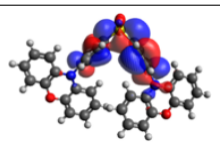	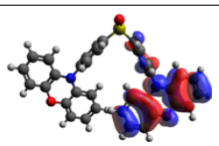	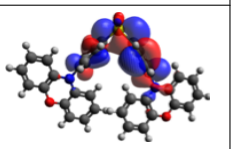

Table B.8. Distribution of frontier molecular orbitals for compounds DMAC-DPS and DPA-DPS at $S_0 \rightarrow S_1$ excitation and $S_0 \rightarrow T_1$ excitation (TDA: B3LYP/6-31+G(d,p)).

Molecule	**B3LYP/6-31+G(d,p)**			
DMAC-DPS	$S_0 \rightarrow S_1$ Excitation		$S_0 \rightarrow T_1$ Excitation	
	HOMO	LUMO	HOMO	LUMO
	S_0 Optimization		S_0 Optimization	
	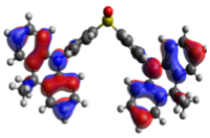	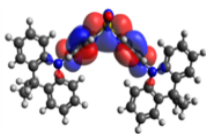	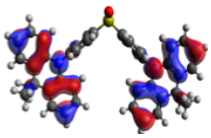	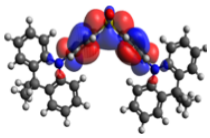
	T_1 Optimization		T_1 Optimization	
	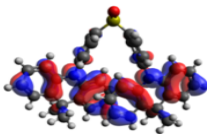	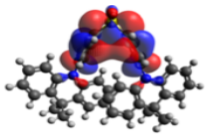	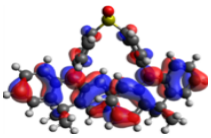	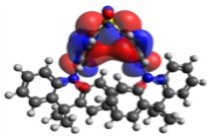
DPA-DPS	S_0 Optimization		S_0 Optimization	
	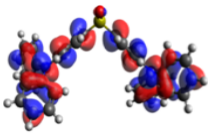	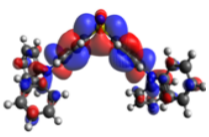	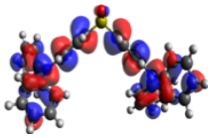	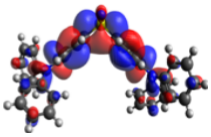
	T_1 Optimization		T_1 Optimization	
	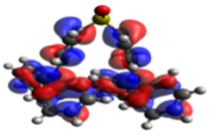	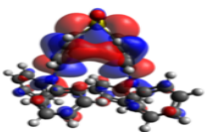	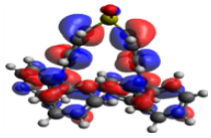	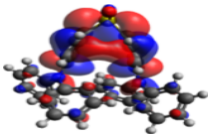

Table B.9. Distribution of frontier molecular orbitals for compound SF2C at $S_0 \rightarrow S_1$ excitation and $S_0 \rightarrow T_1$ excitation (TDA: M062X/6-31+G(d,p)).

Molecule	**M062X/6-31+G(d,p)**			
SF2C	$S_0 \rightarrow S_1$ Excitation		$S_0 \rightarrow T_1$ Excitation	
	HOMO	LUMO	HOMO	LUMO
	S_0 Optimization		S_0 Optimization	
	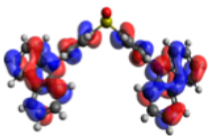	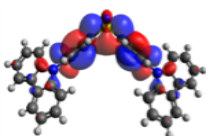	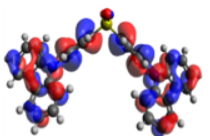	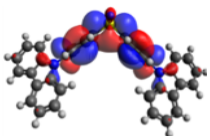
	T_1 Optimization		T_1 Optimization	
	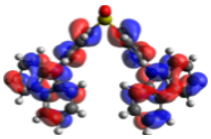	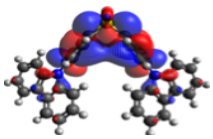	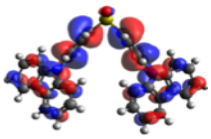	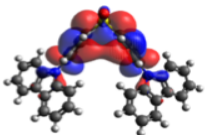

Table B.10. Distribution of frontier molecular orbitals for compounds PTSOPT, PXZ-DPS, DMAC-DPS and DPA-DPS at $S_0 \rightarrow S_1$ excitation and $S_0 \rightarrow T_1$ excitation (TDA: M062X/6-31+G(d,p)).

Molecule	**M062X/6-31+G(d,p)**			
PTSOPT	S_0 Optimization		S_0 Optimization	
	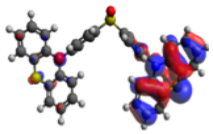		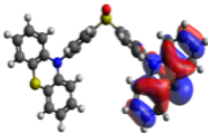	
	T_1 Optimization		T_1 Optimization	
	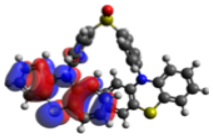		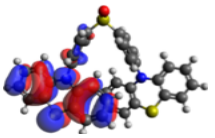	
PXZ-DPS	S_0 Optimization		S_0 Optimization	
	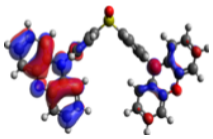		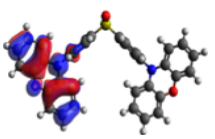	
	T_1 Optimization		T_1 Optimization	
	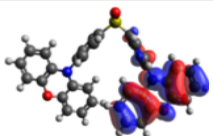		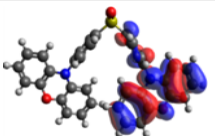	
DMAC-DPS	S_0 Optimization		S_0 Optimization	
	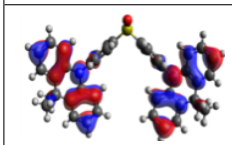		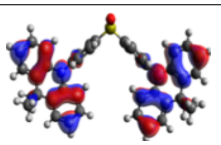	
	T_1 Optimization		T_1 Optimization	
	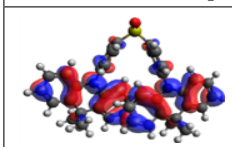		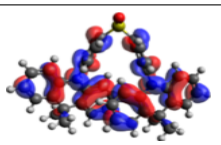	
DPA-DPS	S_0 Optimization		S_0 Optimization	
	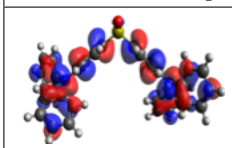		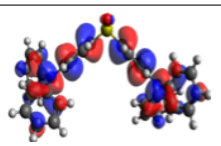	
	T_1 Optimization		T_1 Optimization	
	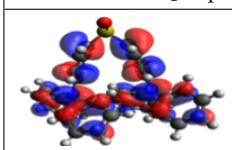		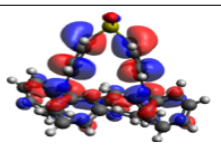	

Table B.11. Distribution of frontier molecular orbitals for compounds SF2C, PTSOPT and PXZ-DPS at $S_0 \rightarrow S_1$ excitation and $S_0 \rightarrow T_1$ excitation (TDA: PBE0/6-31+G(d,p)).

Molecule	**PBE0/6-31+G(d,p)**			
SF2C	$S_0 \rightarrow S_1$ Excitation		$S_0 \rightarrow T_1$ Excitation	
	HOMO	LUMO	HOMO	LUMO
	S_0 Optimization		S_0 Optimization	
	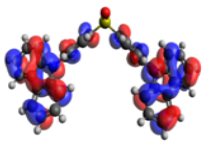	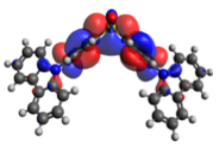	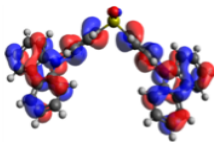	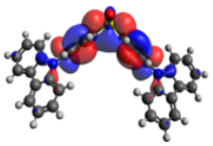
	T_1 Optimization		T_1 Optimization	
	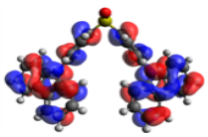	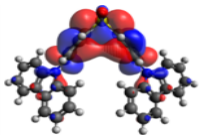	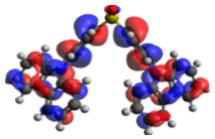	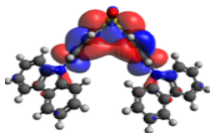
PTSOPT	S_0 Optimization		S_0 Optimization	
	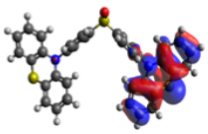	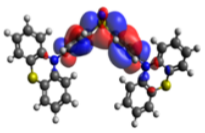	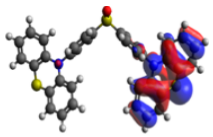	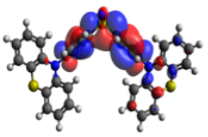
	T_1 Optimization		T_1 Optimization	
	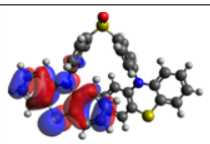	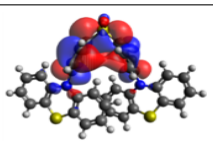	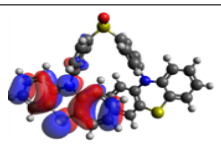	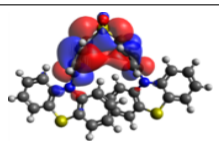
PXZ-DPS	S_0 Optimization		S_0 Optimization	
	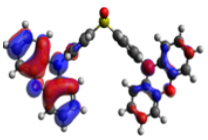	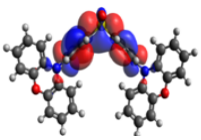	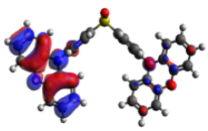	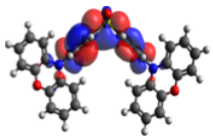
	T_1 Optimization		T_1 Optimization	
	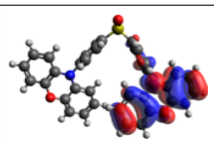	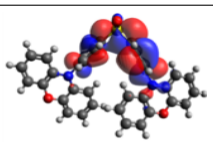	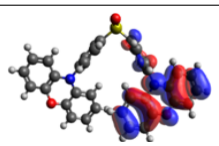	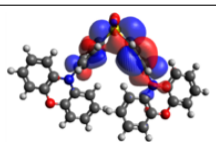

Table B.12. Distribution of frontier molecular orbitals for compounds DMAC-DPS and DPA-DPS at $S_0 \rightarrow S_1$ excitation and $S_0 \rightarrow T_1$ excitation (TDA: PBE0/6-31+G(d,p)).

Molecule	**PBE0/6-31+G(d,p)**			
DMAC-DPS	$S_0 \rightarrow S_1$ Excitation		$S_0 \rightarrow T_1$ Excitation	
	HOMO	LUMO	HOMO	LUMO
	S_0 Optimization		S_0 Optimization	
	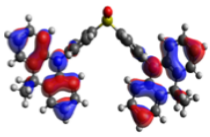	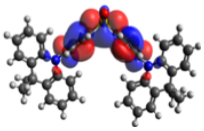	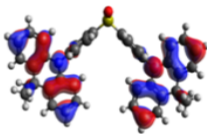	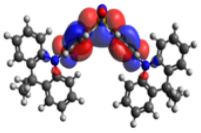
	T_1 Optimization		T_1 Optimization	
	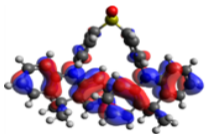	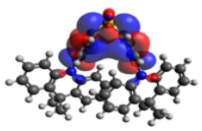	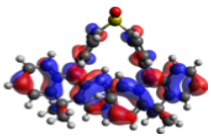	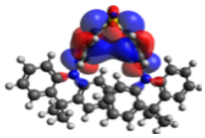
DPA-DPS	S_0 Optimization		S_0 Optimization	
	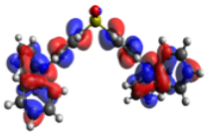	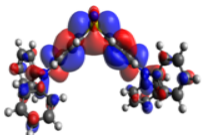	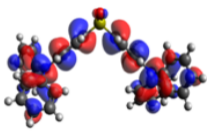	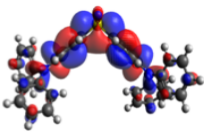
	T_1 Optimization		T_1 Optimization	
	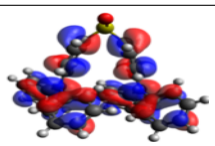	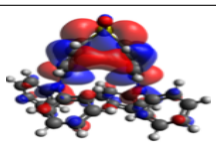	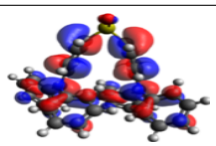	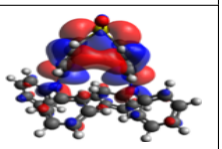

Table B.13. Distribution of frontier molecular orbitals for compounds 1a, 4ASOA and PXZ-DBTO2 at $S_0 \rightarrow S_1$ excitation and $S_0 \rightarrow T_1$ excitation (TDA: B3LYP/6-31+G(d,p)).

Molecule	**B3LYP/6-31+G(d,p)**			
1a	$S_0 \rightarrow S_1$ Excitation		$S_0 \rightarrow T_1$ Excitation	
	HOMO	LUMO	HOMO	LUMO
	S_0 Optimization		S_0 Optimization	
	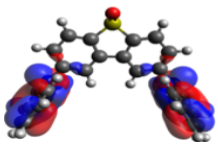	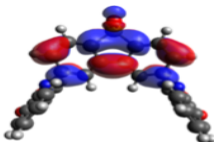	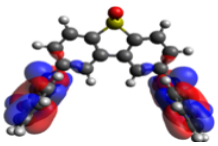	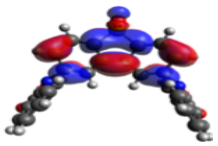
	T_1 Optimization		T_1 Optimization	
	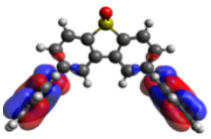	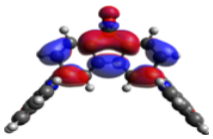	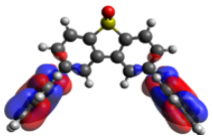	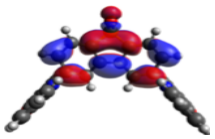
4ASOA	S_0 Optimization		S_0 Optimization	
	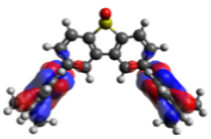	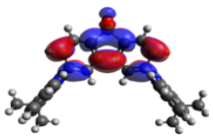	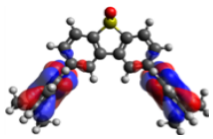	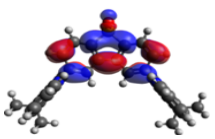
	T_1 Optimization		T_1 Optimization	
	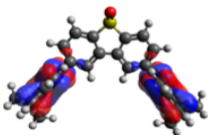	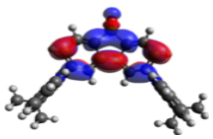	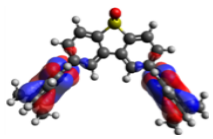	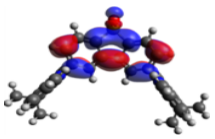
PXZ-DBTO2	S_0 Optimization		S_0 Optimization	
	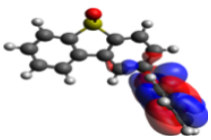	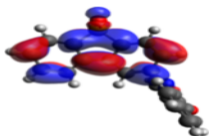	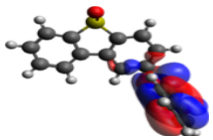	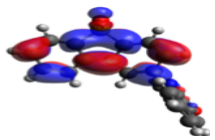
	T_1 Optimization		T_1 Optimization	
	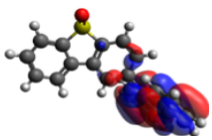	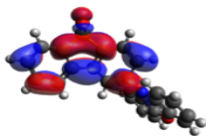	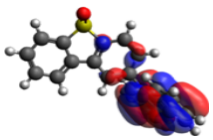	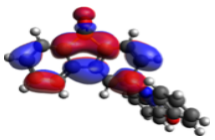

Table B.14. Distribution of frontier molecular orbitals for compounds DPO-TXO2 and DDMA-TXO2 at $S_0 \rightarrow S_1$ excitation and $S_0 \rightarrow T_1$ excitation (TDA: B3LYP/6-31+G(d,p)).

Molecule	**B3LYP/6-31+G(d,p)**			
DPO-TXO2	$S_0 \rightarrow S_1$ Excitation		$S_0 \rightarrow T_1$ Excitation	
	HOMO	LUMO	HOMO	LUMO
	S_0 Optimization		S_0 Optimization	
	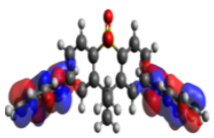	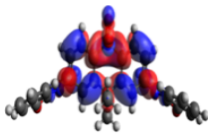	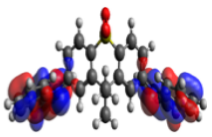	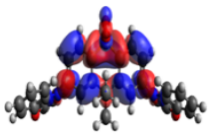
	T_1 Optimization		T_1 Optimization	
	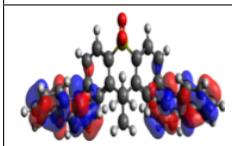	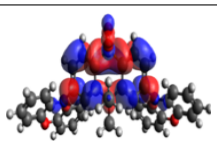	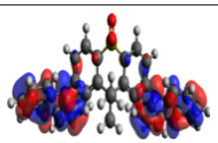	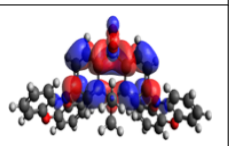
DDMA-TXO2	S_0 Optimization		S_0 Optimization	
	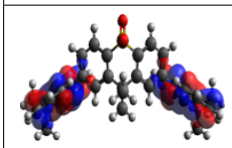	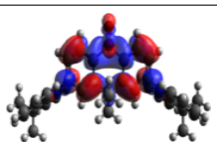	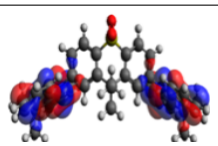	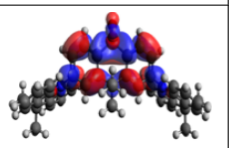
	T_1 Optimization		T_1 Optimization	
	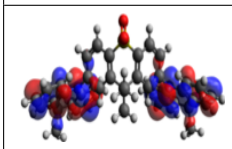	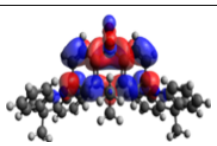	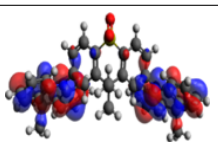	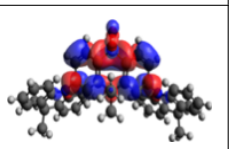

Table B.15. Distribution of frontier molecular orbitals for compound 1a at $S_0 \rightarrow S_1$ excitation and $S_0 \rightarrow T_1$ excitation (TDA: M062X/6-31+G(d,p)).

Molecule	**M062X/6-31+G(d,p)**			
1a	$S_0 \rightarrow S_1$ Excitation		$S_0 \rightarrow T_1$ Excitation	
	HOMO	LUMO	HOMO	LUMO
	S_0 Optimization		S_0 Optimization	
	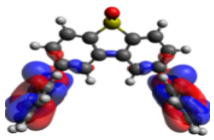	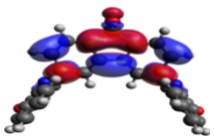	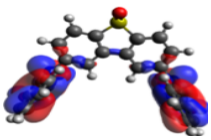	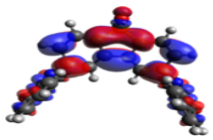
	T_1 Optimization		T_1 Optimization	
		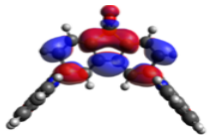	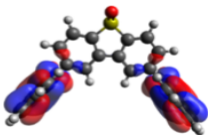	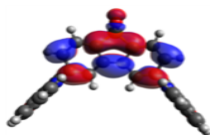

Table B.16. Distribution of frontier molecular orbitals for compounds 4ASOA, PXZ-DBTO2, DPO-TXO2 and DDMA-TXO2 at $S_0 \rightarrow S_1$ excitation and $S_0 \rightarrow T_1$ excitation (TDA: M062X/6-31+G(d,p)).

Molecule	**M062X/6-31+G(d,p)**			
4ASOA	$S_0 \rightarrow S_1$ Excitation		$S_0 \rightarrow T_1$ Excitation	
	HOMO	LUMO	HOMO	LUMO
	S_0 Optimization		S_0 Optimization	
	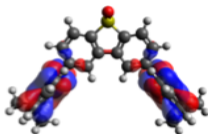	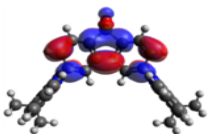		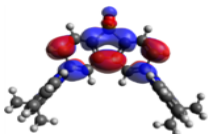
	T_1 Optimization		T_1 Optimization	
		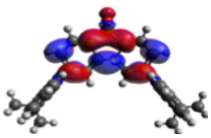		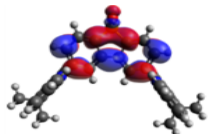
PXZ-DBTO2	S_0 Optimization		S_0 Optimization	
	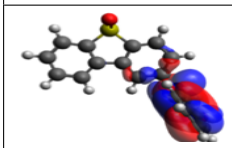	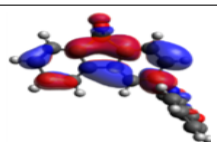	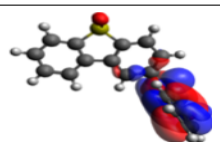	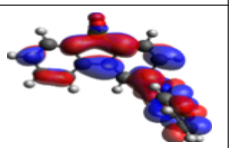
	T_1 Optimization		T_1 Optimization	
	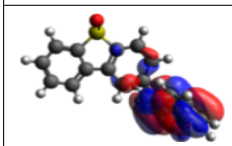	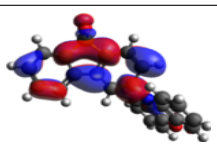	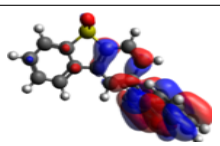	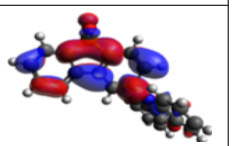
DPO-TXO2	S_0 Optimization		S_0 Optimization	
	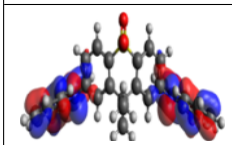	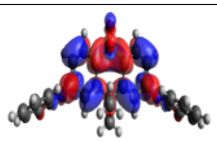	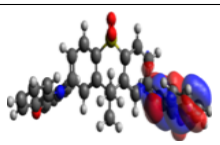	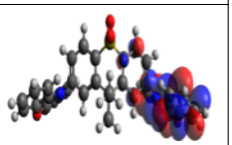
	T_1 Optimization		T_1 Optimization	
	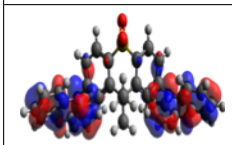	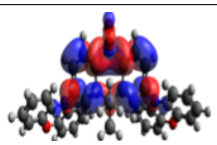	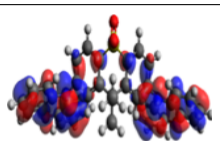	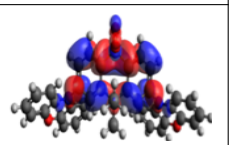
DDMA-TXO2	S_0 Optimization		S_0 Optimization	
	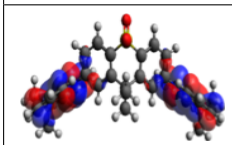	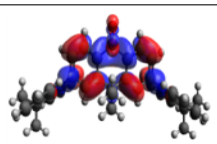	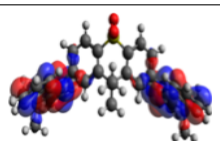	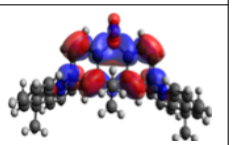
	T_1 Optimization		T_1 Optimization	
	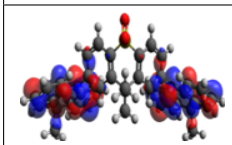	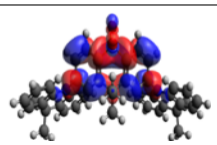	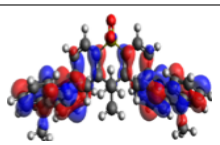	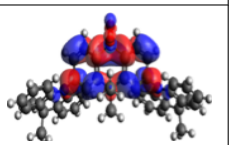

Table B.17. Distribution of frontier molecular orbitals for compounds 1a, 4ASOA and PXZ-DBTO2 at $S_0 \rightarrow S_1$ excitation and $S_0 \rightarrow T_1$ excitation (TDA: PBE0/6-31+G(d,p)).

Molecule	**PBE0/6-31+G(d,p)**			
1a	$S_0 \rightarrow S_1$ Excitation		$S_0 \rightarrow T_1$ Excitation	
	HOMO	LUMO	HOMO	LUMO
	S_0 Optimization		S_0 Optimization	
	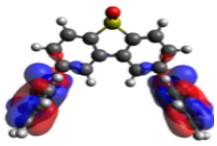		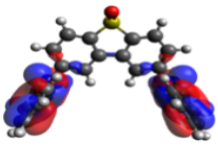	
	T_1 Optimization		T_1 Optimization	
	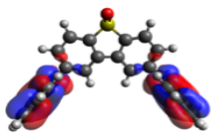		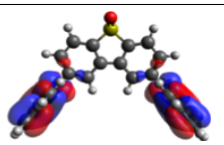	
4ASOA	S_0 Optimization		S_0 Optimization	
	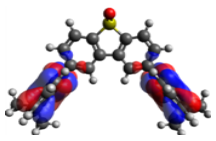			
	T_1 Optimization		T_1 Optimization	
				
PXZ-DBTO2	S_0 Optimization		S_0 Optimization	
	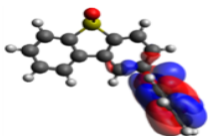		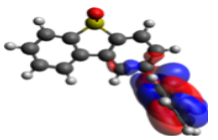	
	T_1 Optimization		T_1 Optimization	
	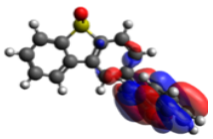		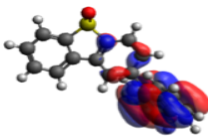	

Table B.18. Distribution of frontier molecular orbitals for compounds DPO-TXO2 and DDMA-TXO2 at $S_0 \rightarrow S_1$ excitation and $S_0 \rightarrow T_1$ excitation (TDA: PBE0/6-31+G(d,p)).

Molecule	**PBE0/6-31+G(d,p)**			
DPO-TXO2	$S_0 \rightarrow S_1$ Excitation		$S_0 \rightarrow T_1$ Excitation	
	HOMO	LUMO	HOMO	LUMO
	S_0 Optimization		S_0 Optimization	
	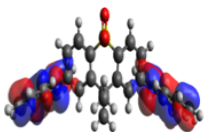	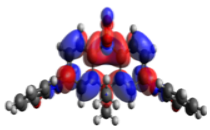	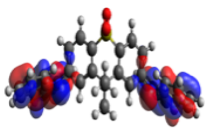	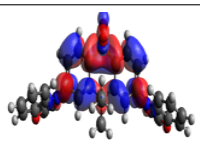
	T_1 Optimization		T_1 Optimization	
	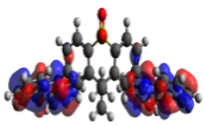	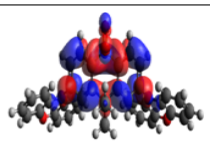	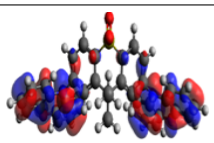	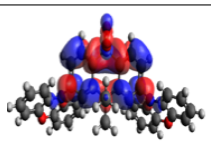
DDMA-TXO2	S_0 Optimization		S_0 Optimization	
	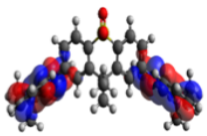	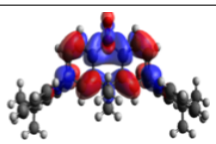	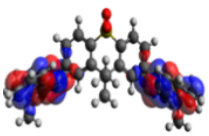	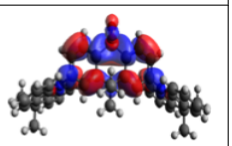
	T_1 Optimization		T_1 Optimization	
	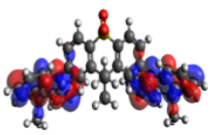	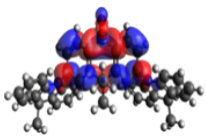	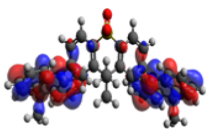	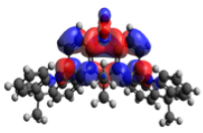

Table B.19. Distribution of frontier molecular orbitals for compounds Cz-TTR, DMAC-TTR, PXZ-TTR and PTZ-TTR at $S_0 \rightarrow S_1$ excitation and $S_0 \rightarrow T_1$ excitation (TDA: B3LYP/6-31+G(d,p)).

Molecule	**B3LYP/6-31+G(d,p)**			
Cz-TTR	$S_0 \rightarrow S_1$ Excitation		$S_0 \rightarrow T_1$ Excitation	
	HOMO	LUMO	HOMO	LUMO
	S_0 Optimization		S_0 Optimization	
	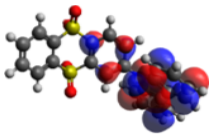	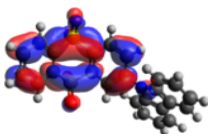	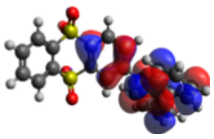	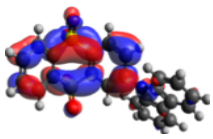
	T_1 Optimization		T_1 Optimization	
	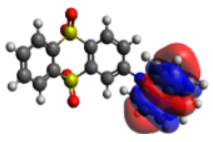	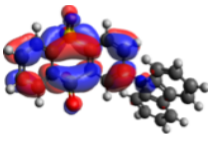	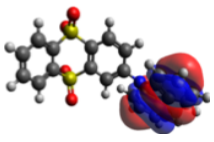	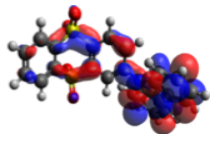
DMAC-TTR	S_0 Optimization		S_0 Optimization	
	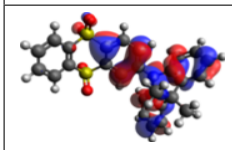	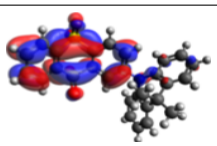	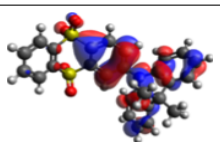	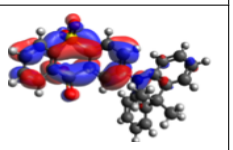
	T_1 Optimization		T_1 Optimization	
	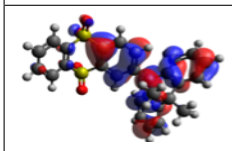	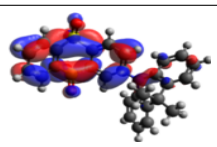	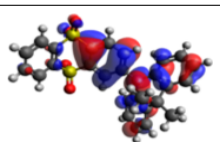	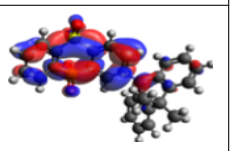
PXZ-TTR	S_0 Optimization		S_0 Optimization	
	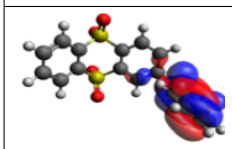	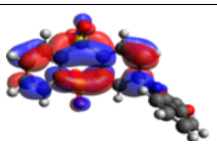	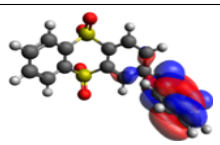	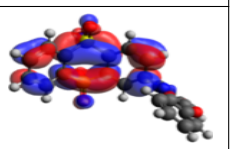
	T_1 Optimization		T_1 Optimization	
	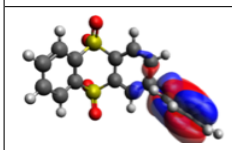	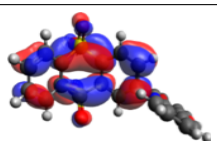	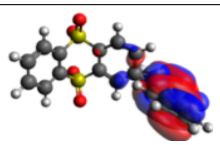	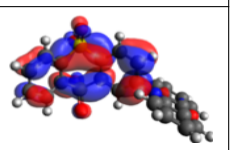
PTZ-TTR	S_0 Optimization		S_0 Optimization	
	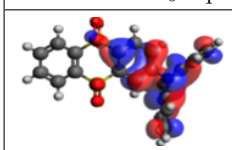	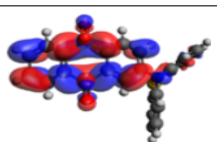	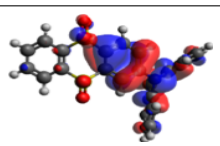	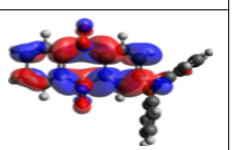
	T_1 Optimization		T_1 Optimization	
	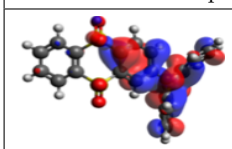	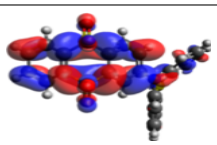	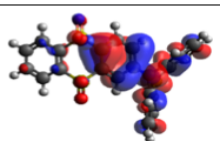	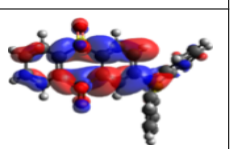

Table B.20. Distribution of frontier molecular orbitals for compounds Cz-TTR, DMAC-TTR, PXZ-TTR and PTZ-TTR at $S_0 \rightarrow S_1$ excitation and $S_0 \rightarrow T_1$ excitation (TDA: M062X/6-31+G(d,p)).

Molecule	**M062X/6-31+G(d,p)**			
Cz-TTR	$S_0 \rightarrow S_1$ Excitation		$S_0 \rightarrow T_1$ Excitation	
	HOMO	LUMO	HOMO	LUMO
	S_0 Optimization		S_0 Optimization	
	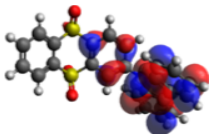	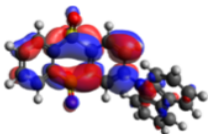	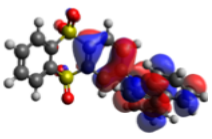	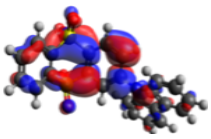
	T_1 Optimization		T_1 Optimization	
	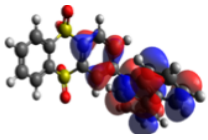	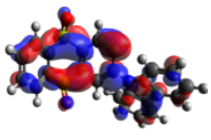	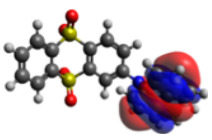	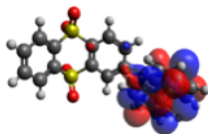
DMAC-TTR	S_0 Optimization		S_0 Optimization	
	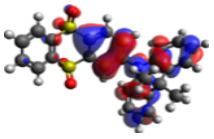	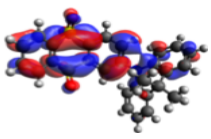	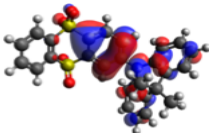	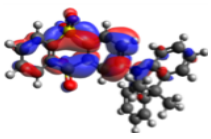
	T_1 Optimization		T_1 Optimization	
	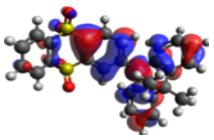	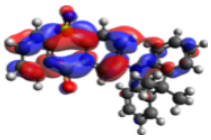	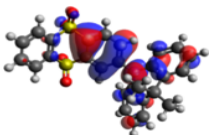	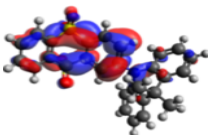
PXZ-TTR	S_0 Optimization		S_0 Optimization	
	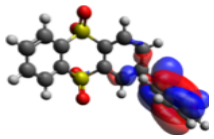	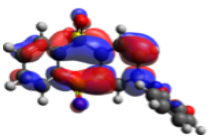	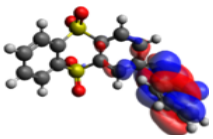	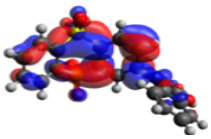
	T_1 Optimization		T_1 Optimization	
	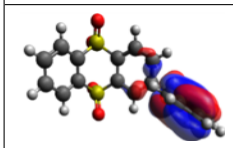	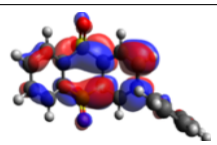	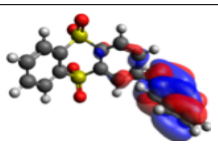	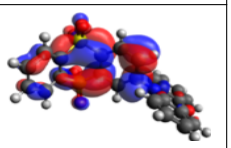
PTZ-TTR	S_0 Optimization		S_0 Optimization	
	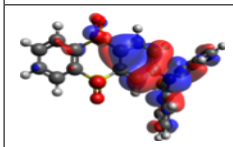	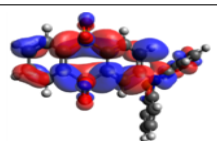	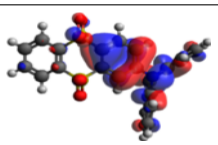	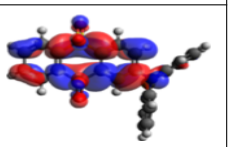
	T_1 Optimization		T_1 Optimization	
	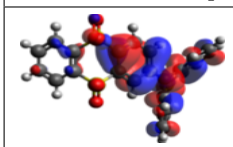	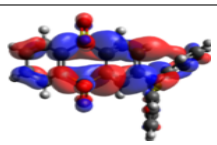	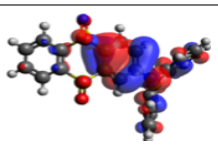	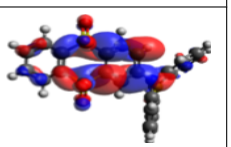

Table B.21. Distribution of frontier molecular orbitals for compounds Cz-TTR, DMAC-TTR, PXZ-TTR and PTZ-TTR at $S_0 \rightarrow S_1$ excitation and $S_0 \rightarrow T_1$ excitation (TDA: PBE0/6-31+G(d,p)).

Molecule	**PBE0/6-31+G(d,p)**			
Cz-TTR	$S_0 \rightarrow S_1$ Excitation		$S_0 \rightarrow T_1$ Excitation	
	HOMO	LUMO	HOMO	LUMO
	S_0 Optimization		S_0 Optimization	
	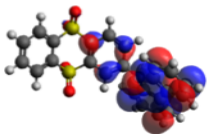	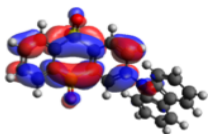	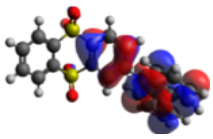	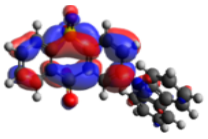
	T_1 Optimization		T_1 Optimization	
	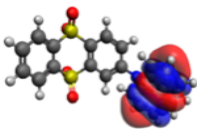	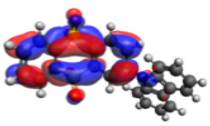	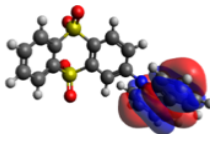	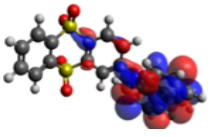
DMAC-TTR	S_0 Optimization		S_0 Optimization	
	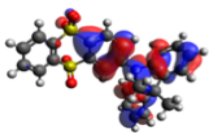	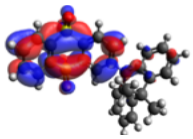	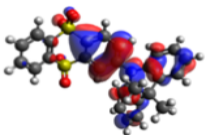	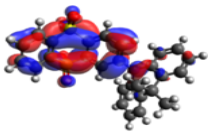
	T_1 Optimization		T_1 Optimization	
	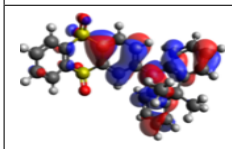	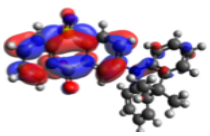	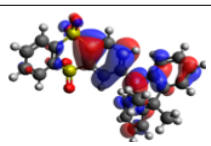	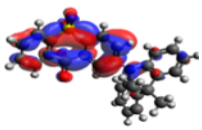
PXZ-TTR	S_0 Optimization		S_0 Optimization	
	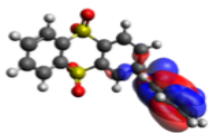	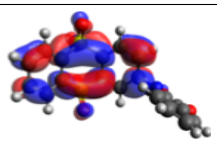	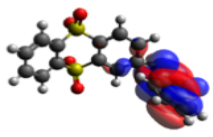	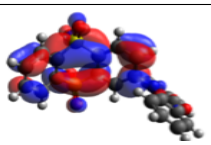
	T_1 Optimization		T_1 Optimization	
	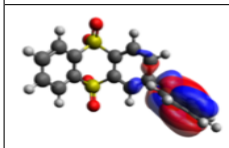	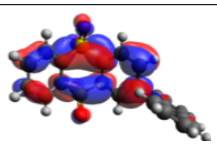	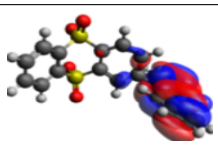	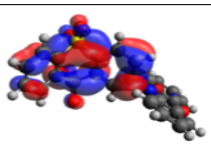
PTZ-TTR	S_0 Optimization		S_0 Optimization	
	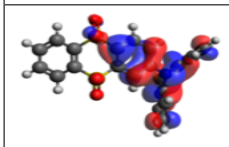	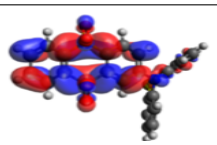	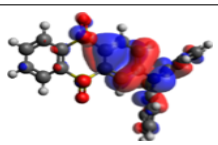	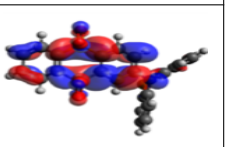
	T_1 Optimization		T_1 Optimization	
	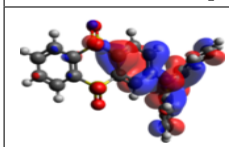	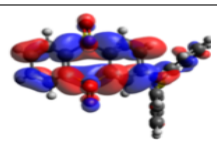	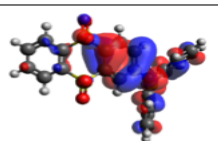	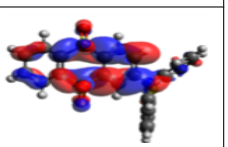

Table B.22. Distribution of frontier molecular orbitals for compounds CzPhDSO2, ACRDSO2, PXZDSO2 and PTZ-Ph-TTR at $S_0 \rightarrow S_1$ excitation and $S_0 \rightarrow T_1$ excitation (TDA: B3LYP/6-31+G(d,p)).

Molecule	**B3LYP/6-31+G(d,p)**			
CzPhDSO2	$S_0 \rightarrow S_1$ Excitation		$S_0 \rightarrow T_1$ Excitation	
	HOMO	LUMO	HOMO	LUMO
	S_0 Optimization		S_0 Optimization	
	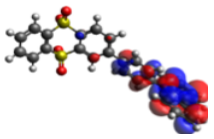	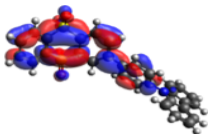	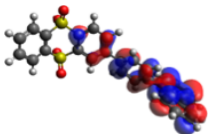	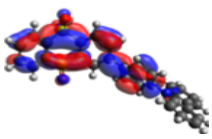
	T_1 Optimization		T_1 Optimization	
	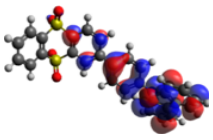	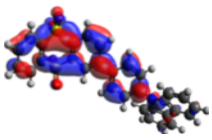	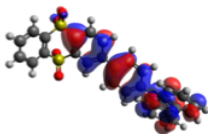	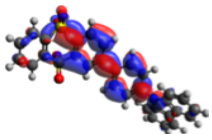
ACRDSO2	S_0 Optimization		S_0 Optimization	
	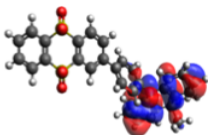	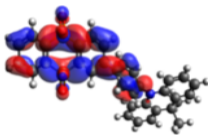	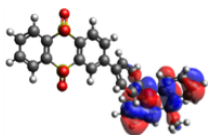	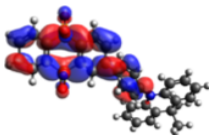
	T_1 Optimization		T_1 Optimization	
	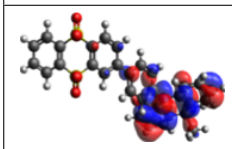	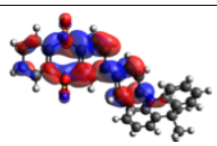	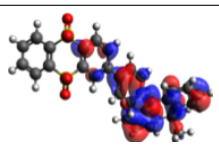	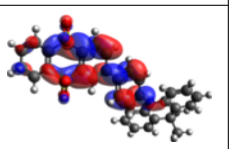
PXZDSO2	S_0 Optimization		S_0 Optimization	
	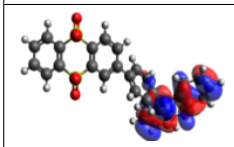	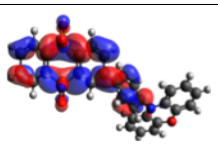	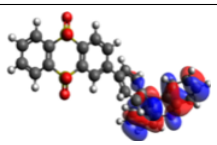	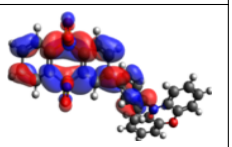
	T_1 Optimization		T_1 Optimization	
	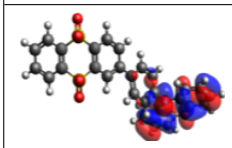	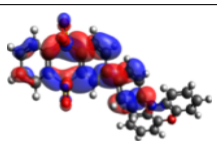	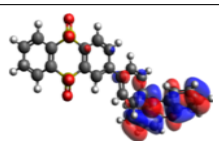	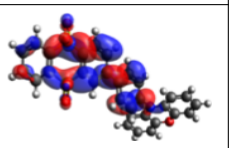
PTZ-Ph-TTR	S_0 Optimization		S_0 Optimization	
	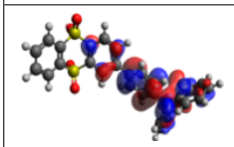	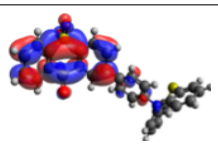	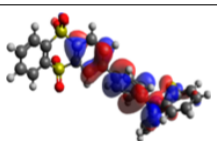	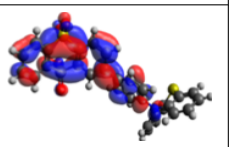
	T_1 Optimization		T_1 Optimization	
	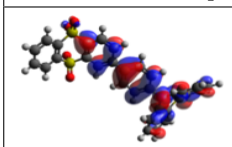	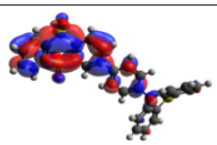	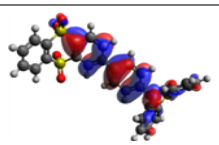	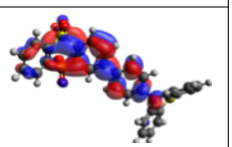

Table B.23. Distribution of frontier molecular orbitals for compounds CzPhDSO2, ACRDSO2, PXZDSO2 and PTZ-Ph-TTR at $S_0 \rightarrow S_1$ excitation and $S_0 \rightarrow T_1$ excitation (TDA: M062X/6-31+G(d,p)).

Molecule	**M062X/6-31+G(d,p)**			
CzPhDSO2	$S_0 \rightarrow S_1$ Excitation		$S_0 \rightarrow T_1$ Excitation	
	HOMO	LUMO	HOMO	LUMO
	S_0 Optimization		S_0 Optimization	
	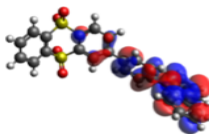	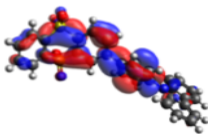	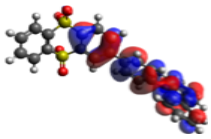	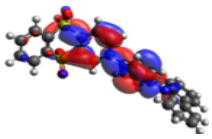
	T_1 Optimization		T_1 Optimization	
	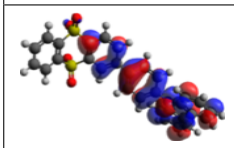	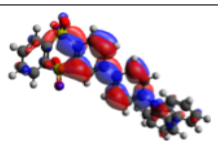	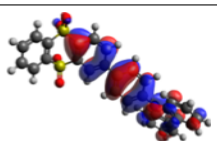	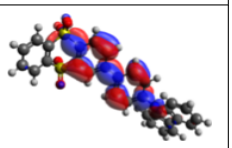
ACRDSO2	S_0 Optimization		S_0 Optimization	
	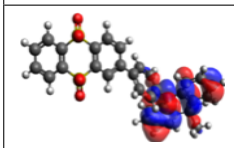	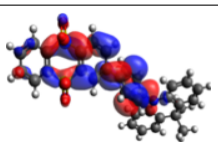	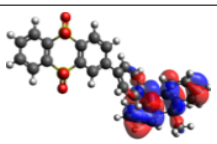	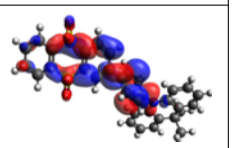
	T_1 Optimization		T_1 Optimization	
	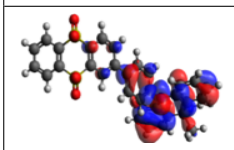	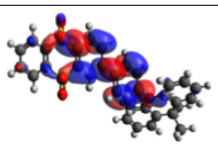	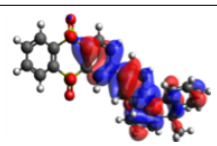	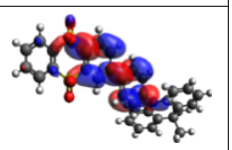
PXZDSO2	S_0 Optimization		S_0 Optimization	
	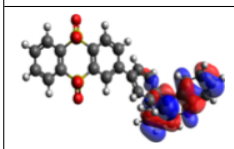	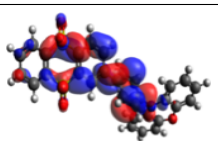	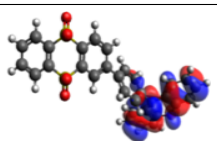	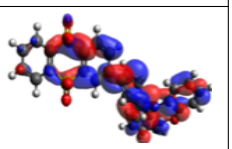
	T_1 Optimization		T_1 Optimization	
	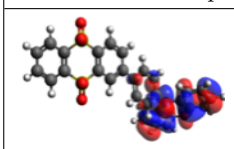	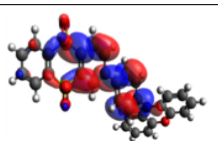	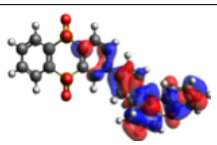	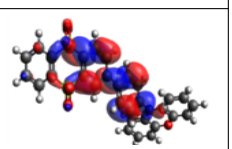
PTZ-Ph-TTR	S_0 Optimization		S_0 Optimization	
	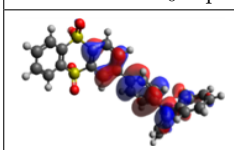	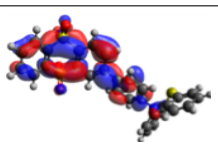	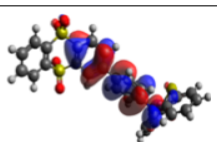	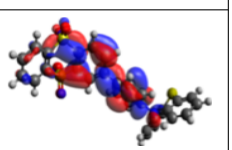
	T_1 Optimization		T_1 Optimization	
	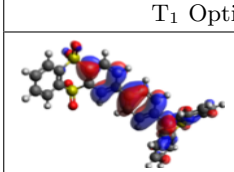	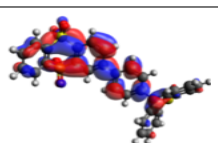	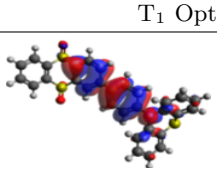	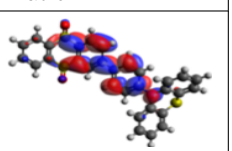

Table B.24. Distribution of frontier molecular orbitals for compounds CzPhDSO2, ACRDSO2, PXZDSO2 and PTZ-Ph-TTR at $S_0 \rightarrow S_1$ excitation and $S_0 \rightarrow T_1$ excitation (TDA: PBE0/6-31+G(d,p)).

Molecule	**PBE0/6-31+G(d,p)**			
CzPhDSO2	$S_0 \rightarrow S_1$ Excitation		$S_0 \rightarrow T_1$ Excitation	
	HOMO	LUMO	HOMO	LUMO
	S_0 Optimization		S_0 Optimization	
	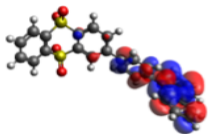	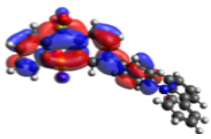	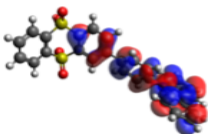	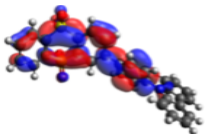
	T_1 Optimization		T_1 Optimization	
	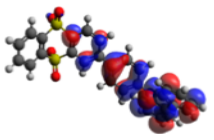	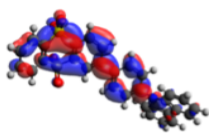	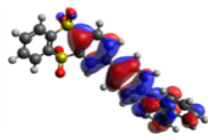	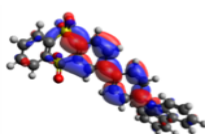
ACRDSO2	S_0 Optimization		S_0 Optimization	
	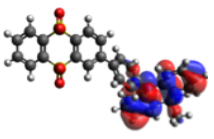	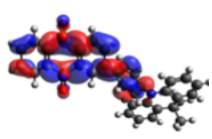	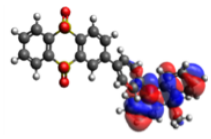	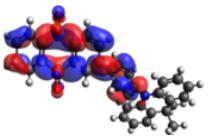
	T_1 Optimization		T_1 Optimization	
	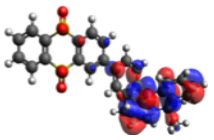	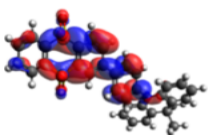	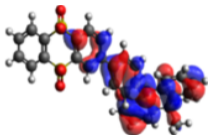	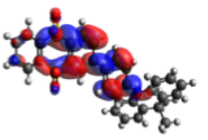
PXZDSO2	S_0 Optimization		S_0 Optimization	
	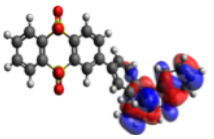	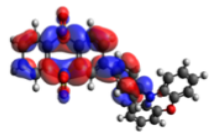	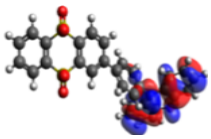	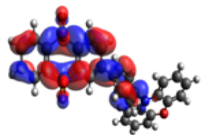
	T_1 Optimization		T_1 Optimization	
	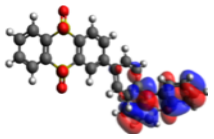	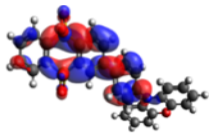	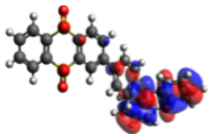	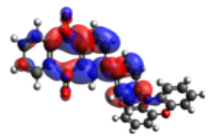
PTZ-Ph-TTR	S_0 Optimization		S_0 Optimization	
	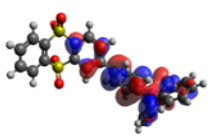	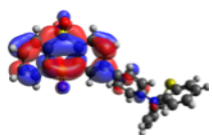	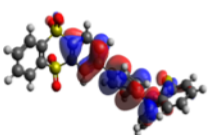	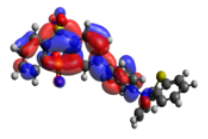
	T_1 Optimization		T_1 Optimization	
	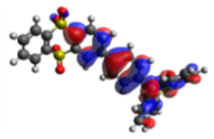	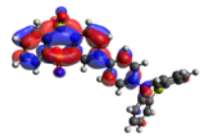	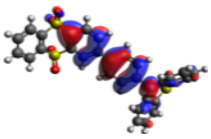	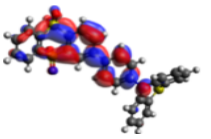

Table B.25. Distribution of frontier molecular orbitals for compounds Ac-OSO, CzSOXO and TXO-PhCz at $S_0 \rightarrow S_1$ excitation and $S_0 \rightarrow T_1$ excitation (TDA: B3LYP/6-31+G(d,p)).

Molecule	**B3LYP/6-31+G(d,p)**			
Ac-OSO	$S_0 \rightarrow S_1$ Excitation		$S_0 \rightarrow T_1$ Excitation	
	HOMO	LUMO	HOMO	LUMO
	S_0 Optimization		S_0 Optimization	
	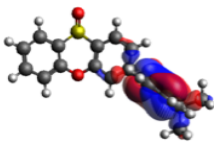	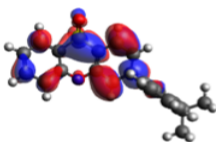	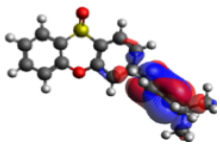	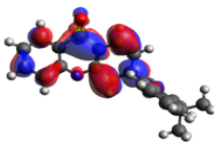
	T_1 Optimization		T_1 Optimization	
		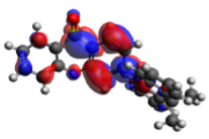	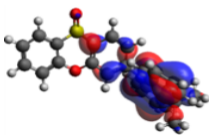	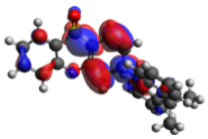
CzSOXO	S_0 Optimization		S_0 Optimization	
		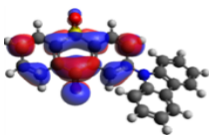	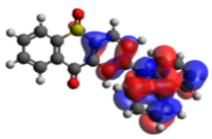	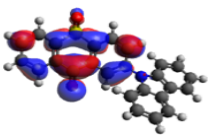
	T_1 Optimization		T_1 Optimization	
	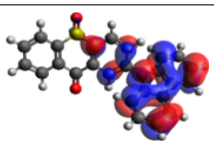	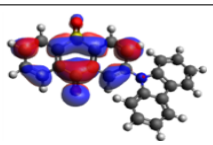	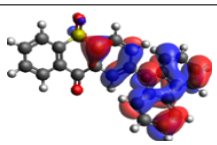	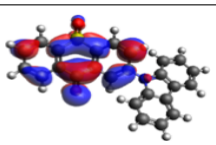
TXO-PhCz	S_0 Optimization		S_0 Optimization	
	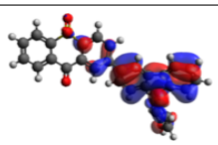	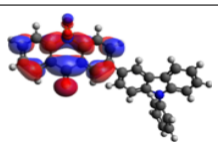	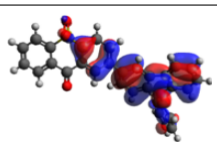	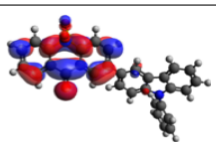
	T_1 Optimization		T_1 Optimization	
	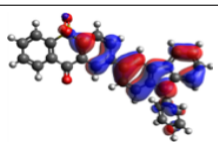	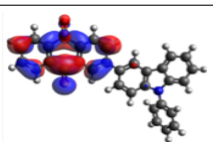	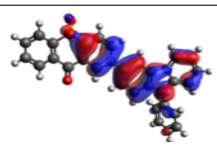	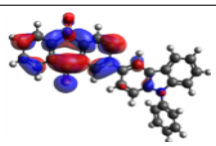

Table B.26. Distribution of frontier molecular orbitals for compounds Ac-OSO, CzSOXO and TXO-PhCz at $S_0 \rightarrow S_1$ excitation and $S_0 \rightarrow T_1$ excitation (TDA: M062X/6-31+G(d,p)).

Molecule	**M062X/6-31+G(d,p)**			
Ac-OSO	$S_0 \rightarrow S_1$ Excitation		$S_0 \rightarrow T_1$ Excitation	
	HOMO	LUMO	HOMO	LUMO
	S_0 Optimization		S_0 Optimization	
	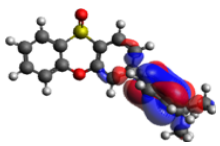	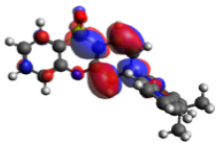	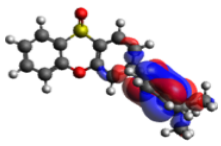	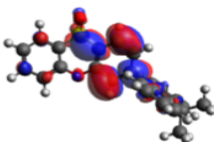
	T_1 Optimization		T_1 Optimization	
	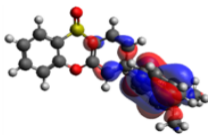	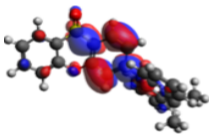	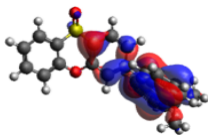	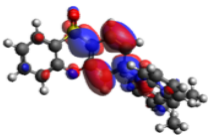
CzSOXO	S_0 Optimization		S_0 Optimization	
	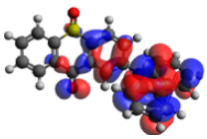	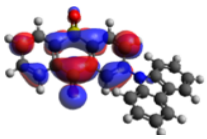	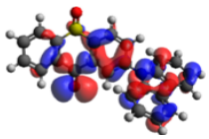	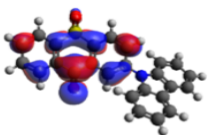
	T_1 Optimization		T_1 Optimization	
	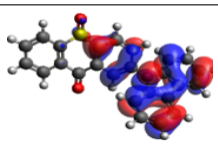	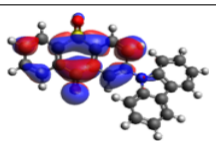	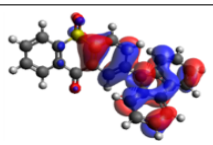	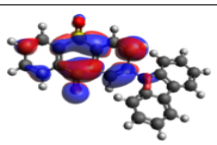
TXO-PhCz	S_0 Optimization		S_0 Optimization	
	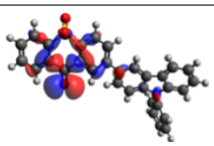	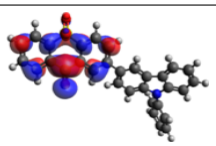	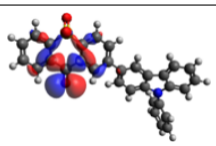	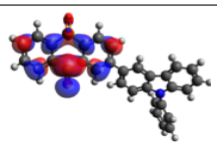
	T_1 Optimization		T_1 Optimization	
	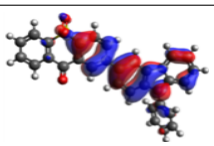	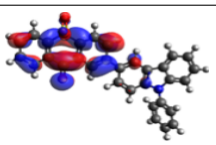	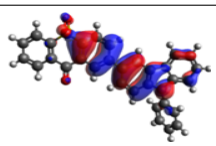	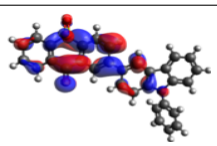

Table B.27. Distribution of frontier molecular orbitals for compounds Ac-OSO, CzSOXO and TXO-PhCz at $S_0 \rightarrow S_1$ excitation and $S_0 \rightarrow T_1$ excitation (TDA: PBE0/6-31+G(d,p)).

Molecule	**PBE0/6-31+G(d,p)**			
Ac-OSO	$S_0 \rightarrow S_1$ Excitation		$S_0 \rightarrow T_1$ Excitation	
	HOMO	LUMO	HOMO	LUMO
	S_0 Optimization		S_0 Optimization	
	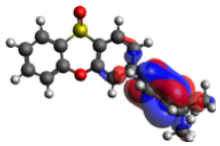	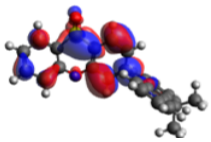	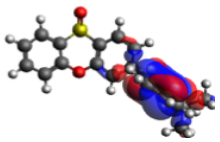	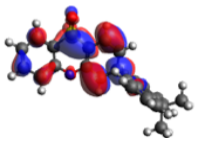
	T_1 Optimization		T_1 Optimization	
	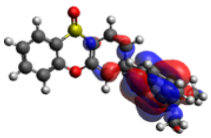	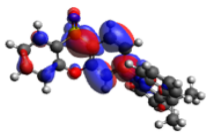		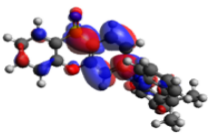
CzSOXO	S_0 Optimization		S_0 Optimization	
	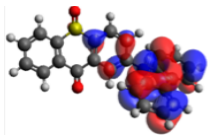	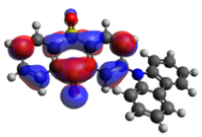	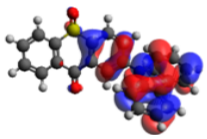	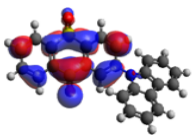
	T_1 Optimization		T_1 Optimization	
	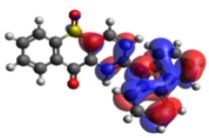	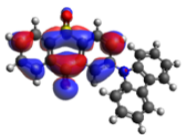	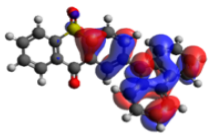	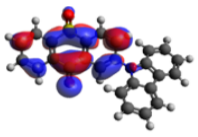
TXO-PhCz	S_0 Optimization		S_0 Optimization	
	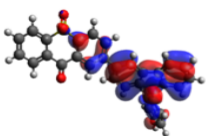	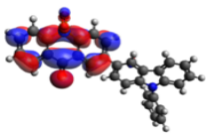	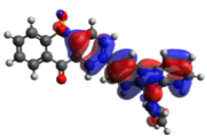	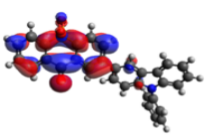
	T_1 Optimization		T_1 Optimization	
	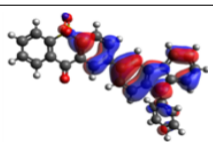	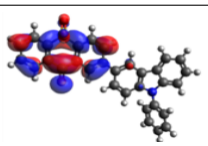	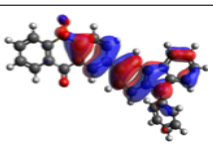	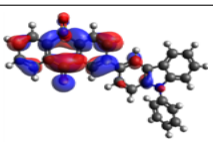

Table B.28. Φ_s indices for compounds in Lowdin (L) and Mulliken (M) charge distributions for the excitations from S_0 to S_1 for Group 1.

GROUP 1					
Compound	**Method**	**S_0 Geometry**		**T_1 Geometry**	
		L	**M**	**L**	**M**
1	B3LYP	0.4078	0.5203	0.4775	0.6364
	M062X	0.5570	0.6595	0.5968	0.7386
	PBE0	0.4402	0.5403	0.4740	0.6156
2	B3LYP	0.2761	0.4080	0.2329	0.3197
	M062X	0.4703	0.5810	0.3306	0.4352
	PBE0	0.3062	0.4296	0.2378	0.3090
3	B3LYP	0.3325	0.4212	0.2544	0.2961
	M062X	0.4383	0.5456	0.4230	0.5027
	PBE0	0.3623	0.4402	0.2882	0.3272
4	B3LYP	0.2234	0.2830	0.2818	0.4323
	M062X	0.3939	0.4601	0.3352	0.4861
	PBE0	0.2457	0.2849	0.2687	0.3757
5	B3LYP	0.6169	0.7551	0.5168	0.6565
	M062X	0.7416	0.8776	0.6402	0.8128
	PBE0	0.6321	0.7530	0.5336	0.6544

Table B.29. Φ_s indices for compounds in Lowdin (L) and Mulliken (M) charge distributions for the excitations from S_0 to T_1 for Group 1.

GROUP 1					
Compound	**Method**	**S_0 Geometry**		**T_1 Geometry**	
		L	**M**	**L**	**M**
1	B3LYP	0.4741	0.5806	0.5654	0.7087
	M062X	0.7721	0.8781	0.8210	0.9206
	PBE0	0.5772	0.6620	0.6361	0.7694
2	B3LYP	0.3332	0.4587	0.2673	0.3560
	M062X	0.7920	0.8824	0.5113	0.6086
	PBE0	0.4181	0.5316	0.2897	0.3616
3	B3LYP	0.3665	0.4563	0.2830	0.3227
	M062X	0.7597	0.8619	0.4744	0.5660
	PBE0	0.4127	0.4895	0.3164	0.3531
4	B3LYP	0.2465	0.3124	0.3092	0.4593
	M062X	0.6062	0.6792	0.4828	0.6695
	PBE0	0.2962	0.3421	0.3105	0.4222
5	B3LYP	0.7512	0.8535	0.6584	0.7700
	M062X	0.8193	0.9671	0.7883	0.9065
	PBE0	0.7646	0.8622	0.6936	0.7956

Table B.30. Φ_s indices for compounds in Lowdin (L) and Mulliken (M) charge distributions for the excitations from S_0 to S_1 for Group 2.

GROUP 2					
Compound	**Methods**	**S_0 Geometry**		**T_1 Geometry**	
		L	**M**	**L**	M
SF2C	B3LYP	0.5460	0.6495	0.5982	0.7400
	M062X	0.7047	0.7487	0.7269	0.8004
	PBE0	0.5720	0.6352	0.6334	0.7505
PTSOPT	B3LYP	0.2042	0.2677	0.2277	0.3531
	M062X	0.3310	0.4202	0.2434	0.3683
	PBE0	0.2633	0.3396	0.2279	0.3387
PXZ-DPS	B3LYP	0.1492	0.3740	0.4886	0.7726
	M062X	0.2485	0.4401	0.5146	0.7627
	PBE0	0.1670	0.3385	0.4407	0.6794
DMAC-DPS	B3LYP	0.0997	0.2021	0.3154	0.4530
	M062X	0.1642	0.2308	0.3938	0.5478
	PBE0	0.1146	0.1862	0.3386	0.4635
DPA-DPS	B3LYP	0.7086	0.7733	0.7266	0.7898
	M062X	0.7594	0.8234	0.7631	0.8279
	PBE0	0.7139	0.7683	0.7423	0.8106

Table B.31. Φ_s indices for compounds in Lowdin (L) and Mulliken (M) charge distributions for the excitations from S_0 to T_1 for Group 2.

GROUP 2					
Compound	**Methods**	**S_0 Geometry**		**T_1 Geometry**	
		L	**M**	**L**	**M**
SF2C	B3LYP	0.7309	0.8289	0.7672	0.9103
	M062X	0.8405	0.8789	0.8563	0.9120
	PBE0	0.7829	0.8346	0.8048	0.9141
PTSOPT	B3LYP	0.2308	0.2941	0.1995	0.3198
	M062X	0.7845	0.9099	0.2758	0.3985
	PBE0	0.3266	0.3964	0.2080	0.3174
PXZ-DPS	B3LYP	0.1589	0.3536	0.3989	0.6627
	M062X	0.4301	0.5961	0.4778	0.7106
	PBE0	0.1862	0.3513	0.3613	0.5742
DMAC-DPS	B3LYP	0.1168	0.2200	0.3653	0.5071
	M062X	0.1692	0.2371	0.5399	0.6931
	PBE0	0.1390	0.2142	0.4174	0.5409
DPA-DPS	B3LYP	0.7835	0.8383	0.8016	0.8888
	M062X	0.8375	0.8890	0.8288	0.8957
	PBE0	0.8080	0.8571	0.8162	0.9005

Table B.32. Φ_s indices for compounds in Lowdin (L) and Mulliken (M) charge distributions for the excitations from S_0 to S_1 for Group 3.

GROUP 3					
Compound	**Method**	**S_0 Geometry**		**T_1 Geometry**	
		L	**M**	**L**	**M**
1a	B3LYP	0.1191	0.1862	0.1038	0.1241
	M062X	0.1854	0.3092	0.1602	0.1786
	PBE0	0.1269	0.1893	0.1116	0.1247
4ASOA	B3LYP	0.1044	0.1141	0.1049	0.1138
	M062X	0.1712	0.1825	0.1567	0.1668
	PBE0	0.1154	0.1214	0.1107	0.1193
PXZ-DBTO2	B3LYP	0.1005	0.1623	0.4006	0.4821
	M062X	0.1435	0.2702	0.5615	0.6611
	PBE0	0.1128	0.1785	0.3802	0.4530
DPO-TXO2	B3LYP	0.1918	0.3178	0.3165	0.3903
	M062X	0.2809	0.4708	0.4694	0.5873
	PBE0	0.2065	0.3355	0.3457	0.4063
DDMA-TXO2	B3LYP	0.2954	0.3781	0.3470	0.4466
	M062X	0.3465	0.4097	0.4591	0.5519
	PBE0	0.2769	0.3364	0.3428	0.4239

Table B.33. Φ_s indices for compounds in Lowdin (L) and Mulliken (M) charge distributions for the excitations from S_0 to T_1 for Group 3.

GROUP 3					
Compound	**Method**	**S_0 Geometry**		**T_1 Geometry**	
		L	**M**	**L**	**M**
1a	B3LYP	0.1443	0.2096	0.1063	0.1275
	M062X	0.3842	0.4907	0.2250	0.2466
	PBE0	0.1615	0.2240	0.1288	0.1446
4ASOA	B3LYP	0.1291	0.1379	0.1104	0.1202
	M062X	0.2102	0.2224	0.1627	0.1767
	PBE0	0.1486	0.1576	0.1255	0.1369
PXZ-DBTO2	B3LYP	0.1357	0.1975	0.3504	0.4336
	M062X	0.5049	0.6072	0.5848	0.6788
	PBE0	0.1739	0.2405	0.3403	0.4141
DPO-TXO2	B3LYP	0.2073	0.3332	0.3001	0.3683
	M062X	0.8393	0.8954	0.5074	0.6271
	PBE0	0.2300	0.3598	0.3420	0.4047
DDMA-TXO2	B3LYP	0.3035	0.3847	0.3690	0.4617
	M062X	0.3422	0.4047	0.5383	0.6278
	PBE0	0.2764	0.3336	0.3832	0.4569

Table B.34. Φ_s indices for compounds in Lowdin (L) and Mulliken (M) charge distributions for the excitations from S_0 to S_1 for Group 4.

GROUP 4					
Compound	**Method**	**S_0 Geometry**		**T_1 Geometry**	
		L	**M**	**L**	**M**
Cz-TTR	B3LYP	0.4345	0.4894	0.2369	0.2810
	M062X	0.5372	0.6048	0.6195	0.6939
	PBE0	0.4719	0.5318	0.2341	0.2715
DMAC-TTR	B3LYP	0.5583	0.6500	0.6746	0.7606
	M062X	0.7150	0.8397	0.7653	0.8827
	PBE0	0.5939	0.7019	0.7014	0.7989
PXZ-TTR	B3LYP	0.5300	0.6635	0.6489	0.7625
	M062X	0.5143	0.6580	0.6361	0.7622
	PBE0	0.5035	0.6330	0.6246	0.7447
PTZ-TTR	B3LYP	0.5016	0.5592	0.5962	0.6693
	M062X	0.6951	0.8025	0.7249	0.8336
	PBE0	0.5368	0.6089	0.6267	0.7187

Table B.35. Φ_s indices for compounds in Lowdin (L) and Mulliken (M) charge distributions for the excitations from S_0 to T_1 for Group 4.

GROUP 4					
Compound	**Method**	**S_0 Geometry**		**T_1 Geometry**	
		L	**M**	**L**	**M**
Cz-TTR	B3LYP	0.5134	0.5785	0.8940	0.9224
	M062X	0.6815	0.7521	0.9528	0.9714
	PBE0	0.5866	0.6587	0.9421	0.9711
DMAC-TTR	B3LYP	0.7291	0.8271	0.7972	0.8798
	M062X	0.7941	0.8950	0.8429	0.9354
	PBE0	0.7643	0.8718	0.8212	0.9159
PXZ-TTR	B3LYP	0.5045	0.6358	0.6014	0.7173
	M062X	0.5156	0.6590	0.6152	0.7430
	PBE0	0.4874	0.6161	0.5735	0.6888
PTZ-TTR	B3LYP	0.7397	0.8112	0.7748	0.8617
	M062X	0.8187	0.9002	0.8268	0.9242
	PBE0	0.7833	0.8687	0.8031	0.9077

Table B.36. Φ_s indices for compounds in Lowdin (L) and Mulliken (M) charge distributions for the excitations from S_0 to S_1 for Group 5.

GROUP 5					
Compound	**Method**	**S_0 Geometry**		**T_1 Geometry**	
		L	**M**	**L**	**M**
CzPhDSO2	B3LYP	0.4579	0.4918	0.5643	0.6276
	M062X	0.7649	0.8196	0.7635	0.8161
	PBE0	0.4890	0.5227	0.5972	0.6682
ACRDSO2	B3LYP	0.2411	0.2797	0.4112	0.4780
	M062X	0.4644	0.5488	0.5449	0.6122
	PBE0	0.2749	0.3273	0.4598	0.5365
PXZDSO2	B3LYP	0.1052	0.1731	0.6138	0.7305
	M062X	0.2247	0.3882	0.7169	0.8632
	PBE0	0.1008	0.1661	0.5940	0.7112
PTZ-Ph-TTR	B3LYP	0.4107	0.4782	0.5992	0.6430
	M062X	0.6631	0.7579	0.7470	0.7856
	PBE0	0.4508	0.5312	0.6346	0.6833

Table B.37. Φ_s indices for compounds in Lowdin (L) and Mulliken (M) charge distributions for the excitations from S_0 to T_1 for Group 5.

GROUP 5					
Compound	**Method**	**S_0 Geometry**		**T_1 Geometry**	
		L	**M**	**L**	**M**
CzPhDSO2	B3LYP	0.6433	0.6826	0.7991	0.8470
	M062X	0.9017	0.9655	0.8941	0.9296
	PBE0	0.7195	0.7595	0.8412	0.8957
ACRDSO2	B3LYP	0.2592	0.3005	0.5612	0.6360
	M062X	0.4545	0.5344	0.8311	0.9064
	PBE0	0.2997	0.3564	0.6476	0.7299
PXZDSO2	B3LYP	0.1089	0.1778	0.5304	0.6416
	M062X	0.5210	0.6610	0.7065	0.8476
	PBE0	0.1094	0.1745	0.5144	0.6232
PTZ-Ph-TTR	B3LYP	0.6692	0.7767	0.7768	0.8203
	M062X	0.8496	0.9997	0.8352	0.8776
	PBE0	0.7389	0.8566	0.8004	0.8520

Table B.38. Φ_s indices for compounds in Lowdin (L) and Mulliken (M) charge distributions for the excitations from S_0 to S_1 for Group 6.

GROUP 6					
Compound	**Method**	**S_0 Geometry**		**T_1 Geometry**	
		L	**M**	**L**	**M**
Ac-OSO	B3LYP	0.1608	0.2226	0.4213	0.4997
	M062X	0.2870	0.3644	0.4516	0.5277
	PBE0	0.2117	0.2638	0.4246	0.5036
CzSOXO	B3LYP	0.4185	0.4671	0.5106	0.5674
	M062X	0.5029	0.5709	0.5565	0.6294
	PBE0	0.4307	0.4800	0.5392	0.5948
TXO-PhCz	B3LYP	0.3224	0.3661	0.4453	0.4768
	M062X	0.4630	0.4849	0.5933	0.6367
	PBE0	0.3561	0.3965	0.4586	0.4881

Table B.39. Φ_s indices for compounds in Lowdin (L) and Mulliken (M) charge distributions for the excitations from S_0 to T_1 for Group 6.

GROUP 6					
Compound	**Method**	**S_0 Geometry**		**T_1 Geometry**	
		L	**M**	**L**	**M**
Ac-OSO	B3LYP	0.1664	0.2267	0.4209	0.5100
	M062X	0.3646	0.4385	0.5842	0.6816
	PBE0	0.2435	0.2953	0.5026	0.5926
CzSOXO	B3LYP	0.4123	0.4655	0.5235	0.5894
	M062X	0.5258	0.5702	0.6481	0.7195
	PBE0	0.4511	0.5060	0.5692	0.6352
TXO-PhCz	B3LYP	0.4321	0.4878	0.5939	0.6276
	M062X	0.4285	0.4437	0.7860	0.8301
	PBE0	0.5306	0.5765	0.6515	0.6840

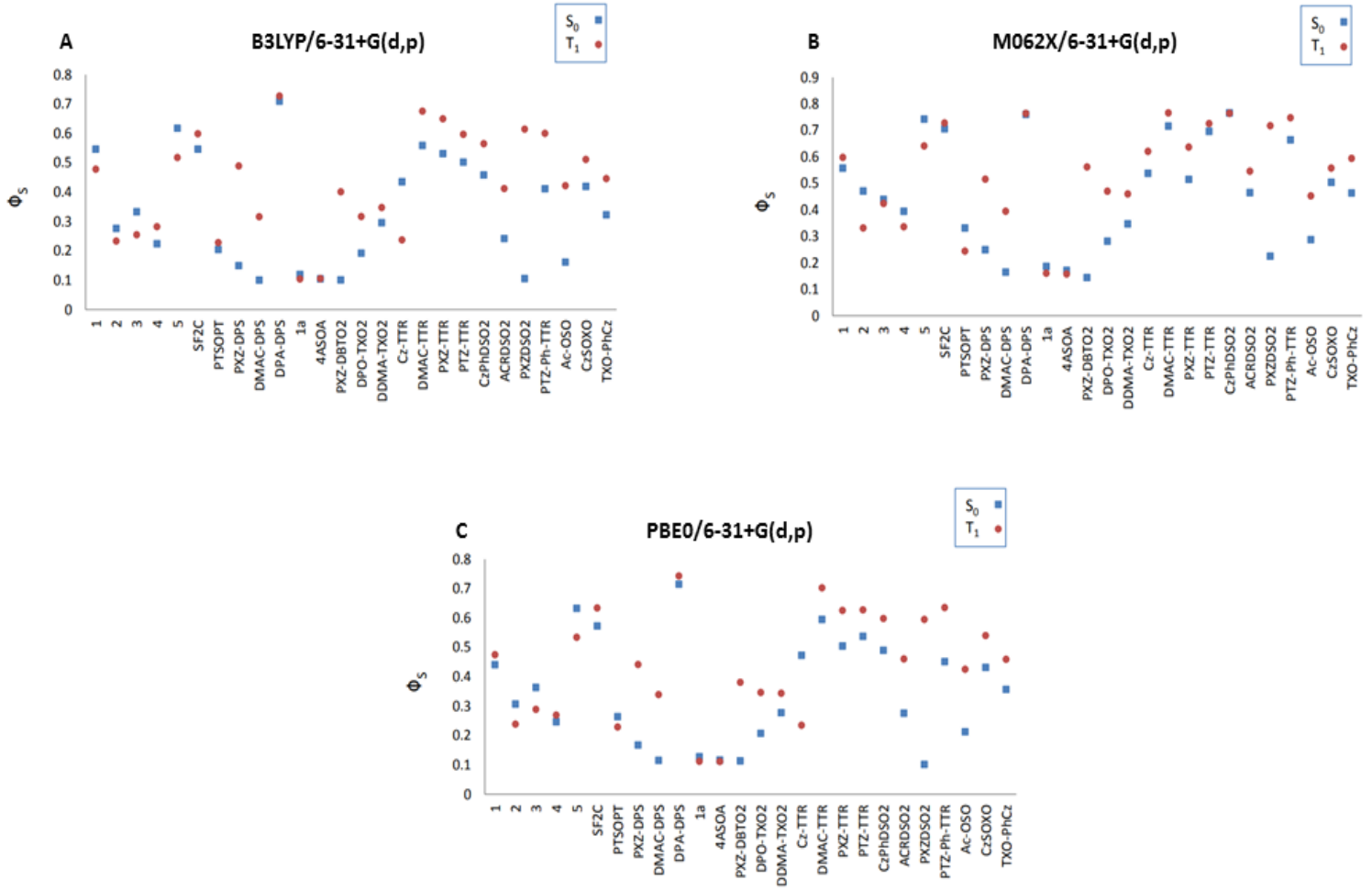

Figure B.1. Φ_s indices of studied compounds at S_0 and T_1 geometries with three different functionals.

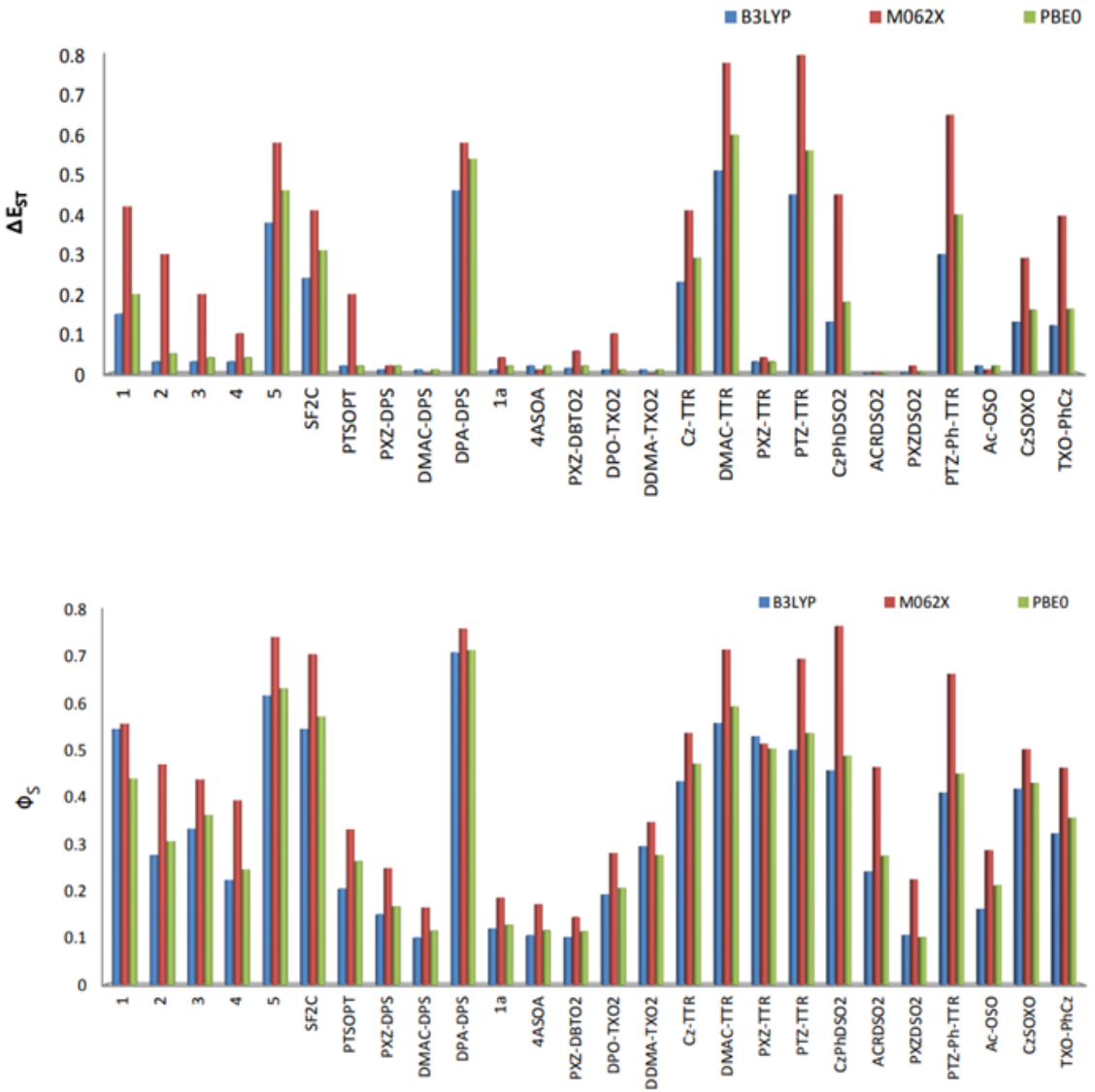

Figure B.2. Calculated ΔE_{ST} and Φ_s indices with B3LYP, M062X and PBE0 functionals

APPENDIX C: ABSORPTION SPECTRA

Table C.1. Experimental and theoretical absorption spectra for Group 1.

Compounds	Theoretical Absorption Spectra	Experimental Absorption Spectra
1	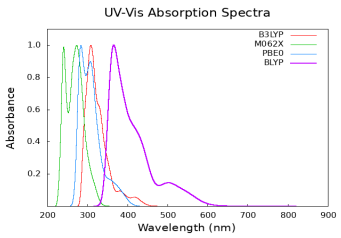	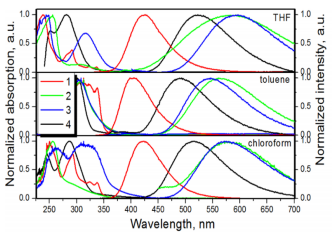
2	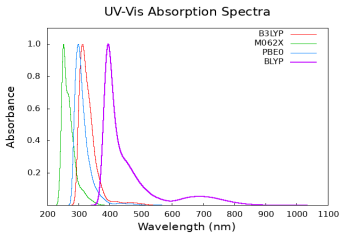	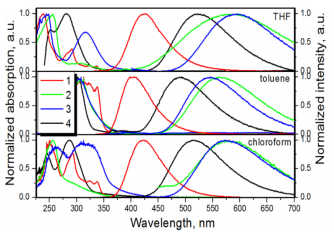
3	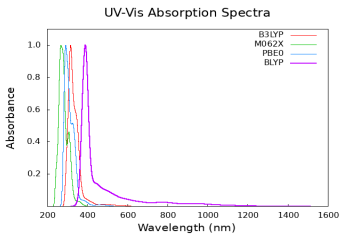	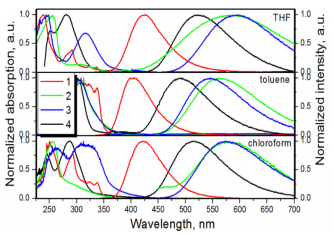
4	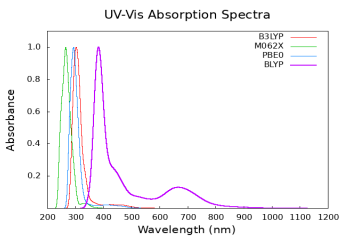	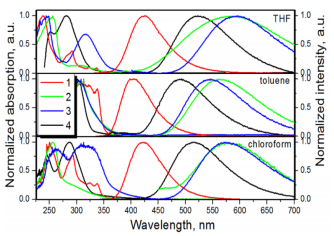
5	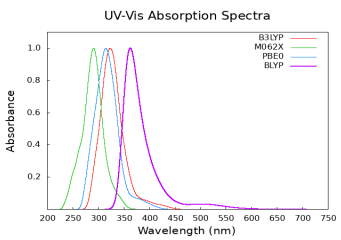	N/A

Table C.2. Experimental and theoretical absorption spectra for Group 2.

Compounds	Theoretical Absorption Spectra	Experimental Absorption Spectra
SF2C	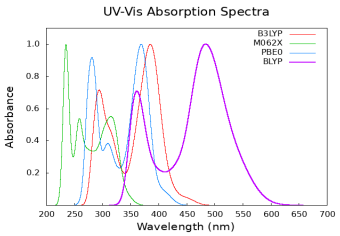	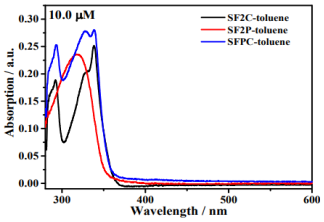
PTSOPT	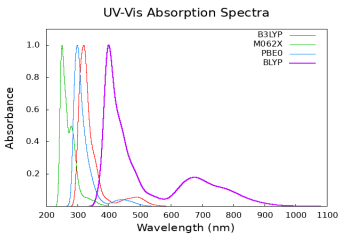	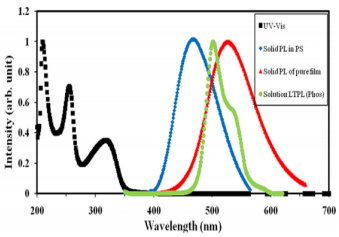
PXZ-DPS	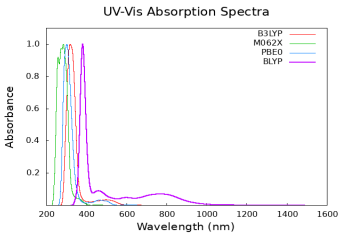	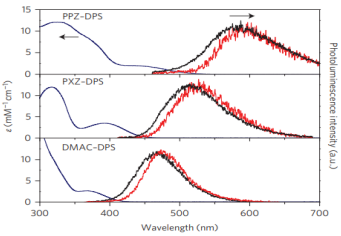
DMAC-DPS	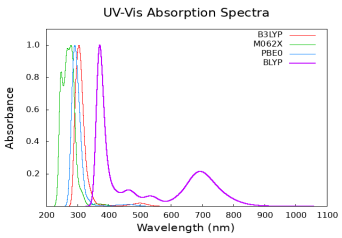	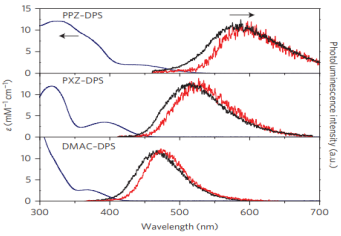
DPA-DPS	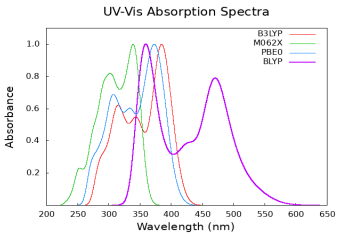	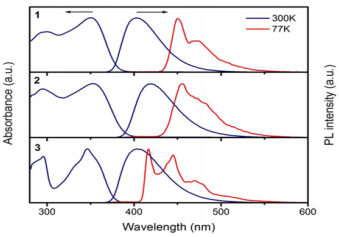

Table C.3. Experimental and theoretical absorption spectra for Group 3.

Compounds	Theoretical Absorption Spectra	Experimental Absorption Spectra
1a	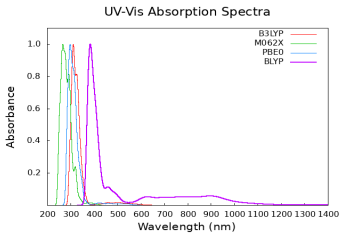	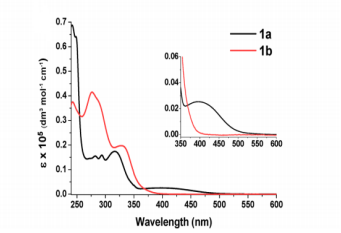
4ASOA	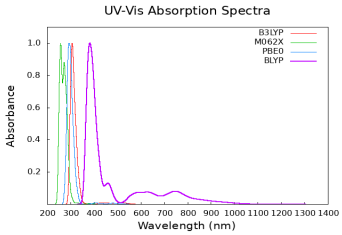	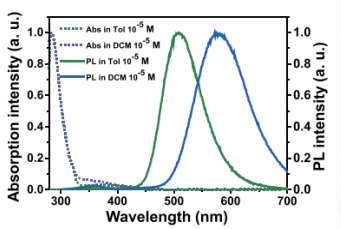
PXZ-DBTO2	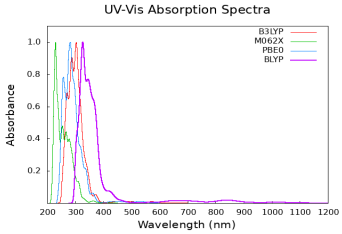	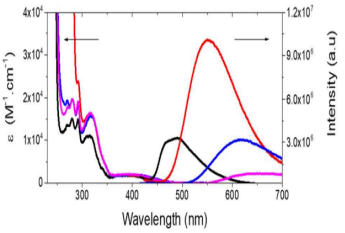
DPO-TXO2	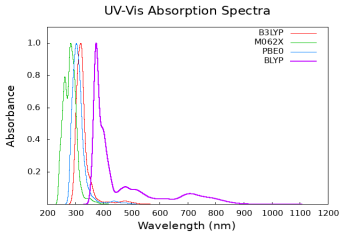	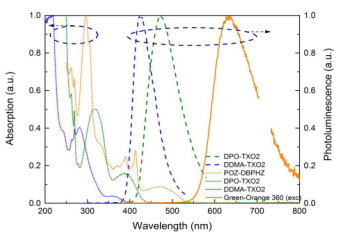
DDMA-TXO2	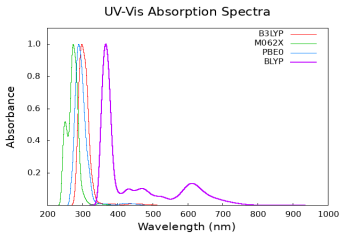	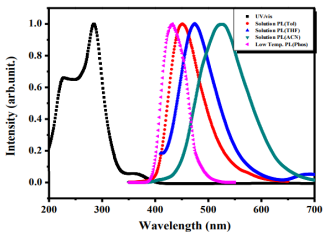

Table C.4. Experimental and theoretical absorption spectra for Group 4.

Compounds	Theoretical Absorption Spectra	Experimental Absorption Spectra
Cz-TTR	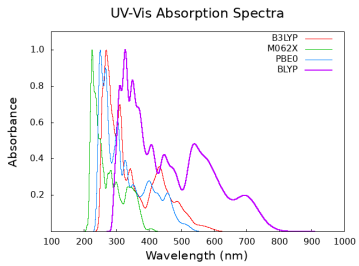	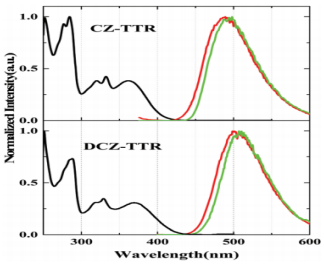
DMAC-TTR	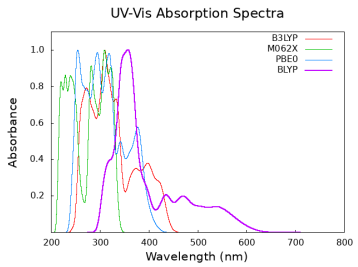	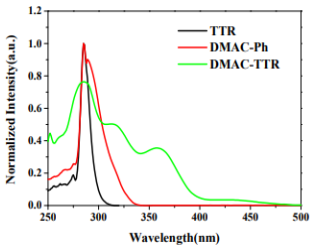
PXZ-TTR	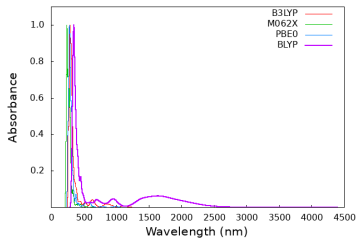	N/A
PTZ-TTR	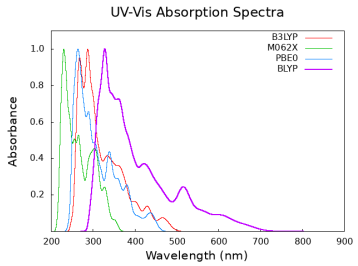	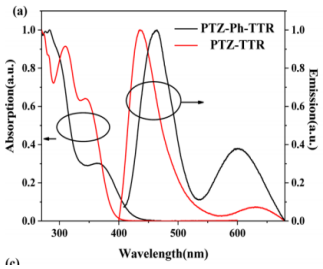

Table C.5. Experimental and theoretical absorption spectra for Group 5.

Compounds	Theoretical Absorption Spectra	Experimental Absorption Spectra
CzPhDSO2	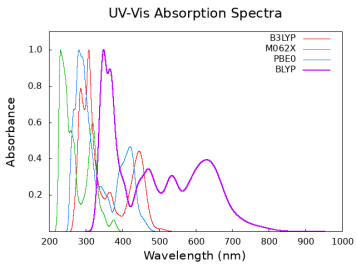	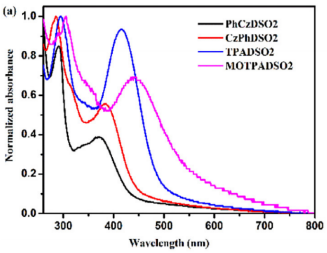
ACRDSO2	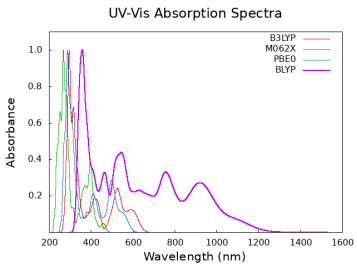	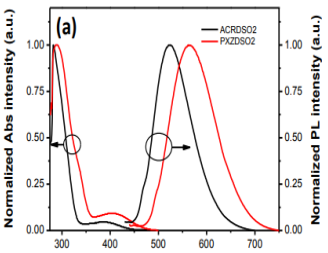
PXZDSO2	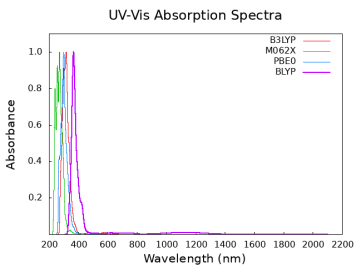	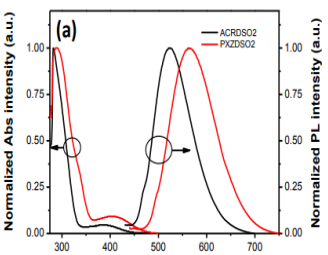
PTZ-Ph-TTR	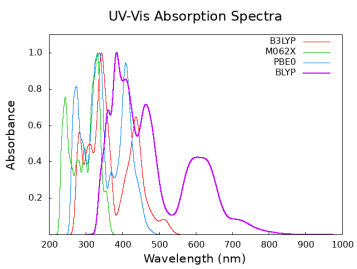	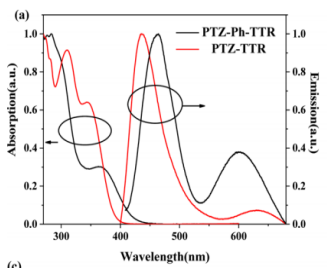

Table C.6. Experimental and theoretical absorption spectra for Group 6.

Compounds	Theoretical Absorption Spectra	Experimental Absorption Spectra
Ac-OSO	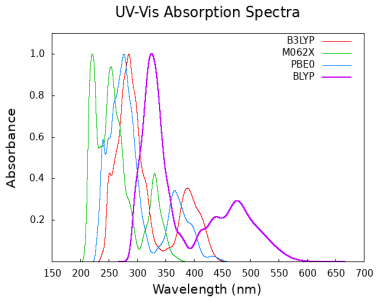	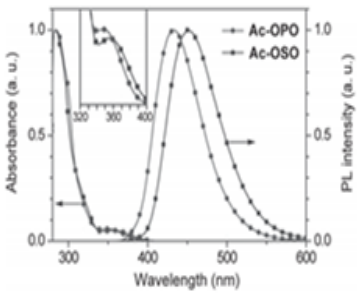
CzSOXO	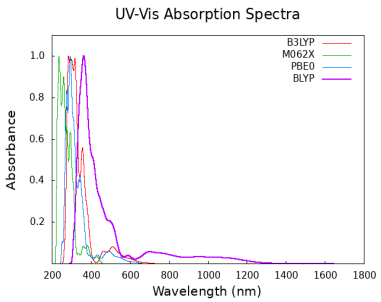	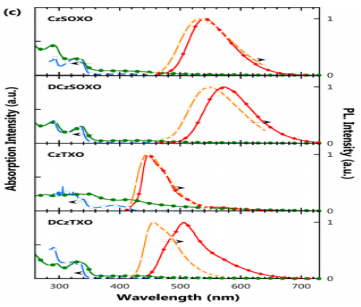
TXO-PhCz	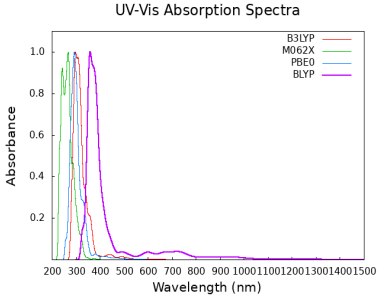	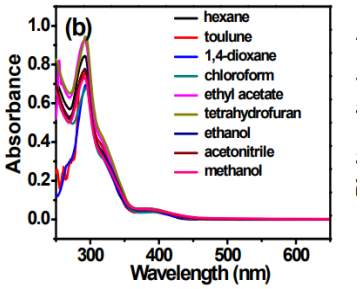

APPENDIX D: EMISSION SPECTRA ANALYSIS

Emission spectra of studied compounds were generated with M062X functional. Generated emission spectra are not successful when compared to experimental spectra. According to comparison between experimental and theoretical emission spectra, there is not good correlation between experimental emission colors and theoretical emission colors. None of the compounds have similar emission color with experimental data. This shows that emission spectra were not successfully reproduced. As expected, M062X functional shows hypsochromic shift (blue shift). According to experimental spectra, the dominant emission colors are blue and green while the dominant color is violet for theoretical spectra. This is the proof for the hypsochromic shift property of M062X functional. Among all of the donor units, PXZ and PTZ containing compounds are prone to generate higher emission wavelength. We expect to get higher emission wavelength by addition of bridge unit to the structure because of the increase at conjugation length. However, compounds CzPhDSO2, PXZDSO2 and PTZ-Ph-TTR have smaller wavelength when compared to non-bridged form. Figure D.1–D.6 contain fluorescence spectra of studied compounds. Hyphen in figures represent the emission band at <380 nm for theoretical part while hyphen in experimental part means that there is no experimental data for this compound in literature. Theoretical wavelenght (nm) that are obtained from phosphorescence spectra calculations can be found in Table C.1.

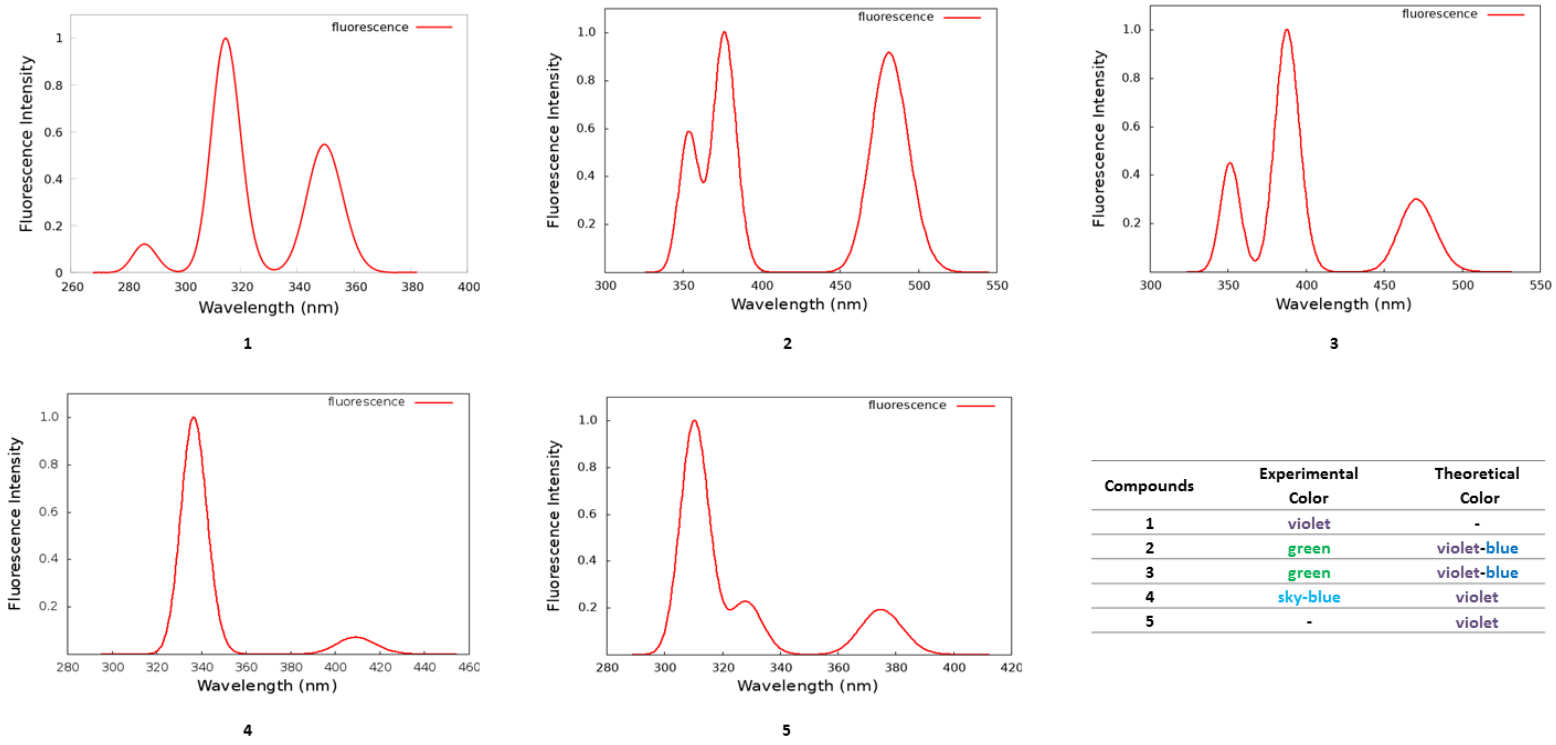

Compounds	Experimental Color	Theoretical Color
1	violet	-
2	green	violet-blue
3	green	violet-blue
4	sky-blue	violet
5	-	violet

Figure D.1. Emission spectra for Group 1 TADF emitters calculated at M062X/6-31+G(d,p) level of theory and experimental-theoretical colors of compounds.

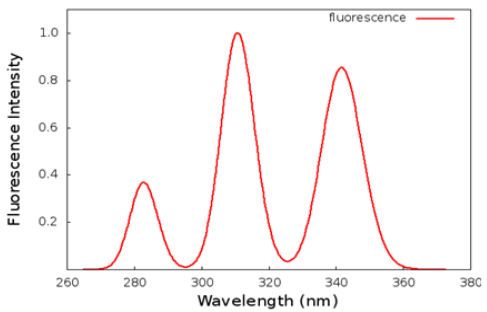

SF2C

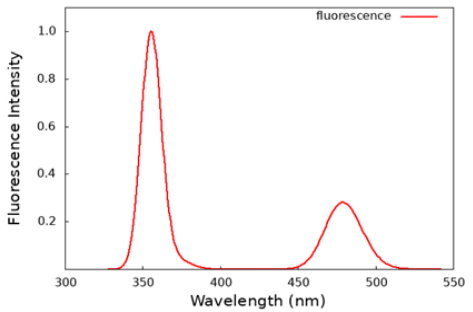

PTSOPT

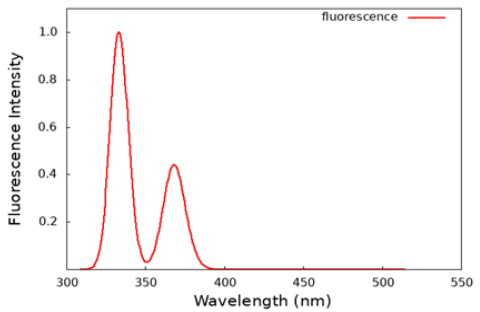

PXZ-DPS

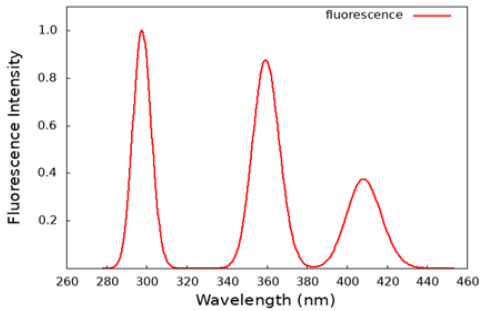

DMAC-DPS

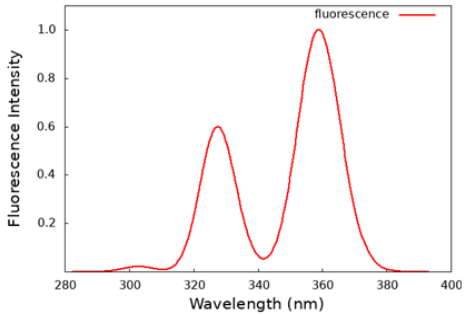

DPA-DPS

Compounds	Experimental Color	Theoretical Color
SF2C	blue	-
PTSOPT	green	blue
PXZ-DPS	blue	violet
DMAC-DPS	blue	violet
DPA-DPS	blue	-

Figure D.2. Emission spectra for Group 2 TADF emitters calculated at M062X/6-31+G(d,p) level of theory and experimental-theoretical colors of compounds.

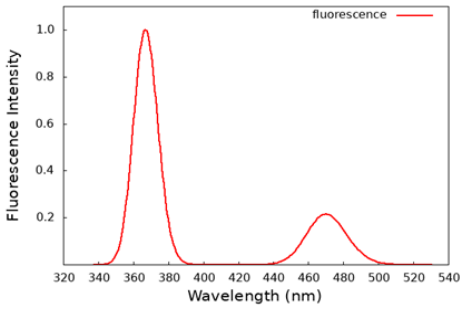

1a

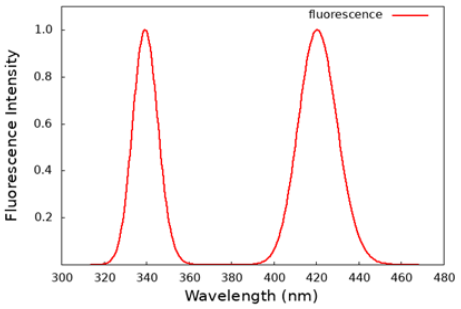

4ASOA

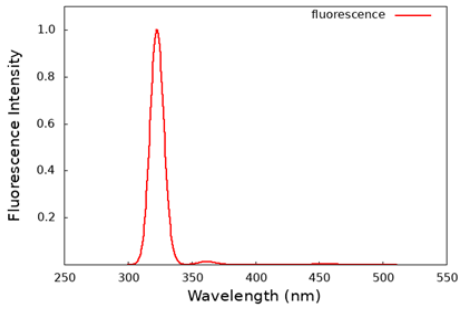

DPO-TXO2

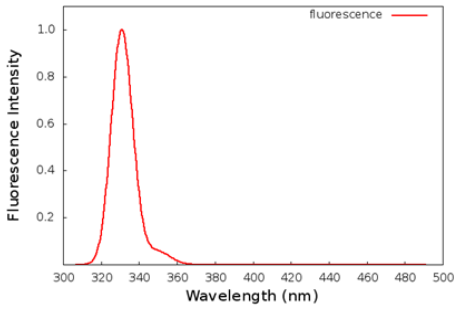

DPO-TXO2

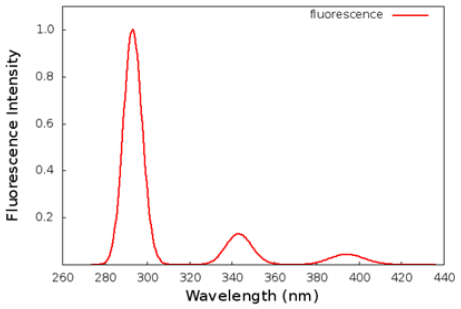

DDMA-TXO2

Compounds	Experimental Color	Theoretical Color
1a	yellow	blue
4ASOA	green	violet
PXZ-DBTO2	green	-
DPO-TXO2	blue-green	-
DDMA-TXO2	blue	violet

Figure D.3. Emission spectra for Group 3 TADF emitters calculated at M062X/6-31+G(d,p) level of theory and experimental-theoretical colors of compounds.

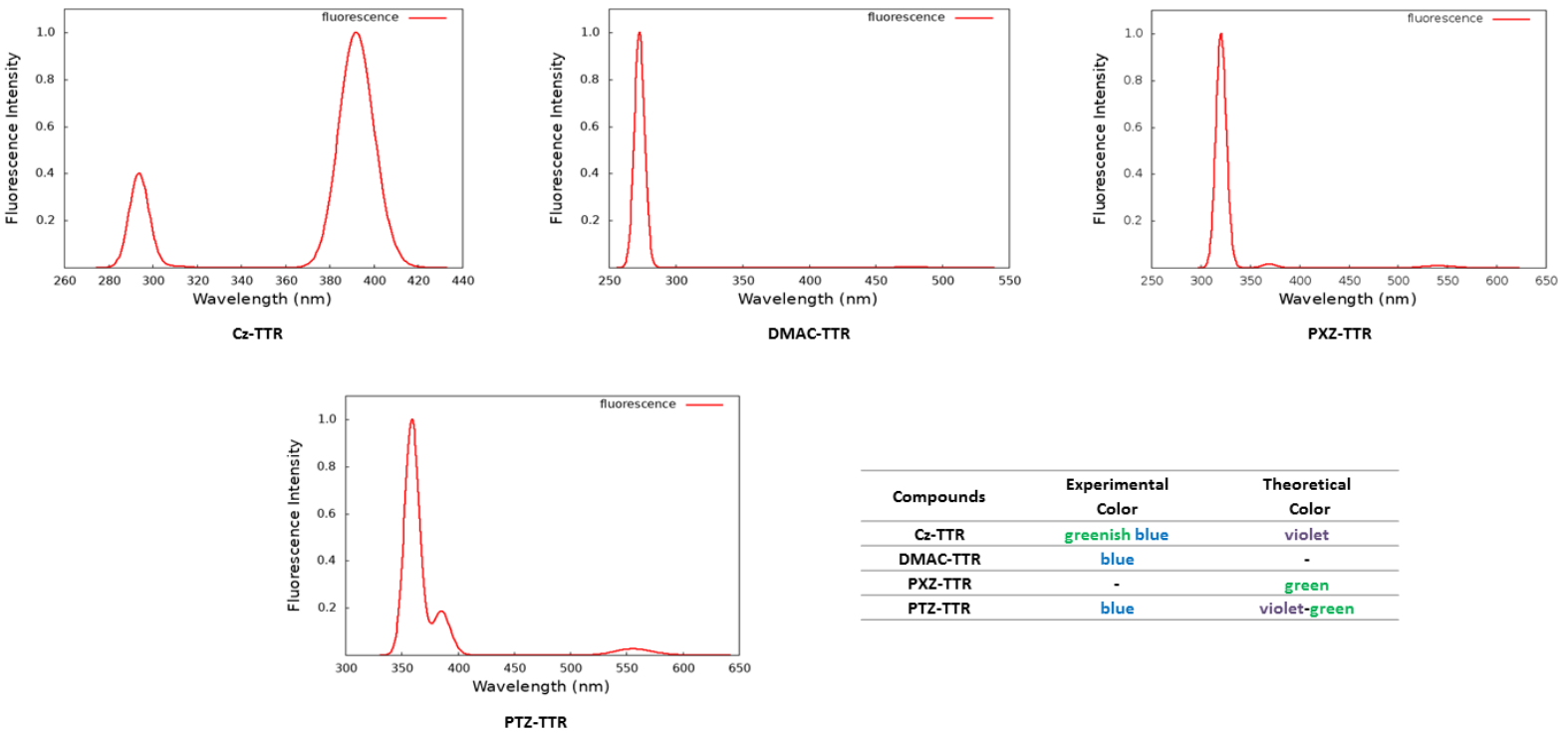

Compounds	Experimental Color	Theoretical Color
Cz-TTR	greenish blue	violet
DMAC-TTR	blue	-
PXZ-TTR	-	green
PTZ-TTR	blue	violet-green

Figure D.4. Emission spectra for Group 4 TADF emitters calculated at M062X/6-31+G(d,p) level of theory and experimental-theoretical colors of compounds.

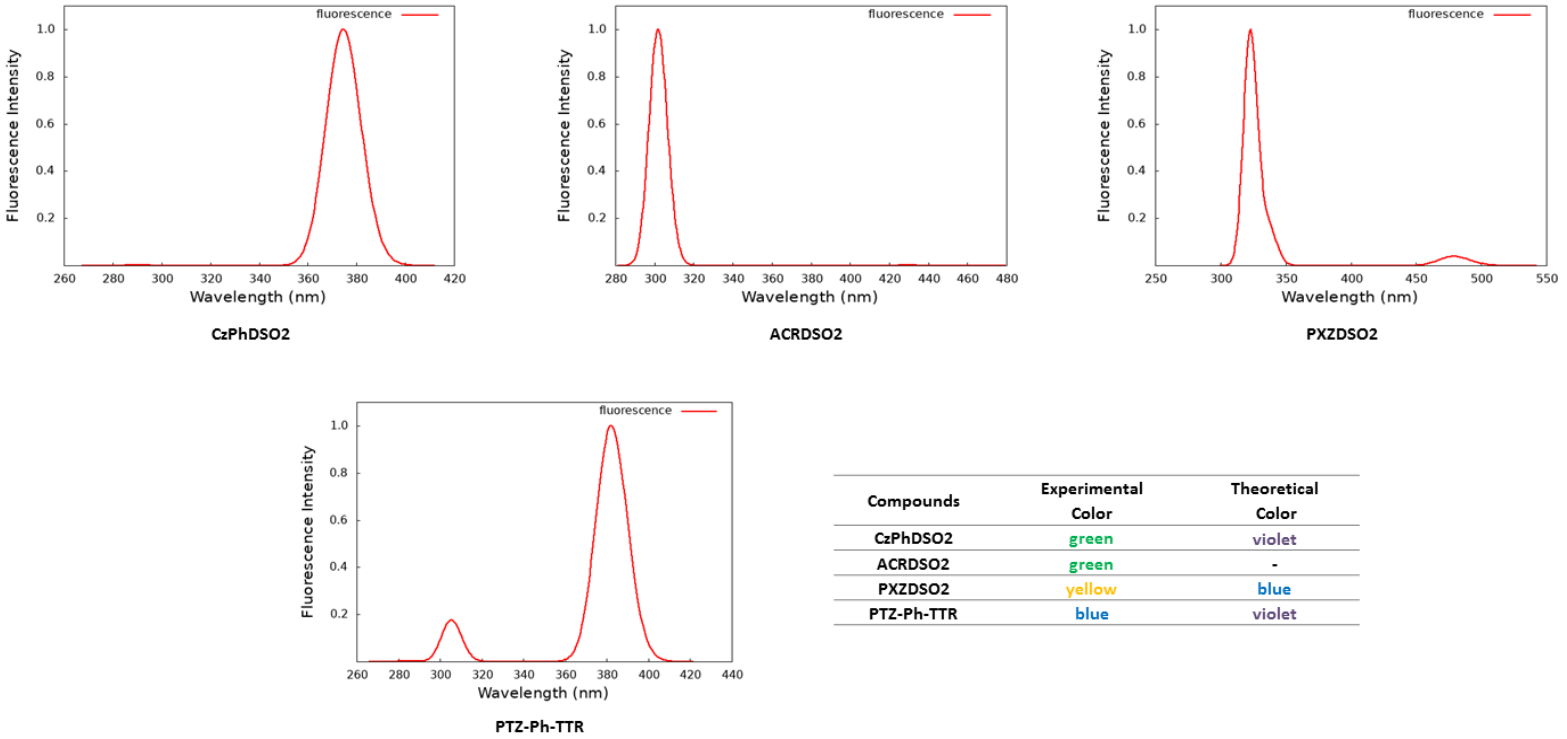

Compounds	Experimental Color	Theoretical Color
CzPhDSO2	green	violet
ACRDSO2	green	-
PXZDSO2	yellow	blue
PTZ-Ph-TTR	blue	violet

Figure D.5. Emission spectra for Group 5 TADF emitters calculated at M062X/6-31+G(d,p) level of theory and experimental-theoretical colors of compounds.

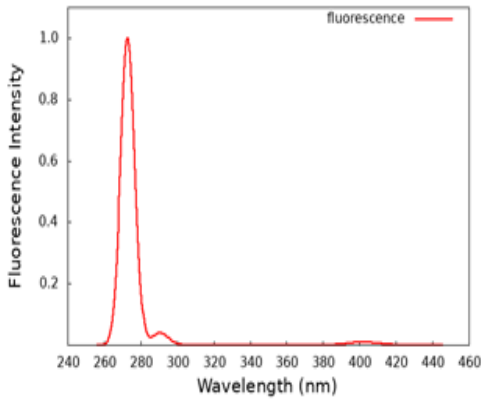

Ac-OSO

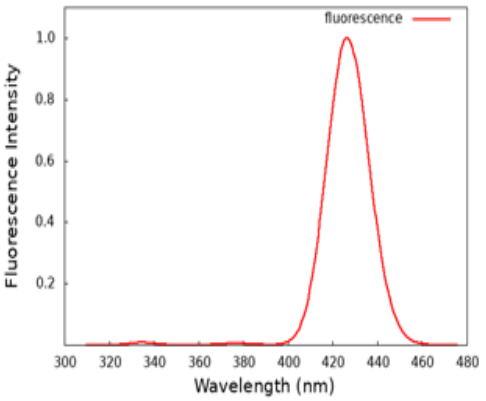

CzSOXO

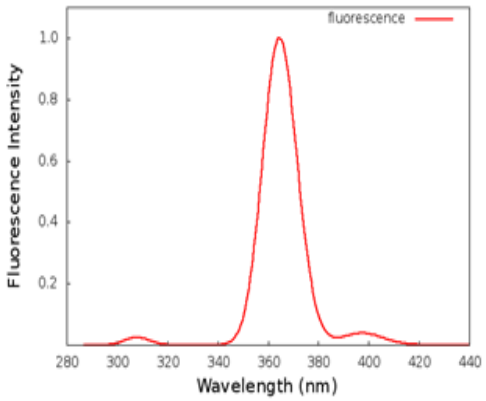

TXO-PhCz

Compounds	Experimental Color	Theoretical Color
Ac-OSO	blue	violet
CzSOXO	green	violet
TXO-PhCz	green	violet

Figure D.6. Emission spectra for Group 6 TADF emitters calculated at M062X/6-31+G(d,p) level of theory and experimental-theoretical colors of compounds.

Table D.1. Phosphorescence wavelengths of studied compounds.

GROUP 1	
Compounds	**Wavelength (nm)**
1	346.06, 335.75, 333.50
2	493.21, 440.19, 369.74
3	437.25, 435.50, 389.36
4	415.88, 350.78, 345.16
5	423.10, 401.15, 350.64
GROUP 2	
Compounds	**Wavelength (nm)**
SF2C	415.72, 368.92, 327.01
PTSOPT	507.70, 450.00, 381.10
PXZ-DPS	483.02, 402.61, 381.45
DMAC-DPS	447.78, 421.56, 345.84
DPA-DPS	516.85, 426.30, 350.18
GROUP 3	
Compounds	**Wavelength (nm)**
1a	458.78, 457.20, 409.67
4ASOA	417.18, 415.75, 408.41
PXZ-DBTO2	469.37, 405.33, 394.09
DPO-TXO2	416.93, 412.45, 387.96
DDMA-TXO2	381.16, 376.76, 336.50
GROUP 4	
Compounds	**Wavelength (nm)**
Cz-TTR	420.18, 364.04, 341.68
DMAC-TTR	472.20, 327.83, 306.15
PXZ-TTR	551.51, 406.06, 372.97
PTZ-TTR	468.60, 326.06, 310.77
GROUP 5	
Compounds	**Wavelength (nm)**
CzPhDSO2	525.40, 347.29, 328.08
ACRDSO2	495.74, 383.59, 338.67
PXZDSO2	498.15, 405.26, 402.29
PTZ-Ph-TTR	542.56, 355.75, 325.35
GROUP 6	
Compounds	**Wavelength (nm)**
Ac-OSO	420.85, 336.67, 318.97
CzSOXO	481.23, 426.58, 377.62
TXO-PhCz	507.46, 423.38, 379.38

APPENDIX E: COPY-RIGHT LIST

E.1. The License for Table C.1

E.2. The License for Table C.2

CCC Marketplace™

This is a License Agreement between Aslıhan Hepgüler ("User") and Copyright Clearance Center, Inc. ("CCC") on behalf of the Rightsholder identified in the order details below. The license consists of the order details, the CCC Terms and Conditions below, and any Rightsholder Terms and Conditions which are included below.

All payments must be made in full to CCC in accordance with the CCC Terms and Conditions below.

Order Date	10-Feb-2022	Type of Use	Republish in a thesis/dissertation
Order License ID	1187543-1		
ISSN	1433-7851	Publisher	WILEY - V C H VERLAG GMBH & CO. KGAA
		Portion	Chart/graph/table/figure

LICENSED CONTENT

Publication Title	Angewandte Chemie	Rightsholder	John Wiley & Sons - Books
Article Title	White-light emission strategy of a single organic compound with aggregation-induced emission and delayed fluorescence properties.	Publication Type	Journal
		Start Page	7181
		End Page	7184
		Issue	24
Author/Editor	Gesellschaft Deutscher Chemiker.	Volume	54
Date	01/01/1962		
Language	English		
Country	Germany		

REQUEST DETAILS

Portion Type	Chart/graph/table/figure	Distribution	Other territories and/or countries
Number of charts / graphs / tables / figures requested	1	Enter territories/countries	Turkey
Format (select all that apply)	Print, Electronic	Translation	Original language of publication
Who will republish the content?	Academic institution	Copies for the disabled?	No
		Minor editing privileges?	No
Duration of Use	Life of current edition	Incidental promotional use?	No
Lifetime Unit Quantity	Up to 499		
Rights Requested	Main product	Currency	USD

NEW WORK DETAILS

Title	BENCHMARKING TADF ACTIVITY OF SULFONE BASED COMPOUNDS	Institution name	Bogazici University
		Expected presentation date	2022-02-13
Instructor name	Aslıhan Hepgüler		

ADDITIONAL DETAILS

The requesting person / organization to appear on the license	Aslıhan Hepgüler

Print

ELSEVIER LICENSE TERMS AND CONDITIONS

Feb 09, 2022

This Agreement between Miss. Aslıhan Hepgüler ("You") and Elsevier ("Elsevier") consists of your license details and the terms and conditions provided by Elsevier and Copyright Clearance Center.

License Number	5244590834030
License date	Feb 09, 2022
Licensed Content Publisher	Elsevier
Licensed Content Publication	Organic Electronics
Licensed Content Title	Aggregation-induced emission type thermally activated delayed fluorescent materials for high efficiency in non-doped organic light-emitting diodes
Licensed Content Author	In Ho Lee,Wook Song,Jun Yeob Lee
Licensed Content Date	Feb 1, 2016
Licensed Content Volume	29
Licensed Content Issue	n/a
Licensed Content Pages	5
Start Page	22
End Page	26
Type of Use	reuse in a thesis/dissertation

Print

SPRINGER NATURE LICENSE TERMS AND CONDITIONS

Feb 09, 2022

This Agreement between Miss. Aslıhan Hepgüler ("You") and Springer Nature ("Springer Nature") consists of your license details and the terms and conditions provided by Springer Nature and Copyright Clearance Center.

License Number	5244670536138
License date	Feb 09, 2022
Licensed Content Publisher	Springer Nature
Licensed Content Publication	Nature Photonics
Licensed Content Title	Efficient blue organic light-emitting diodes employing thermally activated delayed fluorescence
Licensed Content Author	Qisheng Zhang et al
Licensed Content Date	Mar 2, 2014
Type of Use	Thesis/Dissertation
Requestor type	academic/university or research institute
Format	print and electronic
Portion	figures/tables/illustrations
Number of figures/tables/illustrations	1
High-res required	no
Will you be translating?	no

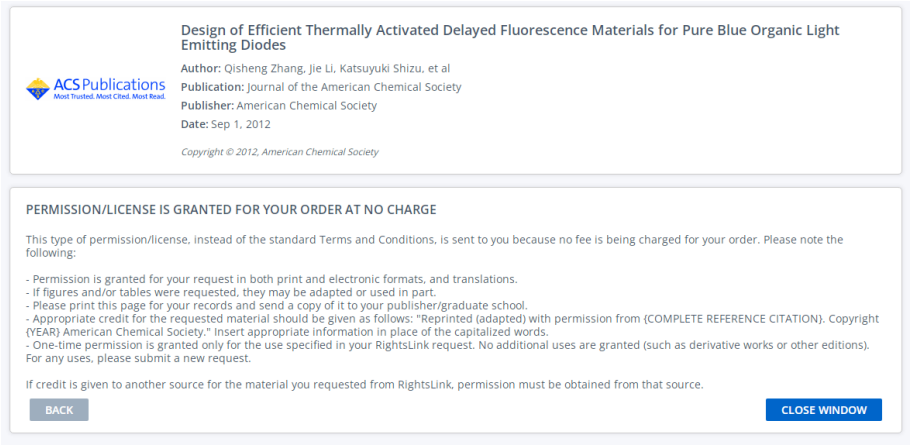

Design of Efficient Thermally Activated Delayed Fluorescence Materials for Pure Blue Organic Light Emitting Diodes

Author: Qisheng Zhang, Jie Li, Katsuyuki Shizu, et al
Publication: Journal of the American Chemical Society
Publisher: American Chemical Society
Date: Sep 1, 2012

Copyright © 2012, American Chemical Society

PERMISSION/LICENSE IS GRANTED FOR YOUR ORDER AT NO CHARGE

This type of permission/license, instead of the standard Terms and Conditions, is sent to you because no fee is being charged for your order. Please note the following:

- Permission is granted for your request in both print and electronic formats, and translations.
- If figures and/or tables were requested, they may be adapted or used in part.
- Please print this page for your records and send a copy of it to your publisher/graduate school.
- Appropriate credit for the requested material should be given as follows: "Reprinted (adapted) with permission from {COMPLETE REFERENCE CITATION}. Copyright {YEAR} American Chemical Society." Insert appropriate information in place of the capitalized words.
- One-time permission is granted only for the use specified in your RightsLink request. No additional uses are granted (such as derivative works or other editions). For any uses, please submit a new request.

If credit is given to another source for the material you requested from RightsLink, permission must be obtained from that source.

BACK CLOSE WINDOW

E.3. The License for Table C.3

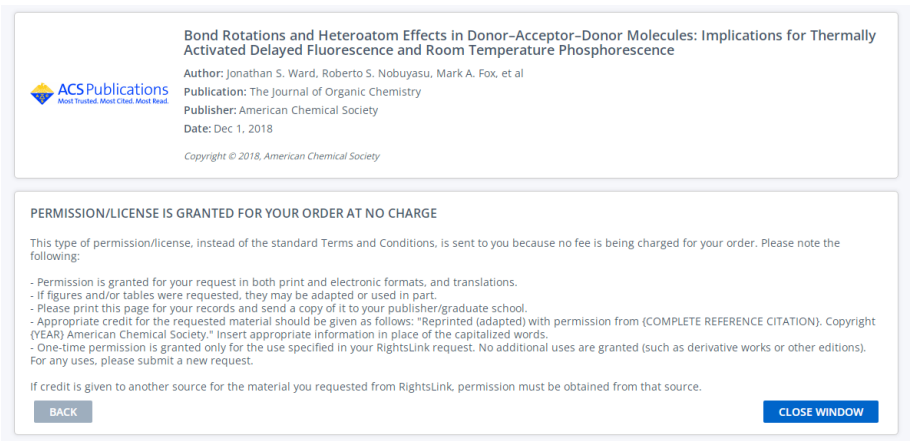

Bond Rotations and Heteroatom Effects in Donor–Acceptor–Donor Molecules: Implications for Thermally Activated Delayed Fluorescence and Room Temperature Phosphorescence

Author: Jonathan S. Ward, Roberto S. Nobuyasu, Mark A. Fox, et al
Publication: The Journal of Organic Chemistry
Publisher: American Chemical Society
Date: Dec 1, 2018

Copyright © 2018, American Chemical Society

PERMISSION/LICENSE IS GRANTED FOR YOUR ORDER AT NO CHARGE

This type of permission/license, instead of the standard Terms and Conditions, is sent to you because no fee is being charged for your order. Please note the following:

- Permission is granted for your request in both print and electronic formats, and translations.
- If figures and/or tables were requested, they may be adapted or used in part.
- Please print this page for your records and send a copy of it to your publisher/graduate school.
- Appropriate credit for the requested material should be given as follows: "Reprinted (adapted) with permission from {COMPLETE REFERENCE CITATION}. Copyright {YEAR} American Chemical Society." Insert appropriate information in place of the capitalized words.
- One-time permission is granted only for the use specified in your RightsLink request. No additional uses are granted (such as derivative works or other editions). For any uses, please submit a new request.

If credit is given to another source for the material you requested from RightsLink, permission must be obtained from that source.

BACK CLOSE WINDOW

Print

ELSEVIER LICENSE TERMS AND CONDITIONS

Feb 09, 2022

This Agreement between Miss. Aslıhan Hepgüler ("You") and Elsevier ("Elsevier") consists of your license details and the terms and conditions provided by Elsevier and Copyright Clearance Center.

License Number	5244710262451
License date	Feb 09, 2022
Licensed Content Publisher	Elsevier
Licensed Content Publication	Journal of Luminescence
Licensed Content Title	Thermally activated delayed fluorescence of Bis(9,9-dimethyl-9,10-dihydroacridine) dibenzo[b,d]thiophene 5,5-dioxide derivatives for organic light-emitting diodes
Licensed Content Author	Jong Uk Kim,Saripally Sudhaker Reddy,Lin-Song Cui,Hiroko Nomura,Sunbin Hwang,Dae Hyeon Kim,Hajime Nakanotani,Sung–Ho Jin,Chihaya Adachi
Licensed Content Date	Oct 1, 2017
Licensed Content Volume	190
Licensed Content Issue	n/a
Licensed Content Pages	7
Start Page	485
End Page	491

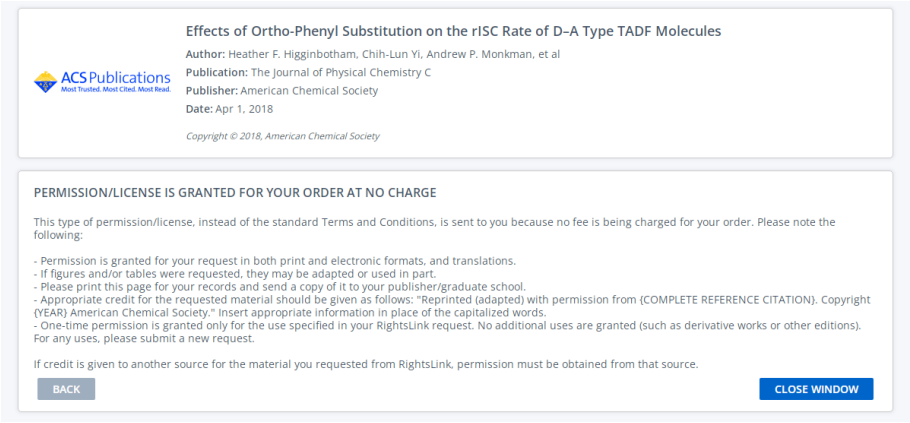

Effects of Ortho-Phenyl Substitution on the rISC Rate of D–A Type TADF Molecules

Author: Heather F. Higginbotham, Chih-Lun Yi, Andrew P. Monkman, et al
Publication: The Journal of Physical Chemistry C
Publisher: American Chemical Society
Date: Apr 1, 2018

Copyright © 2018, American Chemical Society

PERMISSION/LICENSE IS GRANTED FOR YOUR ORDER AT NO CHARGE

This type of permission/license, instead of the standard Terms and Conditions, is sent to you because no fee is being charged for your order. Please note the following:

- Permission is granted for your request in both print and electronic formats, and translations.
- If figures and/or tables were requested, they may be adapted or used in part.
- Please print this page for your records and send a copy of it to your publisher/graduate school.
- Appropriate credit for the requested material should be given as follows: "Reprinted (adapted) with permission from {COMPLETE REFERENCE CITATION}. Copyright {YEAR} American Chemical Society." Insert appropriate information in place of the capitalized words.
- One-time permission is granted only for the use specified in your RightsLink request. No additional uses are granted (such as derivative works or other editions). For any uses, please submit a new request.

If credit is given to another source for the material you requested from RightsLink, permission must be obtained from that source.

BACK CLOSE WINDOW

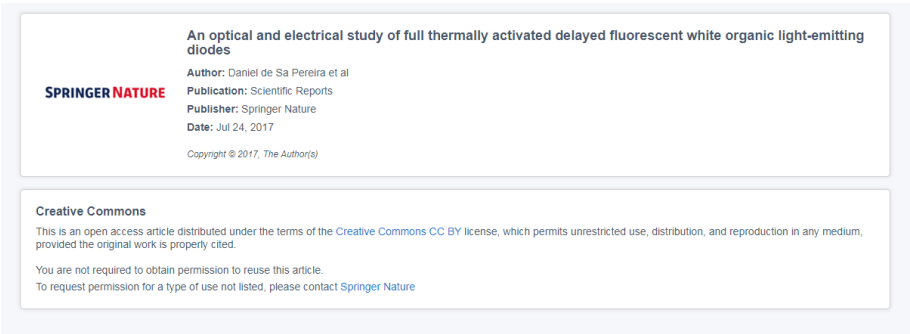

An optical and electrical study of full thermally activated delayed fluorescent white organic light-emitting diodes

Author: Daniel de Sa Pereira et al
Publication: Scientific Reports
Publisher: Springer Nature
Date: Jul 24, 2017

Copyright © 2017, The Author(s)

Creative Commons

This is an open access article distributed under the terms of the Creative Commons CC BY license, which permits unrestricted use, distribution, and reproduction in any medium, provided the original work is properly cited.

You are not required to obtain permission to reuse this article.
To request permission for a type of use not listed, please contact Springer Nature

Print

ELSEVIER LICENSE TERMS AND CONDITIONS

Feb 09, 2022

This Agreement between Miss. Aslıhan Hepgüler ("You") and Elsevier ("Elsevier") consists of your license details and the terms and conditions provided by Elsevier and Copyright Clearance Center.

License Number	5244870893217
License date	Feb 09, 2022
Licensed Content Publisher	Elsevier
Licensed Content Publication	Organic Electronics
Licensed Content Title	Molecular design of deep blue fluorescent emitters with 20% external quantum efficiency and narrow emission spectrum
Licensed Content Author	Inho Lee,Jun Yeob Lee
Licensed Content Date	Feb 1, 2016
Licensed Content Volume	29
Licensed Content Issue	n/a
Licensed Content Pages	5
Start Page	160
End Page	164
Type of Use	reuse in a thesis/dissertation
Portion	figures/tables/illustrations

E.4. The License for Table C.4

Order Date	10-Feb-2022	Type of Use	Republish in a thesis/dissertation
Order License ID	1187545-1		
ISSN	2050-7526	Publisher	Royal Society of Chemistry
		Portion	Chart/graph/table/figure

LICENSED CONTENT

Publication Title	Journal of materials chemistry. C, Materials for optical and electronic devices	Rightsholder	Royal Society of Chemistry
		Publication Type	Journal
		Start Page	4797
Article Title	A comparative study of carbazole-based thermally activated delayed fluorescence emitters with different steric hindrance	End Page	4803
		Issue	19
		Volume	5
Author/Editor	Royal Society of Chemistry (Great Britain)		
Date	01/01/2012		
Language	English		
Country	United Kingdom of Great Britain and Northern Ireland		

REQUEST DETAILS

Portion Type	Chart/graph/table/figure	Distribution	Worldwide
Number of charts / graphs / tables / figures requested	1	Translation	Original language of publication
		Copies for the disabled?	No
Format (select all that apply)	Print, Electronic	Minor editing privileges?	No
Who will republish the content?	Academic institution	Incidental promotional use?	No
Duration of Use	Life of current edition	Currency	USD
Lifetime Unit Quantity	Up to 499		
Rights Requested	Main product		

NEW WORK DETAILS

Title	BENCHMARKING TADF ACTIVITY OF SULFONE-BASED COMPOUNDS	Institution name	Bogazici University
		Expected presentation date	2022-02-13
Instructor name	Aslıhan Hepgüler		

ADDITIONAL DETAILS

Order reference number	N/A

Order Date	11-Feb-2022	Type of Use	Republish in a thesis/dissertation
Order License ID	1188045-1		
ISSN	0935-9648	Publisher	WILEY - V C H VERLAG GMBH & CO. KGAA
		Portion	Chart/graph/table/figure

LICENSED CONTENT

Publication Title	Advanced materials	Rightsholder	John Wiley & Sons - Books
Article Title	Avoiding Energy Loss on TADF Emitters: Controlling the Dual Conformations of D-A Structure Molecules Based on the Pseudoplanar Segments.	Publication Type	Journal
		Start Page	1701476
		Issue	47
		Volume	29
Date	01/01/1989		
Language	English		
Country	Germany		

REQUEST DETAILS

Portion Type	Chart/graph/table/figure	Distribution	Other territories and/or countries
Number of charts / graphs / tables / figures requested	1	Enter territories/countries	Turkey
Format (select all that apply)	Print, Electronic	Translation	Original language of publication
Who will republish the content?	Academic institution	Copies for the disabled?	No
		Minor editing privileges?	No
Duration of Use	Life of current edition	Incidental promotional use?	No
Lifetime Unit Quantity	Up to 499		
Rights Requested	Main product	Currency	USD

NEW WORK DETAILS

Title	BENCHMARKING TADF ACTIVITY OF SULFONE-BASED COMPOUNDS	Institution name	Bogazici University
		Expected presentation date	2022-02-13
Instructor name	Aslıhan Hepgüler		

ADDITIONAL DETAILS

The requesting person / organization to appear on the license	Aslıhan Hepgüler

REUSE CONTENT DETAILS

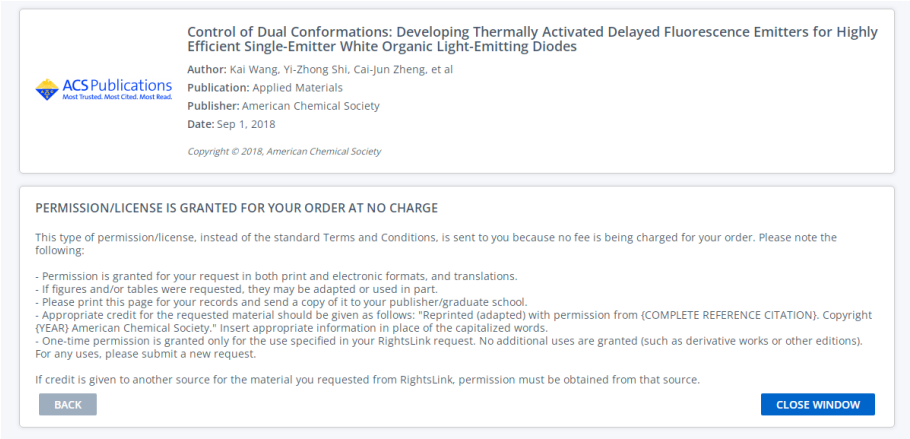

Control of Dual Conformations: Developing Thermally Activated Delayed Fluorescence Emitters for Highly Efficient Single-Emitter White Organic Light-Emitting Diodes

Author: Kai Wang, Yi-Zhong Shi, Cai-Jun Zheng, et al
Publication: Applied Materials
Publisher: American Chemical Society
Date: Sep 1, 2018

E.5. The License for Table C.5

Print

ELSEVIER LICENSE
TERMS AND CONDITIONS

Feb 09, 2022

This Agreement between Miss. Aslıhan Hepgüler ("You") and Elsevier ("Elsevier") consists of your license details and the terms and conditions provided by Elsevier and Copyright Clearance Center.

License Number	5244880401550
License date	Feb 09, 2022
Licensed Content Publisher	Elsevier
Licensed Content Publication	Dyes and Pigments
Licensed Content Title	Highly efficient and color tunable thermally activated delayed fluorescent emitters and their applications for the solution-processed OLEDs
Licensed Content Author	Kaiyong Sun,Yibai Sun,Wei Jiang,Suli Huang,Wenwen Tian,Yueming Sun
Licensed Content Date	Apr 1, 2017
Licensed Content Volume	139
Licensed Content Issue	n/a
Licensed Content Pages	8
Start Page	326
End Page	333

CCC Marketplace™

Order Date	11-Feb-2022	Type of Use	Republish in a thesis/dissertation
Order License ID	1188120-1		
ISSN	0935-9648	Publisher	WILEY - V C H VERLAG GMBH & CO. KGAA
		Portion	Chart/graph/table/figure

LICENSED CONTENT

Publication Title	Advanced materials	Publication Type	Journal
Article Title	Evaporation- and Solution-Process-Feasible Highly Efficient Thianthrene-9,9',10,10'-Tetraoxide-Based Thermally Activated Delayed Fluorescence Emitters with Reduced Efficiency Roll-Off.	Start Page	181
		End Page	187
		Issue	1
		Volume	28
Date	01/01/1989		
Language	English		
Country	Germany		
Rightsholder	John Wiley & Sons - Books		

REQUEST DETAILS

Portion Type	Chart/graph/table/figure	Distribution	Other territories and/or countries
Number of charts / graphs / tables / figures requested	1	Enter territories/countries	Turkey
Format (select all that apply)	Print, Electronic	Translation	Original language of publication
Who will republish the content?	Academic institution	Copies for the disabled?	No
		Minor editing privileges?	No
Duration of Use	Life of current edition	Incidental promotional use?	No
Lifetime Unit Quantity	Up to 499		
Rights Requested	Main product	Currency	USD

NEW WORK DETAILS

Title	BENCHMARKING TADF ACTIVITY OF SULFONE-BASED COMPOUNDS	Institution name	Bogazici University
		Expected presentation date	2022-02-13
Instructor name	Aslıhan Hepgüler		

ADDITIONAL DETAILS

The requesting person / organization to appear on the license	Aslıhan Hepgüler

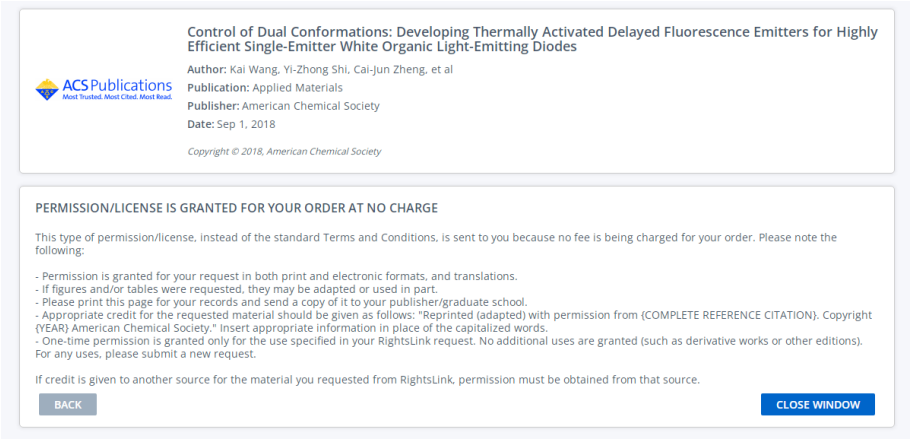

ACS Publications
Most Trusted. Most Cited. Most Read.

Control of Dual Conformations: Developing Thermally Activated Delayed Fluorescence Emitters for Highly Efficient Single-Emitter White Organic Light-Emitting Diodes

Author: Kai Wang, Yi-Zhong Shi, Cai-Jun Zheng, et al
Publication: Applied Materials
Publisher: American Chemical Society
Date: Sep 1, 2018

PERMISSION/LICENSE IS GRANTED FOR YOUR ORDER AT NO CHARGE

This type of permission/license, instead of the standard Terms and Conditions, is sent to you because no fee is being charged for your order. Please note the following:

- Permission is granted for your request in both print and electronic formats, and translations.
- If figures and/or tables were requested, they may be adapted or used in part.
- Please print this page for your records and send a copy of it to your publisher/graduate school.
- Appropriate credit for the requested material should be given as follows: "Reprinted (adapted) with permission from {COMPLETE REFERENCE CITATION}. Copyright {YEAR} American Chemical Society." Insert appropriate information in place of the capitalized words.
- One-time permission is granted only for the use specified in your RightsLink request. No additional uses are granted (such as derivative works or other editions). For any uses, please submit a new request.

If credit is given to another source for the material you requested from RightsLink, permission must be obtained from that source.

BACK CLOSE WINDOW

E.6. The License for Table C.6

CCC Marketplace™

Order Date	11-Feb-2022	Type of Use	Republish in a thesis/dissertation
Order License ID	1188045-3		
ISSN	0935-9648	Publisher	WILEY - V C H VERLAG GMBH & CO. KGAA
		Portion	Chart/graph/table/figure

LICENSED CONTENT

Publication Title	Advanced materials	Publication Type	Journal
Article Title	High-Efficiency Blue Organic Light-Emitting Diodes Based on Thermally Activated Delayed Fluorescence from Phenoxaphosphine and Phenoxathiin Derivatives.	Start Page	4626
		End Page	4631
		Issue	23
		Volume	28
Date	01/01/1989		
Language	English		
Country	Germany		
Rightsholder	John Wiley & Sons - Books		

REQUEST DETAILS

Portion Type	Chart/graph/table/figure	Distribution	Other territories and/or countries
Number of charts / graphs / tables / figures requested	1	Enter territories/countries	Turkey
Format (select all that apply)	Print, Electronic	Translation	Original language of publication
Who will republish the content?	Academic institution	Copies for the disabled?	No
		Minor editing privileges?	No
Duration of Use	Life of current edition	Incidental promotional use?	No
Lifetime Unit Quantity	Up to 499		
Rights Requested	Main product	Currency	USD

NEW WORK DETAILS

Title	BENCHMARKING TADF ACTIVITY OF SULFONE-BASED COMPOUNDS	Institution name	Bogazici University
		Expected presentation date	2022-02-13
Instructor name	Aslıhan Hepgüler		

ADDITIONAL DETAILS

The requesting person / organization to appear on the license	Aslıhan Hepgüler

CCC Marketplace™

Order Date	11-Feb-2022	Type of Use	Republish in a thesis/dissertation
Order License ID	1188045-2		
ISSN	0935-9648	Publisher	WILEY - V C H VERLAG GMBH & CO. KGAA
		Portion	Chart/graph/table/figure

LICENSED CONTENT

Publication Title	Advanced materials	Publication Type	Journal
Article Title	Novel thermally activated delayed fluorescence materials-thioxanthone derivatives and their applications for highly efficient OLEDs.	Start Page	5198
		End Page	5204
		Issue	30
		Volume	26
Date	01/01/1989		
Language	English		
Country	Germany		
Rightsholder	John Wiley & Sons - Books		

REQUEST DETAILS

Portion Type	Chart/graph/table/figure	Distribution	Other territories and/or countries
Number of charts / graphs / tables / figures requested	1	Enter territories/countries	Turkey
Format (select all that apply)	Print, Electronic	Translation	Original language of publication
Who will republish the content?	Academic institution	Copies for the disabled?	No
		Minor editing privileges?	No
Duration of Use	Life of current edition	Incidental promotional use?	No
Lifetime Unit Quantity	Up to 499		
Rights Requested	Main product	Currency	USD

NEW WORK DETAILS

Title	BENCHMARKING TADF ACTIVITY OF SULFONE-BASED COMPOUNDS	Institution name	Bogazici University
		Expected presentation date	2022-02-13
Instructor name	Aslıhan Hepgüler		

ADDITIONAL DETAILS

The requesting person / organization to appear on the license	Aslıhan Hepgüler

REUSE CONTENT DETAILS

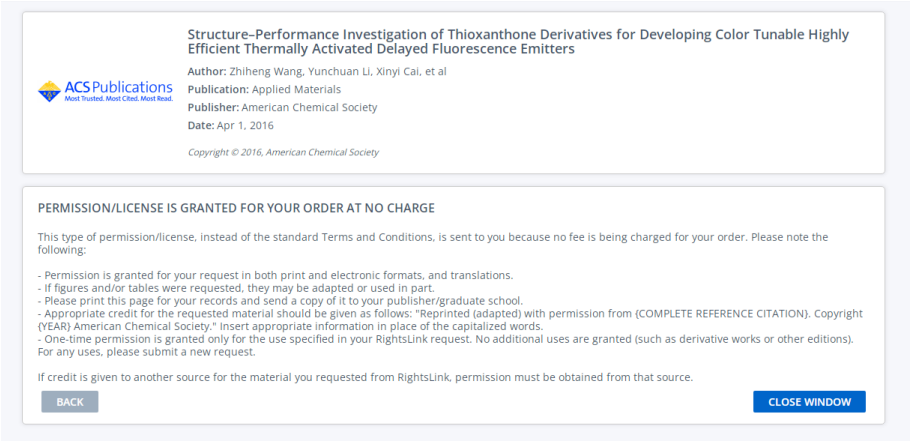

ACS Publications
Most Trusted. Most Cited. Most Read.

Structure–Performance Investigation of Thioxanthone Derivatives for Developing Color Tunable Highly Efficient Thermally Activated Delayed Fluorescence Emitters

Author: Zhiheng Wang, Yunchuan Li, Xinyi Cai, et al
Publication: Applied Materials
Publisher: American Chemical Society
Date: Apr 1, 2016

PERMISSION/LICENSE IS GRANTED FOR YOUR ORDER AT NO CHARGE

This type of permission/license, instead of the standard Terms and Conditions, is sent to you because no fee is being charged for your order. Please note the following:

- Permission is granted for your request in both print and electronic formats, and translations.
- If figures and/or tables were requested, they may be adapted or used in part.
- Please print this page for your records and send a copy of it to your publisher/graduate school.
- Appropriate credit for the requested material should be given as follows: "Reprinted (adapted) with permission from {COMPLETE REFERENCE CITATION}. Copyright {YEAR} American Chemical Society." Insert appropriate information in place of the capitalized words.
- One-time permission is granted only for the use specified in your RightsLink request. No additional uses are granted (such as derivative works or other editions). For any uses, please submit a new request.

If credit is given to another source for the material you requested from RightsLink, permission must be obtained from that source.

BACK CLOSE WINDOW